Benemérita Universidad Autónoma de Puebla

Facultad de Ciencias Físico Matemáticas

Characterization of Multigap Resistive Plate Chambers

Master Thesis in Applied Physics

Author:
Liliana Michelle Ramos Regino

Mentors:
Dra. Cecilia Uribe Estrada

Dr. Guillermo Muñoz Tejeda

December 2023

Abstract

Future high energy physics experiments will require detectors with higher rate capabilities as well as better timing precision, with this in mind, we analyzed data from three Multi Gap Resistive Plate Chambers (MRPCs). The performance studies were done using a cosmic telescope, composed of 2 MRPCs built at CERN and two PMTs, that were installed in BUAP, as well as a MRPC already built at BUAP, to compare results between the performance of the two MRPCs built at CERN and the one from ALICE-BUAP.

The MRPCs from CERN have six gaps made with glass plates and the acquisition geometry is through 24 strips and a honeycomb, while the MRPC from ALICE-BUAP, also made of glass, has two gaps and six pads that help us acquire data. MRPCs (developed in 1996) are gaseous detectors with resistive electrodes and multiple gaps as their name says, a positively charged anode and a negatively charged cathode, in this case, made of glass, separated by a gas volume. MRPCs are known to have a better timing compared to RPCs (developed in 1981) of just one gap.

When a particle enters the gas gap, it interacts with the gas atoms, creating ionized positive ions and electrons, the ions move towards the cathode and the electrons towards the anode, faster than the ions, inducing signals that can be read by the lecture pads or strips. This acquired data then will help us to measure the rate capability, efficiency, the total charge in avalanche mode, the ratio from fast to total signal of the three MRPCs.

The main research in this thesis is related to the characterization of Multigap Resistive Plate Chambers to set up a cosmic telescope with these two MRPCs from CERN and finally start a laboratory of gaseous detectors available to students of BUAP to use and learn how these detectors work.

Acknowledgements

To all the women who fought to be here, before me, specially my mom. To all the women who may come, don't give up.

I am very thankful to my friends and family who stood by me and held me in every step of this journey. Thanks to my mentors, PhD. Cecilia Uribe, PhD. Guillermo Tejeda, and M.Sc. Emigdio Jiménez, who taught me everything I needed to know to write and finish this thesis.

And finally thanks to CONACYT for giving me a scholarship and the instrumentation needed to carry out the experimentation needed to characterize the MRPCs.

Contents

List of Figures

List of Tables

Chapter 1

Introduction

Humanity has always found the way to observe what we can not see, just like Caroline Herschel designed and constructed the best telescopes of her time, Rosalind Franklin photographed the DNA structure, and Jocelyn Bell detected the signals of a pulsar for the first time ever, particle physicists have developed through the last century a significant number of gaseous detectors to understand the smallest portions of existence — elemental particles.

Here we are, in the 21st century, improving the gaseous detectors by increasing the number of gaps for a better time resolution, using gaseous mixtures to reduce greenhouse gases production, and incorporating resistive materials to improve electrical conduction. But to understand how we come to this point, we need to revisit the history and the construction and development of RPCs and MRPCs.

1.1 Historical Insights of the Gaseous Detectors

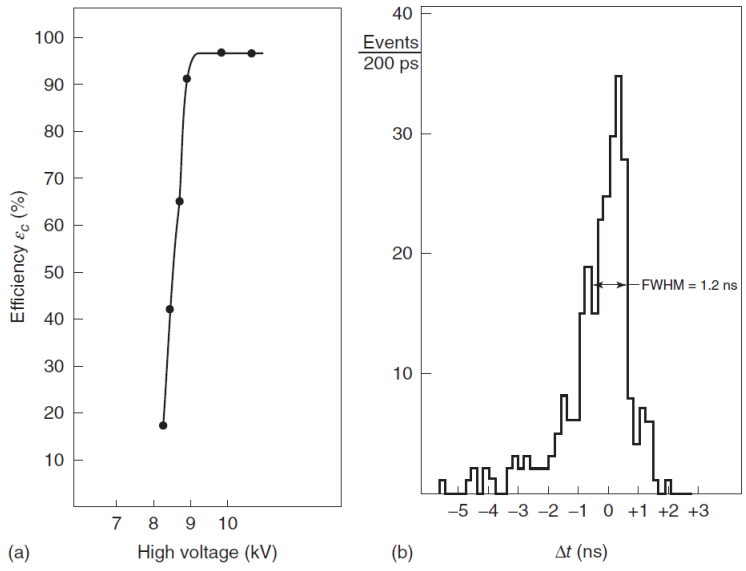

Figure 1.1: Efficiency and time distribution of Santonico and Cardarelli's RPC, where we can observe that its time resolution is of 1.2 ns. (Santonico *et al.*, 1981.)

Particle detectors were created and used for the first time at the beginnings of the 20th century. However, between 1897 and 1901 J.S. Townsend observed and studied the avalanche multiplication of electrons in gases. While detectors with cylindrical geometry were conceived a year earlier, it was not until 1908 that Geiger-Rutherford counters, the first gaseous detectors capable of detecting photons and elementary particles, were used.

In the 1940s a lot of improvements were made, like the development of the first planar detectors, there was an attempt to register radiation using a Parallel Plates Counter (PPC) by Keuffel who published the first results obtained with PPCs. Two years after this publication, Madansky and Pidd published their own PPC model and its results.

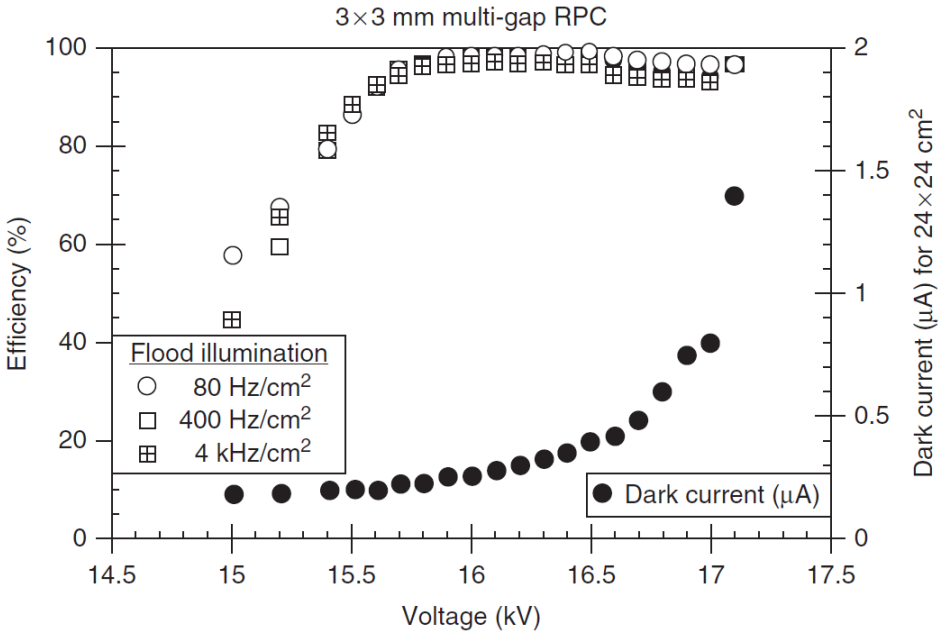

Figure 1.2: Efficiency (left) against Applied Voltage with numerous rate capacities and its Dark current (right) against the Applied Voltage from C. Williams' group first MRPC. (Williams *et al.*, 1996.)

During the 1950s, Geiger counters were among the few electronic detectors of elementary particles, and Wilson cameras were used for visualization. In fact, it was in 1955 when the first two cosmic rays photographs were taken with a Flash camera and a year after this event, the first prototype of Planar Scintillator Counters (PSCs) were proposed. Twelve years later, in 1968, G. Charpak invented the Multi-Wire Proportional Chamber (MWPC) [6].

While Geiger Counters were popular in the two decades before, in the 1970s Scintillator Counters gained popularity , however this was about to change when the Novosibirsk group began designing the first planar detectors with resistive plates. Although they initiated this development, they were not the ones to complete the creation of RPCs, we had to wait ten years to finally use them. Just when wired detectors with resistive cathodes were very popular, Rinaldo Santonico and Roberto Cardarelli constructed the first prototype of the actual Resistive Plate Chamber (RPC) with phenolic laminates compressed at high temperatures in Rome [1] Fig. (1.1) shows us the efficiency and time

distribution of the first RPCs.

A year after this, the Conversi group developed flash cameras and Pestov developed a special glass used as anodes. Subsequently, scientists began using Iarocci's tube as a cathode in particle detectors and thin gaps were employed in MWPCs in ATLAS experiment. Between 1986 and 1991, the SLAC-Novosibirsk collaboration utilized PSCs in physical experiments.

Within the new decade, the usage of RPCs in cosmic ray experiments became so popular that researchers began investigating and developing an optimum configuration in the gap width and separation thickness between them, and explored the use of a pure avalanche mode and double gap RPCs in High Energy Physics (HEP). However, it wasn't until 1996 that the group led by M. C. S. Williams created and tested a Multi-gap Resistive Plate Chamber with three gaps separated by 3 mm each and compared its results to a RPC of one gap of 9 mm, the multi-gap RPC showed better efficiency than the single-gap RPC [10]. In Fig. (1.2) we can observe the efficiency and dark current of the first MRPC.

The first years of the new century brought about the normalization of RPCs usage in significant experiments as ATLAS (A Toroidal LHC ApparatuS), TOF (Time Of fLIGHT) from ALICE (A Large Ion Collider Experiment), and CMS (Compact Muon Solenoid) at the LHC (Large Hadron Collider), the MONOLITH (Massive Observatory for Neutrino Oscillations or limits on their existence) project and the EEE (Extreme Energy Event) experiment. As we can see in the map of Fig. (1.3), in the EEE experiment high school students actively participate in the construction and data taking of six gap glass MRPCs which are arranged in cosmic telescopes consisting of three MRPCs each; of the 52 stations worldwide, 46 are in high schools [2].

Figure 1.3: Site map of the EEE net at the end of 2016. The red points are the High Schools who have MRPCs, while the blue points are High Schools that participate in the project but do not have a detector within its installations. (Abbrescia, 2018.)

1.2 Women in the history of the development of particle detectors

This thesis began with an analogy to women in other scientific fields who revolutionized their respective domains, but what about this one? There is limited information available about them, the names that could be retrieved from some readings include Anna Peisert, Elena Aprile, and Archana Sharma [5].

In 1983, Anna Peisert (Fig. (1.4) shows us a photograph of her in Fermilab) studied the time resolution of Parallel Plates Avalanche Chambers (PPAC), another precursor to the RPCs and MRPCs, PPACs were known for their superior rate capability compared to MWPCs. The following year she conducted a study on the drift and diffusion of electrons in gaseous detectors.

Between 1991 and 2008, Elena Aprile's research focused on the use of xenon in scintillator detectors, ionization chambers, projection chambers for gamma rays, and xenon chambers as well as the application of various gases including xenon, argon and krypton in photocathodes.

Archana Sharma worked with Micro-pattern Gaseous Detectors in 1999, she studied the first Townsend coefficient in argon mixtures, and muon tracking in gaseous detectors, she also worked with tracking detectors in the FINUDA experiment. She has been working with MRPCs since 2009.

Figure 1.4: Photo of physicist Anna Peisert with a photon detector at Fermilab.(Sauli, 2014.)

These are just three of the many women who curretly work in the field of particle physics and specifically with particle detectors. It is important to acknowledge their contributions since a significant portion of the literature in this field is authored by

men, making it difficult to find the valuable contributions of women that undeniably exist [19].

1.3 RPCs Advantages

The reasons why we are using RPCs and why they are very popular and used in multiple projects and experiments are listed below:

- Continuous operation.
- Capable of various events detection, even simultaneously.
- A good spatial resolution, and this one is even better for MRPCs, where we can get micrometer resolution.
- Easy and inexpensive to build, so they can be used to cover vast areas. That is why RPCs are used in large experiments such as ATLAS, CMS and ALICE (A Large Ion Collider Experiment), where they cover an area of 15000 m^2, and as mentioned before, they can be constructed by high school students.
- Superior time resolution, because of its planar geometry, which we will explain further in this thesis (see Section 2.1.1). And if we have a smaller width between the electrodes (gap thickness), it gets better. Simultaed time resolution is not bigger than experimental time resolution (Fig.(1.5)).

Some of the projects where MRPCs have been used are PyramidScan, Project MURAVES and DIAPHANE, that studies the insides of pyramids and volcans. MRPCs are also used in Positron Emission Tomography (PET), Thermal Neutron Detection, Homeland Security, X-Ray Imaging and Muon Tomography [4].

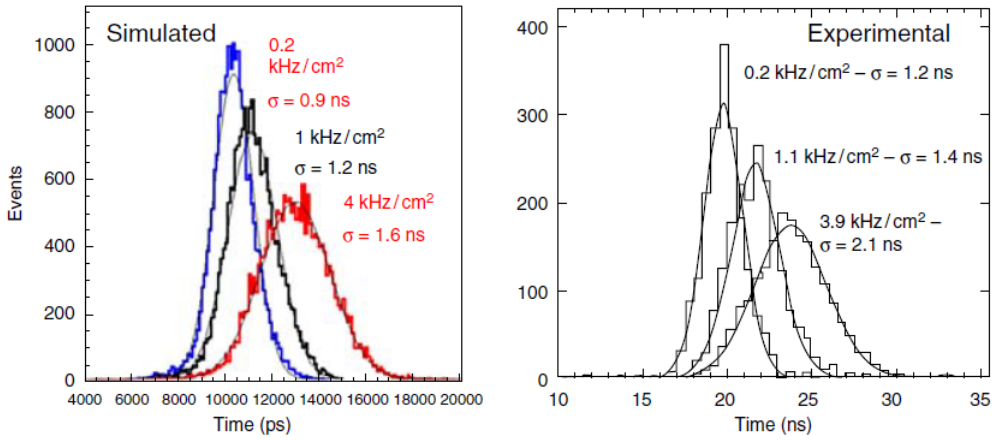

Figure 1.5: Time distribution simulations (left) and experimental time distribution results (right), for three different values of rate capacities. When the rate increases the resolution gets worse since the Effective Voltage decreases.(Abbrescia, 2018.)

Chapter 2

Physical processes and RPCs' Design

2.1 General Design

As shown in Fig (2.1), RPCs consist of two highly resistive parallel plates, a positively charged anode and a negatively charged cathode, made of Bakelite or glass. Both electrodes are connected to a High Voltage (HV) source and to ground, so that the current can circulate fluently [1].

This two plates are separated by a gas mixture volume, normally Freon (R134a) or a mixture of $C_2F_4H_2$ and SF_6, but before filling the RPC with the chosen gas, the MRPCs should be cleaned by filling them with Argon or Nitrogen gas to remove impurities that can cause chemical reactions which can speed up any aging effect as well as increase the number of noise pulses and dark current. Noise pulses and dark current, also known as background counting rate, can make it difficult to analyze the data we obtain from the detector.

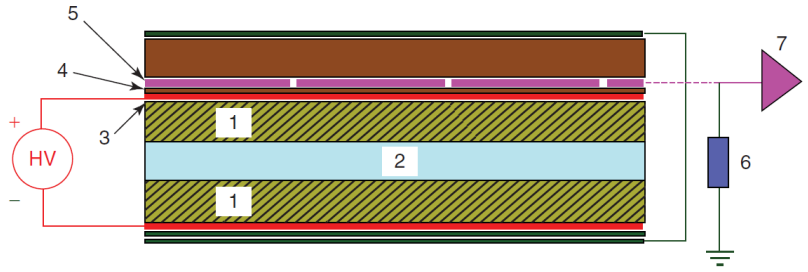

Figure 2.1: Scheme of Santonico and Cardarelli's RPC. (1) Bakelite electrodes, (2) gas gap, (3) HV connection, (4) Mylar insulator, (5) lecture strips, (6) resistor, (7) electronics used to read the signals. (Santonico *et al.*, 1981.)

In the case of MRPCs, we got separations between the plates, we call them gas gaps, and we can have any number of gaps we can physically build, this is the major difference between MRPCs and RPCs.

2.1.1 Geometry and materials

The reason behind the geometry of the RPCs is that a planar geometry give us a better time resolution, since, theoretically, its electric field is even and intense enough in all its surface, thus a primary electron can originate an avalanche instantly after being generated anywhere in the surface of the detector. Time resolution is given by

$$\sigma_t = \frac{1}{\alpha * \nu_d} \log\left(\frac{I_{thr}}{I_s}\right), \tag{2.1}$$

where $\alpha*$ is the Townsend coefficient that gives us the probability of a free electron giving us an additional pair of ion-electron per length unit, ν_d is the drift velocity, I_{thr} is the current threshold from the time where the signal crosses and I_s is the ignal current amplitude. When we consider the case for a single primary electron, with no probability of a second one, we have the following equation:

$$\sigma_t = \frac{1.28}{\alpha * \nu_d}, \tag{2.2}$$

where the constant 1.28 is obtained when the limit of the number of initiated avalanchges is zero [6]. For the MRPCs, we use

$$\sigma_t = \frac{1}{\sqrt{N_g \lambda g}} \frac{U}{\alpha * \nu_d}, \tag{2.3}$$

where N_g is the number of gaps, λ is the number of clusters per unit of length, g is the thickness of the gap and U is a factor of order 1 used for the statistical nature of the avalanche, representing the variation of the primary ionization developing into aalanches[6]. This equation give us a hint of how to improve the time resolution, it improves when we reduce the distance between the electrodes, meaning the thickness of the gas gap gets smaller.

Another important consideration towards the electrodes, goes to the materials that they are made of. When they are made of Bakelite, we apply a polymerized linseed oil layer to prevent the formation of droplets that can interact with the water vapor of the chamber and create hydrofluoric acid, which can damage the detector, and to make the surface softer (to avoid discharges and to have an uniform electric field). The electrodes are also coated with a conductive paint with graphite (for a better high voltage connection).

When the electrodes are made of glass, which has a smoother surface than Bakelite, the treatment with linseed oil for the inner surface is not necessary. The spacers (to form the gap) do not need glue to get attached to the electrodes and the high voltage contacts do not need welding. The MRPC normally uses fishing lines as spacers (being hold by plastic screws) and an envelope (it could be an aluminium box) to contain the gas, instead of a frame glued to the electrodes, thus reducing any possibility of gas leak.

2.1.2 The Development of Multiple Gaps

Multiple gaps are used precisely because they give us a better time resolution than when we only have one gap, an important factor in this thesis, than RPCs of just one gap. In this case, just the exterior plates are painted with conductive graphite paint so we can connect them to a HV source.

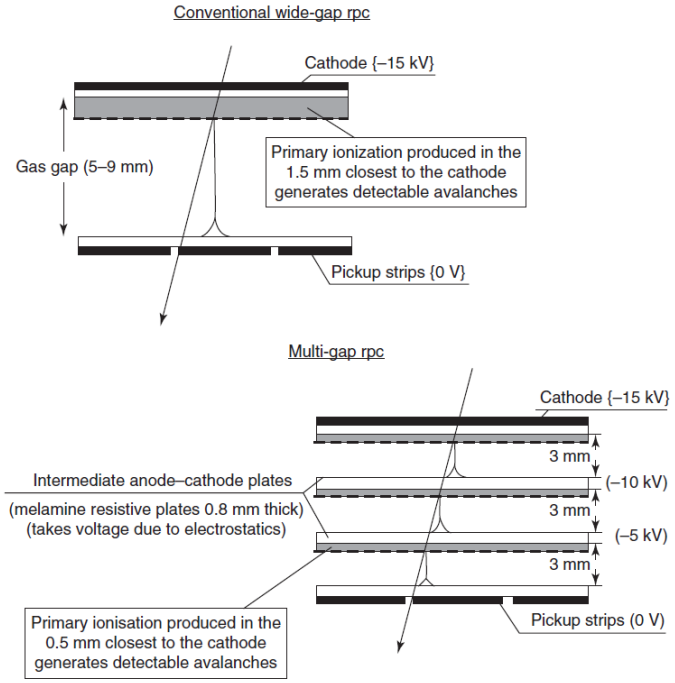

Figure 2.2: Diagram and operational principle of the first MRPC compared to a conventional RPC of 9 mm gap. (Williams *et al.*, 1996.)

We make the separations between gaps with fishing lines and screws or separators made of a non-conductive material, such as plastic or filaments used to print 3D separators to have a more accurate construction.

Characteristic	Narrow gap RPC	Wide gap RPC	First MRPC
Number of gaps	1	1	3
Size of gaps	2mm	8 mm	3 mm
Gas mixture	60% argon and 40% isobutane	60% argon and 40% isobutane	86% argon, 8.5% CO_2, 0.5% C_4F_{10} and 5% DME.
Resistivity	$10^{10} - 10^{11}\Omega$cm	$10^{10} - 10^{11}\Omega$cm	$10^{11} - 10^{13}\Omega$cm
Efficiency	100% at 19.2 kV	100% at 16.9 kV	100% from 16 to 16.5 kV
Time resolution	4 ns	7.5 ns	4 ns
Charge	9.1 pC	1.8 pC	2 pC

Table 2.1: Comparison between a narrow gap RPC, a wide gap RPC and the first MRPC ever built, the three were made of melamine phenolic foils with a detection area of 24 $\times 24 cm^2$

Fig. 2.2 shows the comparison between the 3 gap MRPC of 3 mm each created by Williams group and a conventional RPC of 9 mm gap, and how in the first one the primary ionization occurred in the 0.5 mm closer to the cathode compared to the last one where it occurred in the 1.5 mm closer to the cathode.[10] Table 2.1 shows the re-

sults between this first MRPC, a narrow gap RPC and a wide gp RPC built in 1996 by Williams group, Although the narrow gap RPC had an equal time resolution than the MRPC, the charge was higher, and even when the charge was smaller for the wide gap RPC, the time resolution was worse than the ones from the MRPC and narrow RPC, the efficiency plateau remined at 100% for various applied voltages, while for the narrow and wide RPC it was at 100% at just one applied voltage. [16]

2.2 Physical Processes of the RPCs

2.2.1 Avalanche Formation

When a charged particle enters the gas gap, it ionizes the gas molecules creating pairs of electron-ion due to its interaction as shown in Fig. (2.3). Since there is an applied electrical field between the electrodes, the ions move towards the cathode and the electrons towards the anode, inducing signals in both electrodes [6].

The electrons continue to move and if the electrical field is intense enough, they can create avalanches that end up amplifying the signals, so we can get data about the performance of our detector such as the time resolution and the rate capability. The electric field is computed by:

$$E = \frac{V}{g}, \tag{2.4}$$

where V is the applied voltage and g is the distance between two gaps. Typically, the electric field in an MRPC is on the order of a few kV/cm [15], it varies from experiment to experiment, it just needs to be strong enough to initiate and sustain the avalanche process, which has two temporal parts:

- The time when the electron avalanche reaches the anode (known as the fast signal).
- The time when the positive ions reach the cathode (known as the slow signal).

Both end up forming one signal, we will explain this in detail later on this thesis (see Section 2.3.4).

Although, positrons can also produce electron-ion pairs, they are not typically created in the avalanche process since they are not abundant in our everyday environment, nor in experimental setups, since there is more matter than anti-matter and electrons are more common and the anti-particles of positrons. When positrons appear, they do not last long since they encounter an electron, collide, and produce gamma ray positrons, that process is called positron annihilation.

2.2.2 Operational modes: Avalanche and Streamer

RPCs can operate in avalanche and streamer mode. An avalanche is the process where ionizing particles pass through a gas-filled gap, causing a chain reaction of electron multiplication. Avalanche mode is characterized by the controlled multiplication of electrons, by applying an operational voltage in the efficiency plateau of the MRPC, as they drift towards the anode, leading to a significant increase in the signal we retrieve.

The transition from avalanche to streamer occurs when the size of the avalanche gets closer or exceeds the Raether limit. Streamer mode means that the ion avalanche that

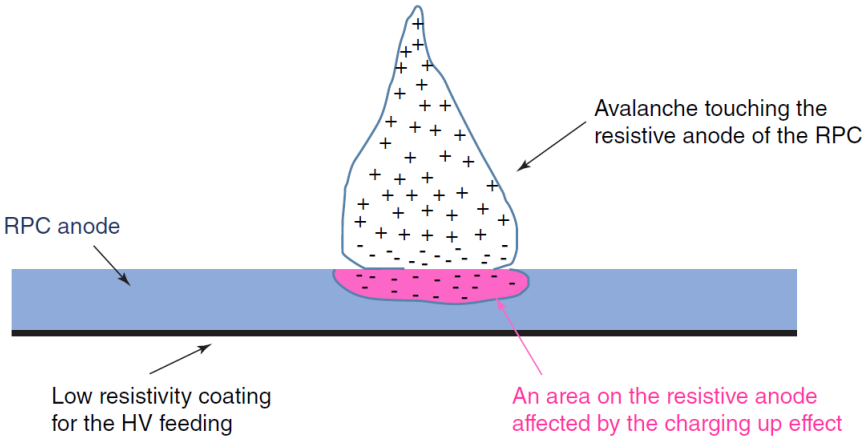

Figure 2.3: Representation of an avalanche generated by the moving electrons inside the RPC and how it creates an affected area by a local discharge in the anode. (Abbrescia, 2018.)

reaches the resistive cathode does not auto-quench, on the contrary, it causes a low current discharge, the signals we obtain from this mode are from the order of nanocoulombs, which are larger than the signals from avalanche mode, which are from the order of picocoulombs [6].

The avalanche mode was chosen in the LHC experiments and in the research for this thesis as it reduces the charge that travels through the detector thus increasing the rate capability and reducing aging effects. The development of avalanches depends on the size of the detectors, when it is small enough, we assume that the electric field depends on an external one.

2.3 Measurements and their meanings

2.3.1 Efficiency

Efficiency is a measurement of the probability of detecting a signal. We couple coincidences with the PMTs from Ecocampus BUAP, as triggers, to get the MRPCs' efficiency, meaning

$$Eff = \frac{N_c}{N_{PMTs}}, \tag{2.5}$$

where N_{PMTs} is the number of signals measured between just the PMTs, and N_c is the number of coincidences between the three detectors, including the MRPC [11].

2.3.2 Rate Capability

Rate capability is the ability of the detector to stay efficient (up to 95%) even when exposed to a high flux of incident particles. This can be improved by reducing the thickness of the gas gap or the resistivity of the electrodes. Currently CMS and ATLAS RPCs have a rate capability of 2 kHz/cm^2, but since 1995, there is experimental evidence of MRPCs having a rate capability around 1 kHz/cm^2 [6]. MRPCs are known to have a stable rate capability for several years even in harsh environments such as the

ones at GIF (Gamma Irradiation Facilitiy) at CERN.

Normally, and if we had a variable source of impinging particles, we would estimate the rate capability of the detector by operating it at the voltage, that we would keep constant, where the efficiency is in the plateau, wich means a constant maximum efficiency, we would increase the flux of particles until the efficiency decreases and is lower than 90% [9]. But as we do not have such technology, we use cosmic rays and a counter, we increase the applied voltage and save the number of impinged particles every two minutes in each strip.

2.3.3 Fast Signals to Total Signals Ratio

A fast signal is related to the electron avalanche mentioned in Section 2.1.1, and usually it is registered with an appropriate current amplifier. This fast signal is only 5 to 20% of the total charge signal. The slow one is induced by the positive ion avalanche towards the cathode, to measure it we use Photo-Multiplier Tubes (PMTs) as triggers, then we will couple coincidences with an oscilloscope and a digitizer.

The total signal is the analogue sum of the fast and the slow partof the signal. Just like in Fig. (2.4), what we see in a digitizer or an oscilloscope is the fast signal, we only use it since the slow one is hundreds of times slower than the fast one [9].

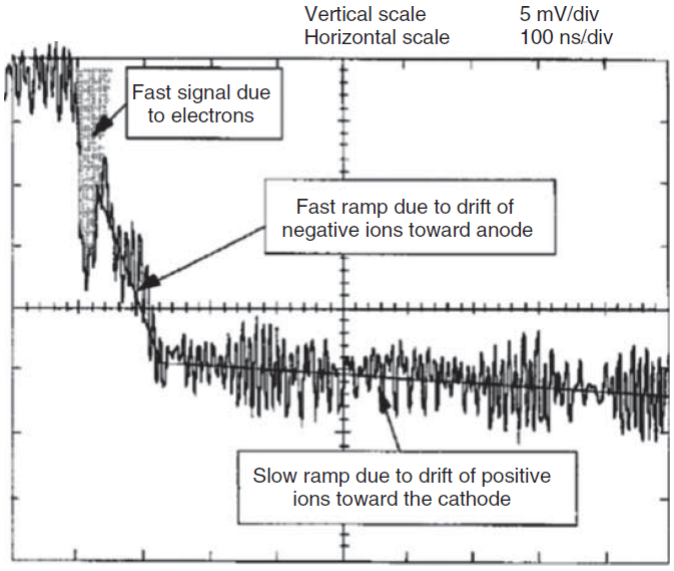

Figure 2.4: Voltage (mV/div) vs. Time (ns/div) showing an avalanche signal, the first part is due the movement of electrons, the fast ramp is due the movement of negative ions and the slow ramp is due the drift of positive ions. (Cerron Zeballos *et al.*, 1997)

2.3.4 Total Charge in Avalanche Mode

The electric charge depends on the position where the avlanche is formed

$$q(x) = \sum_{j=1}^{n_{cl}} q_e n_0^j M_j e^{\alpha^*(x-x_0^j)}, \tag{2.6}$$

where n_0^j is the the number of the primary electrons contained in the j-th cluster, group of particles prouced by an avalanche, q_e is the charge of the electron, M_j is used to take into consideration the stochastic fluctuationof the avalanches, $\alpha^* = \alpha - \eta$ is the first effective coefficient of Townsend, which depends on the Townsend coefficient and the attachment coefficient

$$dn_e = (\alpha - \eta) n_e dx, \tag{2.7}$$

and it also depends on the time

$$q(t) = \sum_{j=1}^{n_{cl}} q_e n_0^j M_j e^{\alpha^* \nu_d t} = q_e e^{\alpha^* \nu_d t} \sum_{j=1}^{n_{cl}} n_0^j M_j, \tag{2.8}$$

where we use the fact that the length covered by the electrons after $t = 0$ is proportional to the module of the drift velocity of the electrons, $x = \nu_d \cdot t$, with a time range between $0 < t \leq \frac{g - x_0^{n_{cl}}}{\nu_d}$ [6].

2.3.5 Time resolution

Time resolution is the time interval measured between two particles crossing the detector. It can be expressed in terms of its full width at half maximum (FWHM), or in terms of the standard deviation:

$$\sigma_t = \sqrt{\frac{\sigma_{PuM}^2 + \sigma_{PdM}^2 - \sigma_{PTMs}^2}{2}}, \tag{2.9}$$

where σ_{PuM}^2 is the standard deviation between the PMT up and the MRPC, σ_{PdM}^2 is the one between the PMT down and the MRPC and σ_{PTMs}^2 is the standard deviation between both PMTs [12]. This is the equation we will be using in the data analysis because of the experimental setup, which is a type of arrangement made to obtain coincidences between the detectors.

Errors are calculated by

$$ERR = \frac{\sqrt{err_2^2 + err_3^2 - err_1^2}}{2} \tag{2.10}$$

where err_1 is the error associated to the time resolution between the triggers, PMT UP and PMT DOWN, err_2 is the error associated between the MRPC and the PMT UP, and err_3 is the error associated between the MRPC and the PMT DOWN. The type of error we are talking about is a parameter error, it is a measure of the uncertainty associated with the estimation of a parameter, in this case for time resolution, in a mathematical model or data analysis. These parameters are stimated from the data the program in c++, made by a master student from FCFM-BUAP, is working with.

Chapter 3

Experimental Setup

3.1 Aluminium Box Construction

We constructed two aluminium boxes ($0.4m \times 0.272m \times 0.05m$), shown in Fig (3.1), to contain the MRPCs and the gas that would flow through them. We used the milling machine CNC-3040Z-DQ with an end mill of 2mm from Ecocampus BUAP and the program Aspire 9.5 to design and generate a code for the machine to work. To put all the pieces together we used several screws and white silicone, and to prevent sparks a layer of Kapton tape was attached in the upper and bottom lids of the box.

Figure 3.1: Aluminium box with a layer of kapton tape, Each one has a volume of $5.44 \times 10^{-3} m^2$.

The disadvantage of this type of boxes is that they consumes an unnecessary amount of gas, since it should fill all the box as shown in Fig (3.2a). Another option, which is used at Ecocampus, is the making of acrylic boxes that inject the gas directly in the detector area, they are similar to Fig (3.2b) and we can see one of those acrylic boxes in Fig. (3.20).

To avoid gas leaks on the aluminium box we used heat on the plastic tubes as well as white silicone, to seal it properly. For the HV connectors we made an extra parts, a 5 cm aluminium square, so the protected wiires are not in contact with the PCB (Printed Circuit Boards) and the aluminium box could have more physical stability.

One of the MRPCs has an acrylic lid so students can see the insides of the chamber. To make sure there was no gas leak, we let air flow through the closed boxes, not freon or argon since they are expensive, while we closed momentarily the plastic tubes, and used a lighter to see if the flame moved, and if that was the case we sealed that part with more white silicone.

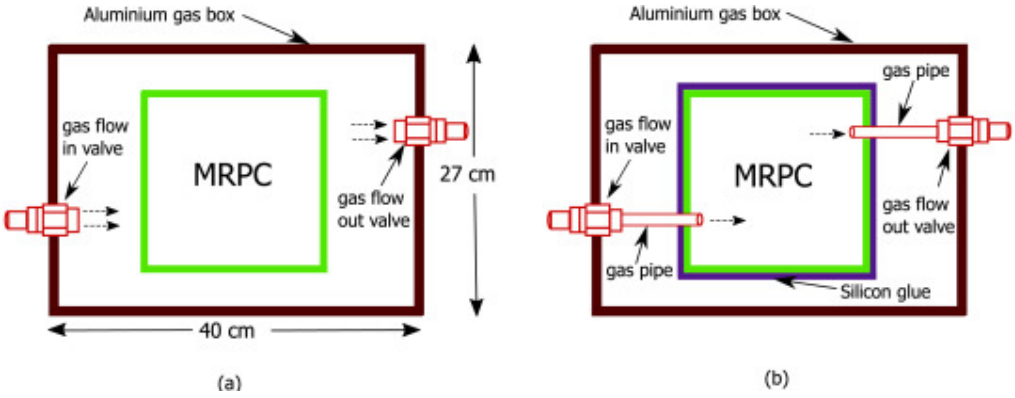

Figure 3.2: Diagram of both types of boxes. (Liu *et al.*, 2019.)

3.2 CERN MRPC features

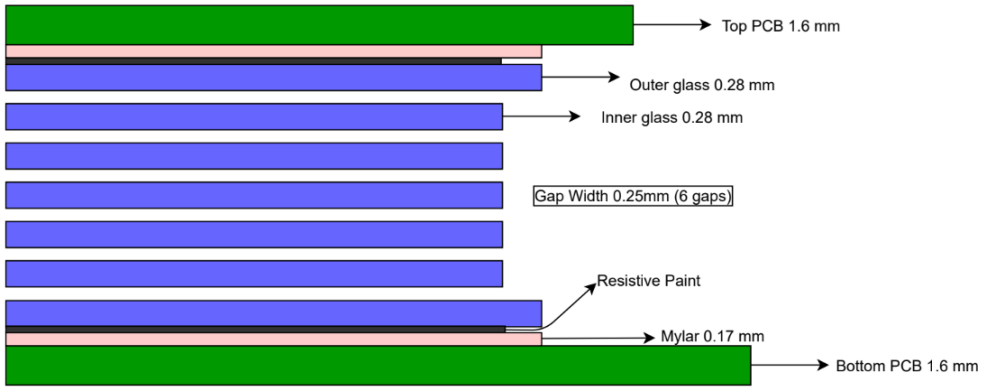

Figure 3.3: CERN MRPCs' geometry.

As shown in Fig. (3.3), the two MRPCs built at CERN have six gas gaps (0.25 mm gap width) and a 0.28 mm glass thickness. The area of the two outer glass is slightly larger than the inner glass ($22 \times 22 cm^2$ vs $18 \times 18 cm^2$). The MRPC have 24 lecture strips and was supposed to use a gas mixture of $C_2F_4H_2$ (98%) and SF_6 (2%), but we ended using just Freon since we do not have yet a gas mixer. For electric continuity to acquire the

signals we had to weld the pins between the Top and Bottom PCBs.

From Fig. (3.4), we can observe that the MRPCs have two cables, the upper was the one we connected to positive voltage while the one below was for the negative one, so the electric field could exist.

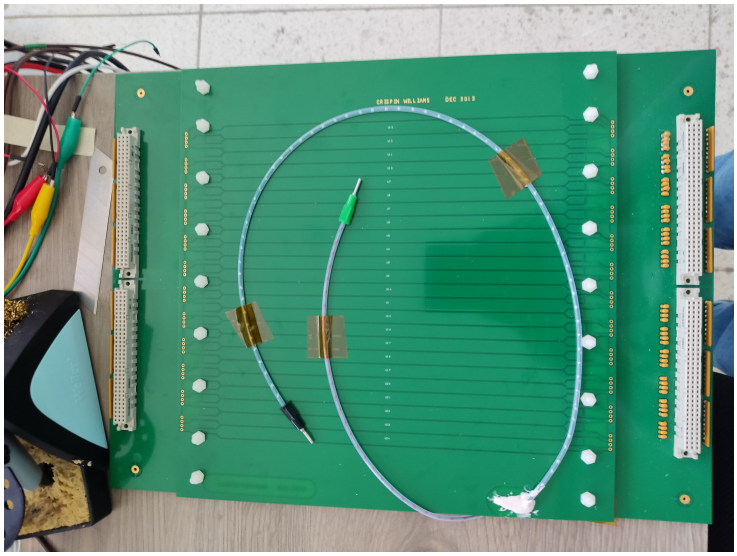

Figure 3.4: Upper view of CERN MRPC.

From side to side we could appreciate the six gaps and seven glasses (Fig. (3.5), where the first and last one are larger than the middle ones.

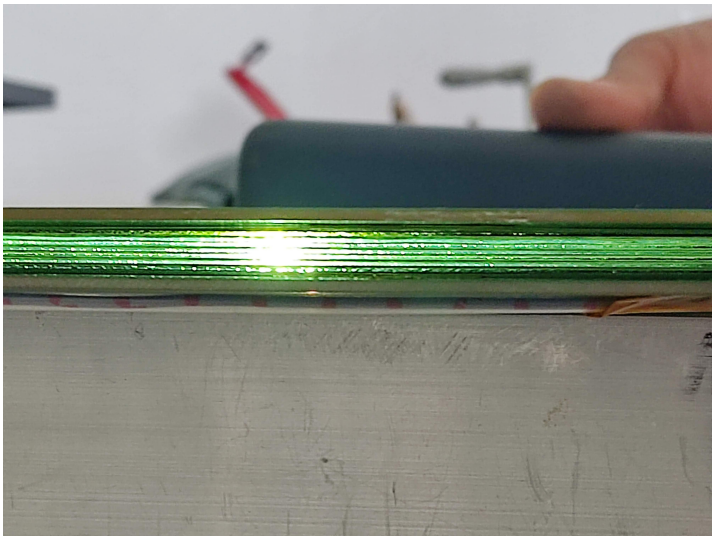

Figure 3.5: Lateral side of the MRPC.

In Fig. (3.6) the MRPC inside the aluminium boxes we built. We can see not just where we connected the cables but the tubes to fill the chamber with Freon gas.

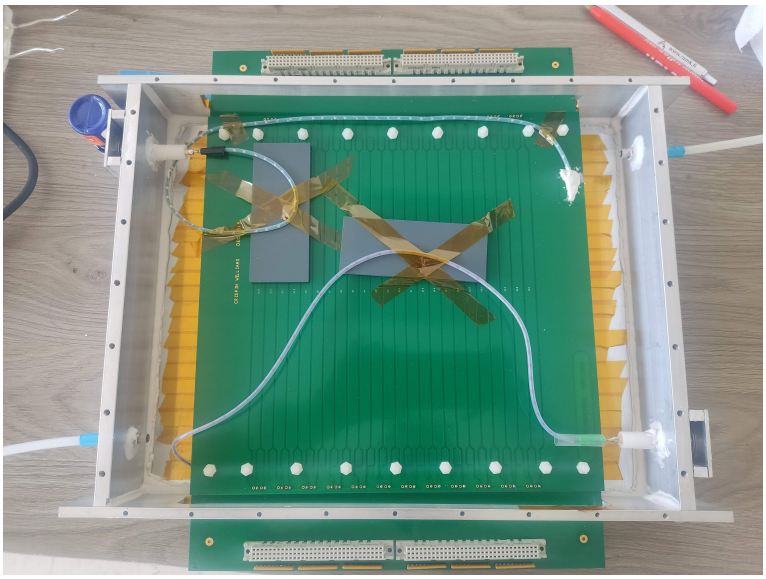

Figure 3.6: MRPC inside the aluminium chamber.

The strip maping (Fig. (3.7)) was much more complicated due to the interconnected pines between both PCBs, there were 48 possible signals, we only connected 24 for each detector, naming the strips by letters. and ended up using only 12 strips named A, C, E, G, I, K, M, O, Q, S, U and W. We divided them in 4 sections, the first one was A-C-E, the second one -I-K, the third one was M-O-Q, and the fourth one was S-U-W.

Figure 3.7: Strips arrangement of the CERN MRPCs.

3.3 High Voltage Converters

We used two different types of DC-HVDC Converters, models Q101-5R, for the positive ones (Fig. (3.8)), and Q101N-5R, for the negative ones (Fig. (3.9)), three electric resistances of 1 MΩ and one of 1 GΩ.

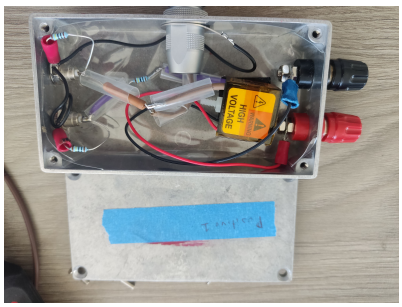

Figure 3.8: Positive HV converter.

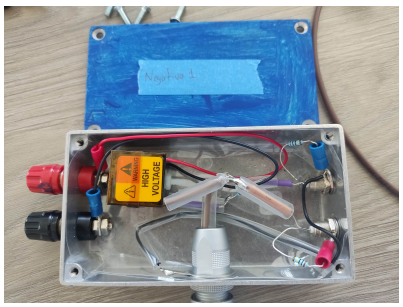

Figure 3.9: Negative HV converter.

The electric diagram (Fig. (3.10))is the same for both types of converters, and the input voltage increases two thousand times per volt in the output voltage. However, three of these converters do not work anymore. We suspect that they unweld internally due to the heat produced by the voltage.

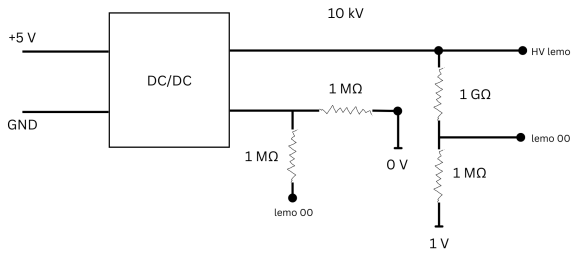

Figure 3.10: Electric diagram of the HV Converters.

However the experimental results (Fig. (3.11)) that we obtained from the negative converter were consistent with the theoretical ones from its data sheet (Fig. (3.12)), the only difference is that it is expressed in percentages. We show the lineal conversion of one of the negative HV boxes, but as they no longer worked, we constructed some wires using the HV lemos and the wires for the HV source.

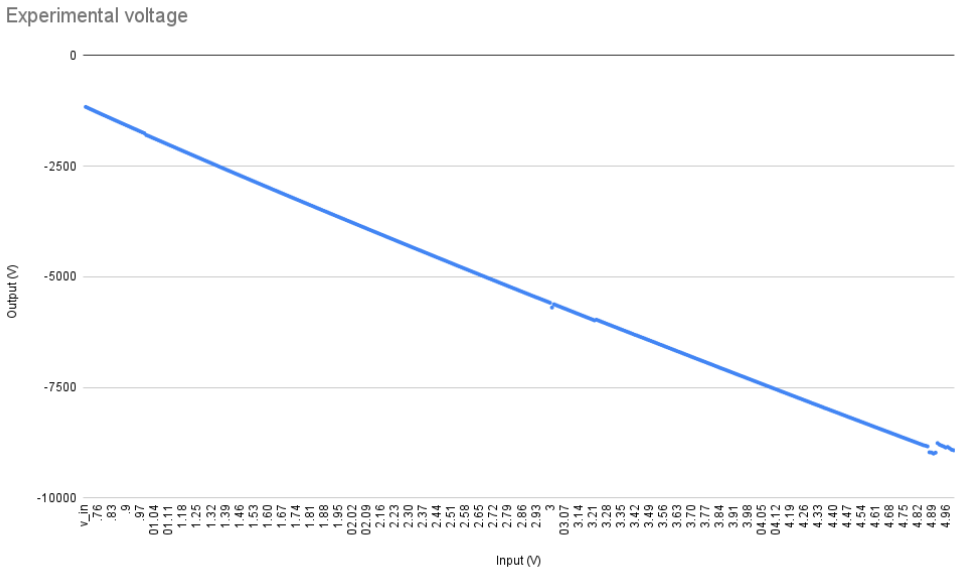

Figure 3.11: Experimental results of one of the HV converters, plotting the input vs. output voltage.

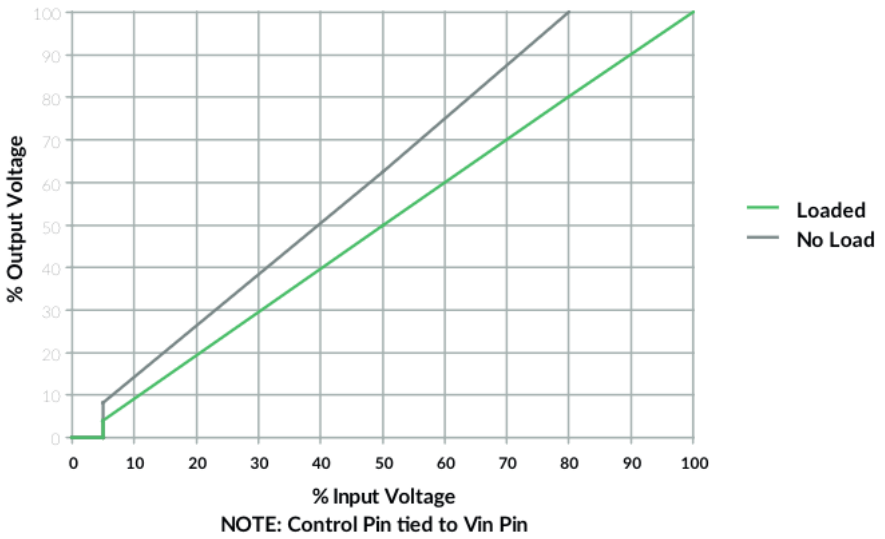

Figure 3.12: Typical output vs. input voltage of the DC-HV converters from the manufacturer's data sheet.

3.4 Instrumentation

We used several instruments to acquire, clean and translate the data, all of them were in a rack, as shown in Fig. (3.13).

1. Fan-in-fan-out (CAEN V925): It has four sections, each one produces the sum of the signals we put on to the inputs on the output connectors. We use it since we need two signals, one to construct the trigger with the PMTs and the other one for the digitizer to save.

2. Amplifier (CAEN V974 and V975): V974 has four channels, it increases the amplitude of a signal, negative or positive, from 1 to 10 times. V975 has eight channels, it increases the amplitude of a signal, positive or negative, 10 times. If we need to amplify the amplitude of signals we see on the oscilloscope or computer. We can directly connect the RPC to the amplifiers, because we do not need two outputs, although both models have one input and two outputs per section.

3. Discriminator (LeCroy 621L): It has four sections, it has a good impedance match which allows it to eliminate reflections and multiple-pulsing, it can help with possible phototube malfunctions. We use it to retrieve the signals from each PMT and convert them to TTL (Transistor-Transistor Logic) signals.

4. Quad Coincidence (LeCroy 622): It has four sections, each one can apply an AND/OR logical functions to the two inputs creating one output signal. It is used in coincidence applications with LeCroy 62IL with an AND logical function for the two input signals from the two PMTs to obtain the trigger output signal.

5. Translator (CAEN V976): It has four sections, 16 inputs and 16 outputs, each one operates as a TTL to NIM (Nuclear Instrumentation Module) signal conversor or viceversa, or with logic functions AND/OR. We use it to change the TTL signal to a NIM signal because the program made by other master students from BUAP reconstruct these NIM signals.

6. Digitizer (CAEN DT542B): A digitizer converts the analog data into digital one. With this digitizer we obtain information about the time resolution and charge from the particles that crosses our detectors so we can store it in the computer and reconstruct the signals.

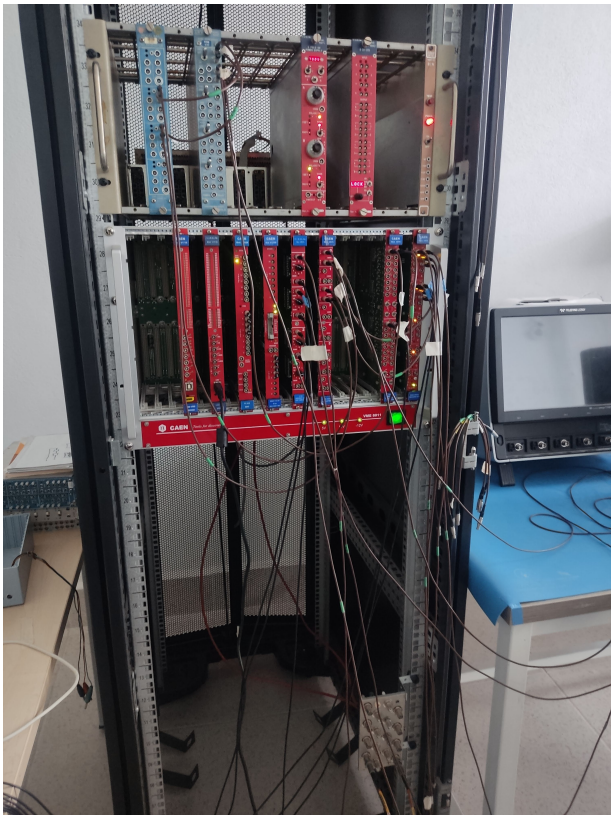

Figure 3.13: Rack with multiple instruments to acquire, clean and translate data from detectors. Above, from left to right, the first blue item is LeCroy 621L, then LeCroy 622, then a 2 fold HV power supply, then CAEN N842 (we do not use these last two). Below, from left to right, CAEN V1718 (we do not use it), then CAEN V974, V975, V976 and V925.

We also used four PMTs, two had an hexagonal plastic scintillator (Fig. (3.14) and (3.15)) with an area of $41.56cm^2$ each, we will call them hexagonal PMT up and hexagonal PMT down through all the thesis. The other two had a square plastic scintillator with an area of $121cm^2$ each, we are going to refer to them as Square PMT up and Square PMT down too.

These PMTs are used to couple coincidences, through the quad coincidence device, in other words, the simultaneous detection of two or more particles that crosses the area of the PMTs, to do that, we place one the plastic scintillator are above the other one with the photomultiplication tubes at different angles so we have less interference. The MRPC is placed between the PMTs, so when a particle crosses the area of the three detectors (the MRPC an the two PMTs) we can save the electric signals, reconstruct and analyse them.

Figure 3.14: PMT up.

Figure 3.15: PMT down.

3.5 Setup of CERN MRPCs

We used three different setups for the MRPCs, two for the MRPC from CERN and one for the ALICE-BUAP MRPC. For the CERN MRPC Fig. (3.16) shows the first one consisted in putting the MRPC between two PMTs (up and down) with scintillator plastics, besides these two there was a SiPM above the MRPC, since another student was taking data with that detector too and it didn't interfere with our data acquisition. We went strip by strip, moving the PMTs and SiPM along the way coordinately.

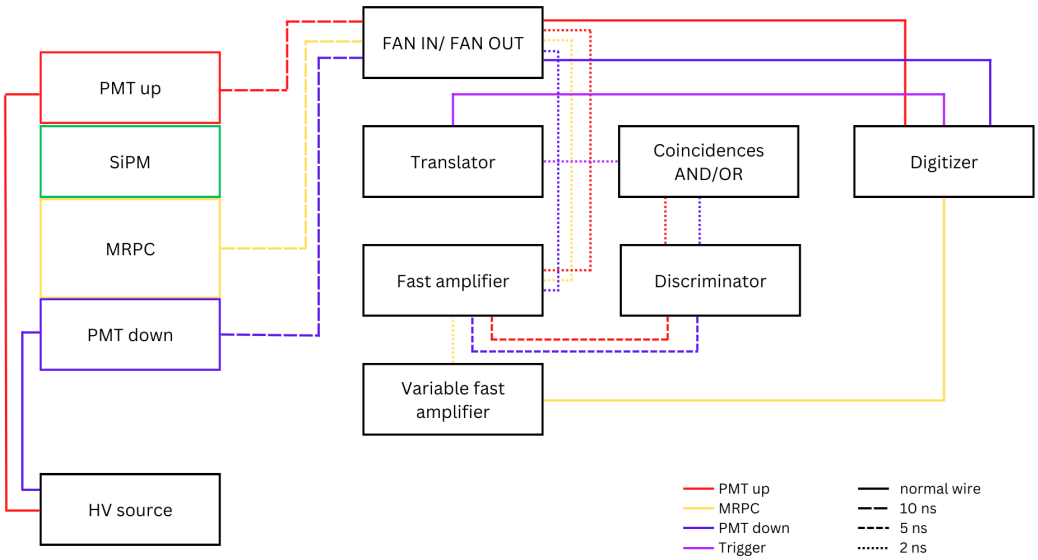

Figure 3.16: First experimental setup to acquire data for the CERN MRPC.

The plastic scintillators of the PMTs were hexagonal, as we can see in Fig. (3.17), we

used a box so the weight of the MRPC would not pressure the PMT down, and because it was a little too far from the MRPC's surface, we put the PMT down above a wooden bar. The photo multiplier tube was heavier than the plastic scintillator, so we used a plastic box in a way the PMT would not move while acquiring the data.

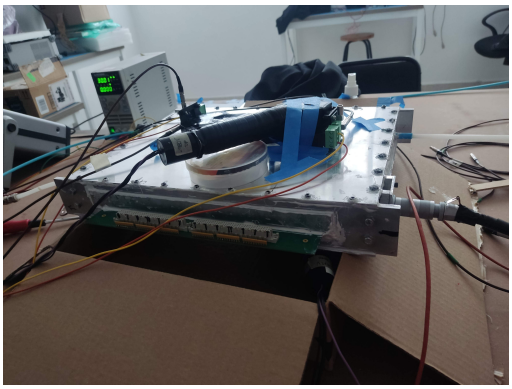

Figure 3.17: First setup for the CERN MRPC.

The MRPC was connected to a Power supply CAEN DT1471ET, channels 2, for the positive voltage, and channel 3, for the negative one, since the PMT up was connected to channel 0 at 979 V and PMT down to channel 1 at 983 V. Freon gas was applied to the aluminium box with a rate of 1 bubble per second.

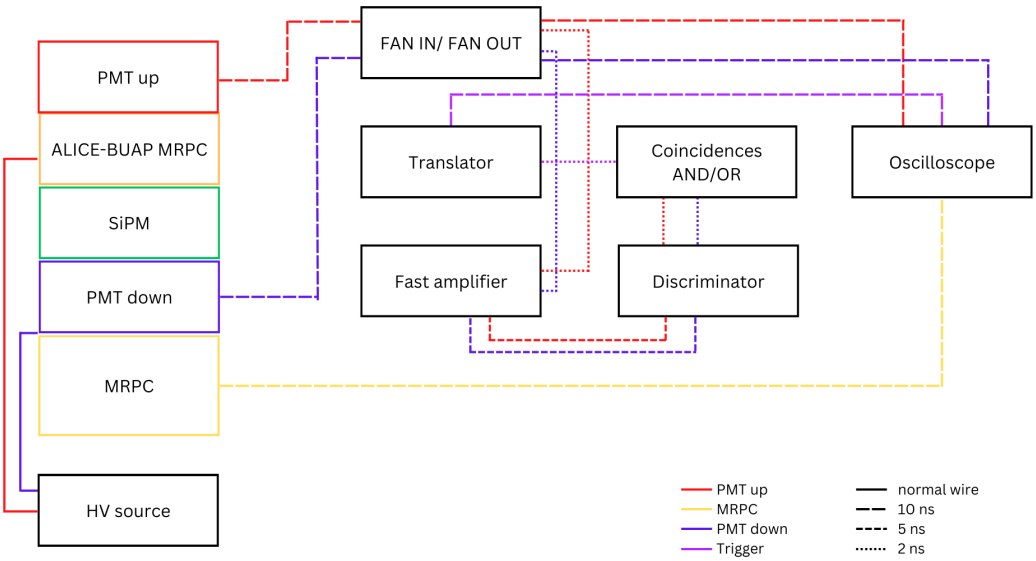

Figure 3.18: Second experimental setup to acquire data from the CERN MRPC.

The strip was connected to the input of a variable fast amplifier CAEN V974, to amplify the signal 10 times, to easily observe the signal and choose a range to consider it either a signal or just noise, and then the output went to the digitizer. We used wires with different lenghts, the longer ones were of 10 ns, the shorter ones were of 2 ns, that is

the time it takes for the signal to travel from one end to another, we tried to make the traveling as fast as it could be physically possible since some instruments were farther away from the others.

For the second setup, other students were taking data too, so the arrangement had a bigger height than the first one. As we can see in Fig. (3.19) and (3.18), there was a square PMT Up, then a BUAP MRPC, then a SiPM, then another square PMT Down and finally our MRPC. The gas filled both MRPCs, but every type of detector used a different voltage source. We used an oscilloscope to save the data and analyze it later on.

Figure 3.19: Second setup for the CERN MRPC.

The voltages for the PMTs are the operating voltages recommended by the peers from Ecocampus BUAP, the applied voltage for the MRPC was chosen since some papers operate similar MRPCs at those voltages.

- The PMT up has an applied voltage of 979 V, connected to the oscilloscope's third channel.
- The PMT down has an applied voltage of 974 V, connected to the oscilloscope's fourth channel.
- The MRPC has an applied voltage of 12, 12.8, 13.4, 14, 14.3, 14.6 and 15 kV for the strips G and I, connected to the channels 1 and 2 of the oscilloscope, although we used only the 14 to 15 kV because we had too little coincidences for lower voltages since it was more difficult to align the PMTs with a lot of detectors between them and the MRPCs actually working better above 14.3 kV. [11, 13, 14]

We used two different setups, shown in Fig. (3.16) and (3.18), because other students and researchers needed to work too, and we had to adapt our experimental setup to theirs, we used the oscilloscope since we do not have enough wires that the digitizer needed.

3.6 ALICE-BUAP MRPC features

Figure 3.20: ALICE-BUAP MRPC's interior.

Originally we were supposed to work with a four pad MRPC shiwn in Fig. (3.20), but one of the pads was damaged because of humidity, and the first attempt was to change said MRPC for a similar one, so we opened it, it had a foamy sheet above a cooper sheet so there would not be any conduction between the cooper sheet and the aluminium upper lid. Below the cooper sheet there was an acrylic box similar to the scheme in Fig. (3.2), the electronic connections could be seen and the tubes for the gas too.

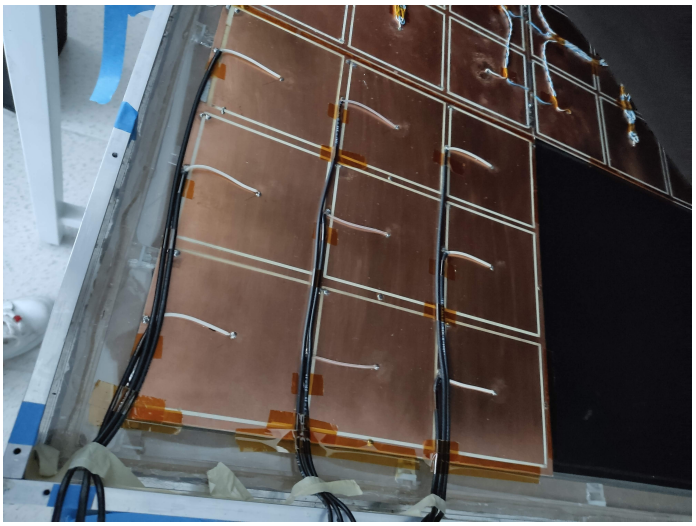

Figure 3.21: Cooper sheet of the ALICE-BUAP MRPC used.

The MRPC we put inside had a lot of noisy signals so we ended up using the big MRPC built by PhD. Guillermo Tejeda, MSc. Emigdio Jimenez and students from FCFM-BUAP, with pads of $9 \times 9\text{cm}^2$. The pads were connected to the cooper sheet as Fig. (3.21) shows.

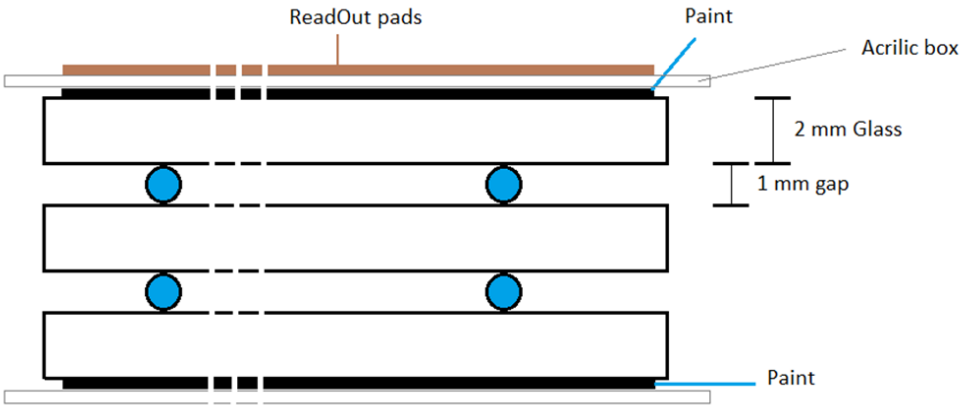

Figure 3.22: MRPCs design from ALICE-BUAP.

Fig. (3.22) shows the MRPC from BUAP, which has two gaps of 1 mm, it is made of glass of 2 mm width. The total are is of 90 cm $\times$ 120 cm and it is divided in 64 pads, but we just used an area of 27 cm $\times$ 18 cm, meaning 6 pads originally but we had less data for pad 5, so we did not consider it, and we had to start working with the MRPC from CERN.. ALICE-BUAP MRPC operates with Freon gas and has a resistivity of 3 $M\Omega \times cm$.

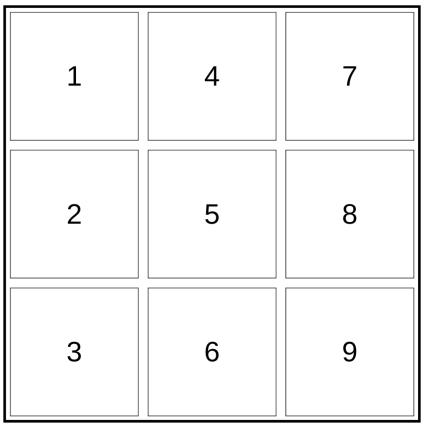

Figure 3.23: Scheme of the pad arrangement of the ALICE-BUAP MRPC.

The pad mapping of this detector is divided in 9 parts of 10 cm^2, as shown in Fig. (3.23). We only worked with pads from 1 to 6; when we observed the signals from pads 7, 8 and 9 with the oscilloscope, we mainly observed noise and very few signals.

3.7 Setup of ALICE-BUAP MRPC

For the setup shown in Fig. (3.24), we used two hexagonal plastic scintillators attached to PMTs, one named PMT up (Fig. (3.14)), and the other named PMT down (Fig. (3.15)) since they go on top and bottom of the MRPC. The PMTs are wired to an amplifier where they connect to the discriminator model 621L and a Quad Coincidence model 622C then to a Quad And/Or model CAEN V976 and then to the trigger entry from the digitizer.

The PMTs were connected to a different voltage source and the gas (Freon) filled all the volume of the MRPC, not only the five pads we were analyzed. The MRPC's pad was connected to the FAN IN/FAN OUT and then amplified 100 times, 10 times with a fast amplifier and then 10 times more with a variable fast amplifier that is then connected with the digitizer so we can acquiere data. It was amplified that much because the signal was small, amplifying it helped us to observe the signal better and chose the range where we could consider it a signal and not noise.

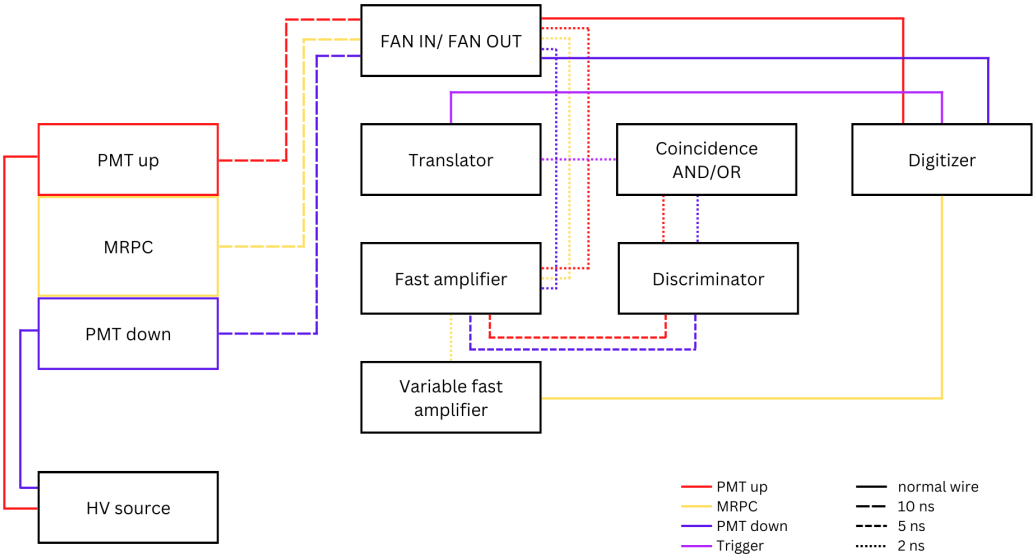

Figure 3.24: Experimental setup to acquire data for the ALICE-BUAP MRPC.

The voltages for each detector and channel entries of the digitizer are the following:

- The PMT up has an applied voltage of 979 V, connected to the digitizer second entry, channel one.
- The PMT down has an applied voltage of 974 V, connected to the digitizer third entry, channel two.
- The RPC has an applied voltage of 11 kV, 11.5 kV and 12 kV for each of the six pads, connected to the digitizer first entry, channel zero. These voltages are the efficiency plateau of the MRPC from ALICE-BUAP.

3.8 Area of the detectors

A strip of the CERN MRPCs has an area of 9.8 cm^2, a pad of the ALICE-BUAP MRPC has an area of 81 cm^2, while the hexagonal PMTs have an area of 41.56 cm^2 each, and squared PMTs have an area of 121 cm^2 each.

For the data analysis of the MRPCs, we used a division factor to consider the actual area where we are detecting particles

$$\text{division factor} = \frac{\text{area of the strip or pad}}{\text{area of the plastic scintillator of the PMT}}, \tag{3.1}$$

so we could compute a new efficiency per area we compute with

$$Eff' = \frac{Eff}{\text{division factor}}, \tag{3.2}$$

and finally a normalized efficiency per area, so we could match the efficiency in a scale from 0 to 100,

$$\text{Normalized Eff} = \frac{(Eff' - \text{min Eff}) \times 100}{\text{max Eff}}, \tag{3.3}$$

where min Eff and max Eff are the minimum and maximun, respectiely, from all of the efficiencies from each trial with a certain voltage at a certain strip or pad.

For the ALICE-BUAP MRPC, where we used the hexagonal PMTs, the division factor iss 1.94. For the first run of the CERN MRPC the factor is 0.23 since we used the hexagonal PMT, and for the second run the factor is 0.089 since we used the squared PMT. Figures (3.25) and (3.26) shows the difference in area between all the detectors.

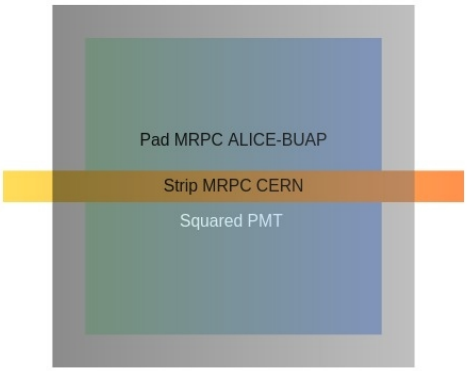

Figure 3.25: MRPC's strip and pad compared to the squared PMT.

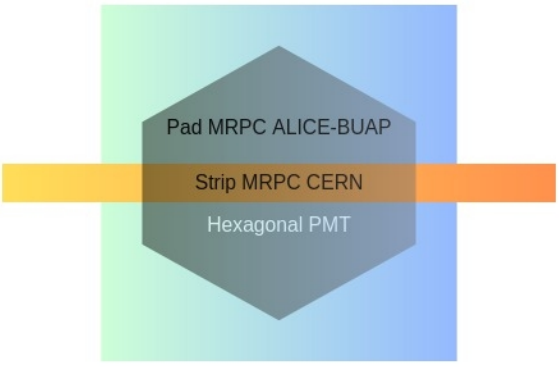

Figure 3.26: MRPC's strip and pad compared to the hexagonal PMT.

3.9 Data acquisition and analysis

3.9.1 Data acquisition process

To acquire the data we used a rack with different instruments so we could create the trigger making the PMTs coincidence putting one above the other with diferent angles, and in some cases amplify the signal if necessary we couple the PMTs with the quad

coincidence instrument, LeCroy 622 with an AND logical function obtaining an output trigger signal. We used the digitizer from Fig. (3.27) and the oscilloscope from Fig. (3.28) to observe and save the signals that we analysed later on in different setups, because we did not have enough wires for the digitizer since several students and researchers needed to work with the digitizer, so we used the oscilloscope to acquire the data.

Figure 3.27: Digitizer CAEN DT5742B.

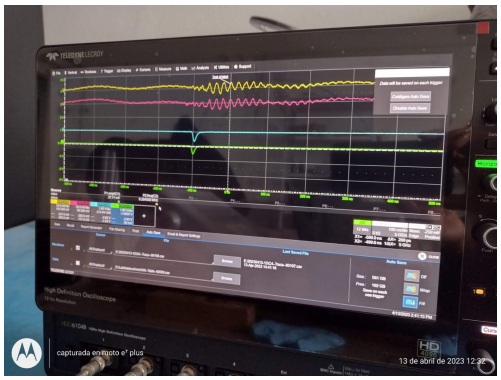

Figure 3.28: Oscilloscope TELEDYNE LECROY HDO6104B.

With the oscilloscope we retrieved signals like the ones shown in Fig. (3.28), where the blue and green signals were the ones for the PMT up and down respectively, the pink and yellow lines were the ones we were using for two strips of the CERN MRPC, it showed sporadic signals so taking a photo of the signals was rather difficult. In the other hand, with the digitizer we registered signals like the one in Fig. (3.29), where every channel was for a different detector, in this case, the blue and green one were for the hexagonal PMTs and the red one was for the ALICE-BUAP MRPC.

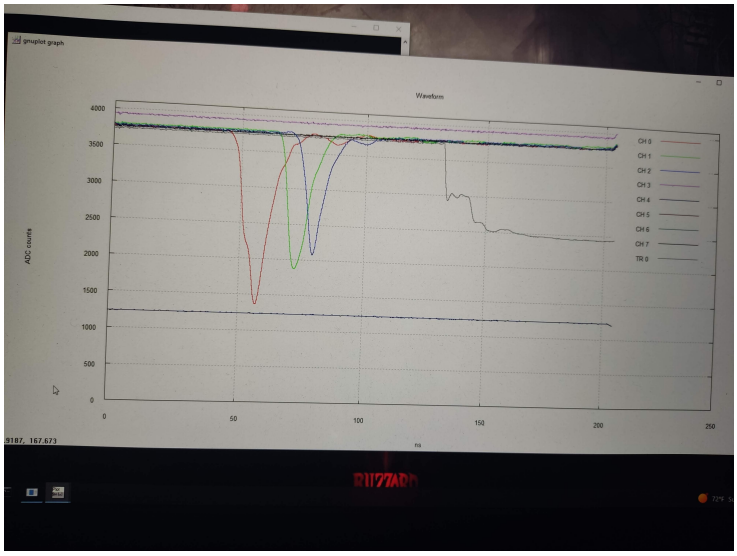

Figure 3.29: A signal from the digitizer.

For the oscilloscope, Fig. (3.30) and (3.31) show the signals we could observe while operating both MRPCs. In this case, the oscilloscope's model was TELEDYNE LECROY Wave Pro 715Zi-A. For Fig. (3.30) the scale was of 20 mV/div and 50 ns/div, for Fig. (3.31) it was of 10 mV/div and 50 ns/div, all of the signals of the MRPC from CERN were more noisy and smaller than the ones from ALICE-BUAP MRPC.

Figure 3.30: ALICE-BUAP MRPC's signal.

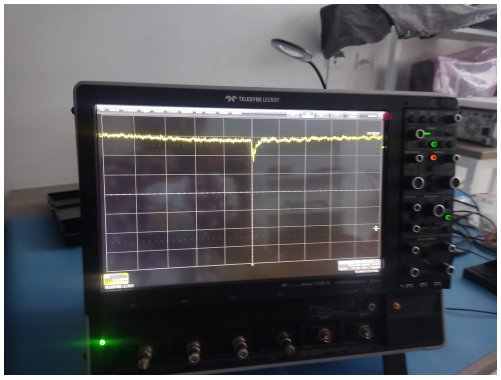

Figure 3.31: CERN MRPC's signal.

3.9.2 Data analysis

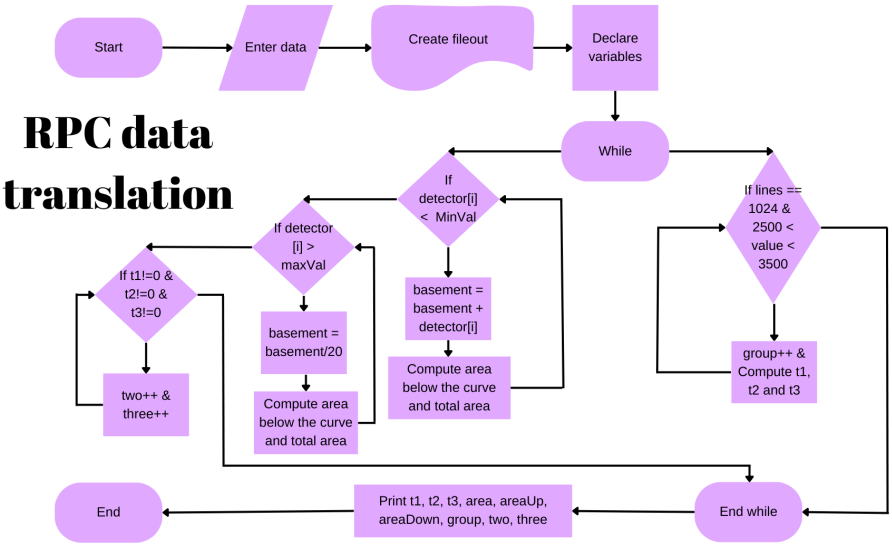

Figure 3.32: Flux diagram of the process between the data acquisition with the digitizer and the translation of said binary data to plot the histograms of time resolution and charge.

Once we collected the data from the signals stored, we proceeded to reconstruct the data so we could plot, the flux diagram in Fig. (3.32) allows us to understand the procedure. The program uses limits to know whether it was a signal or just noise, for a MRPC signal we considered signals in the range from 3500 and 3000 ADC counts for the CERN

MRPC and between 3500 and 2500 ADC counts for the ALICE-BUAP mrpc; for the PMTs, the signals we considered were the ones in the range between 3500 and 2500 ADC counts, with that information we obtain the time for the coincidences between the three detectors and the are above and below the curve for the cgharge; the program also accumulates the number of total signals and coincidences between the two PMTs and the three detectors, so it can save these numbers in columns in a file we can name.

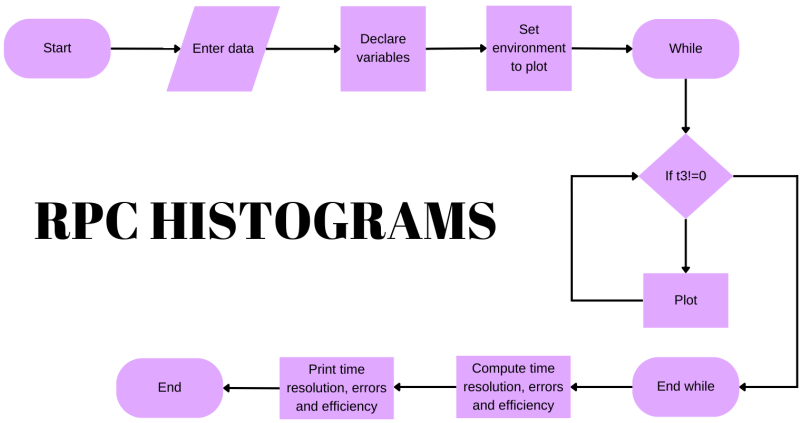

Figure 3.33: Flux diagram for the plotting of the data in histograms.

We use the file we obtain from the first program to plot histograms of time and charge, and with this data we can compute and print the time resolution, the parameter errors associated to the time resolution, and the efficiency of the detector with equations (2.9), (2.10) and (2.5) respectively as shown in Fig. (3.33).

Chapter 4

Results

4.1 Gas consumption

As we worked with gaseous detectors, the use of different kinds of gases and their impact it is very important. As scientists we try to do the less harm to Earth when we perform our experiments, however Freon and similar gases used in MRPCs are polluting agents that can damage the ozone layer [17]. In Ecocaampus BUAP, that is the only gs we have to operate the MRPCs, that is why we try to regulate our usage of the gas through the containers in Fig. (4.1).

In order to check for gas leaks, we injected air in the MRPCs, using a thank of compressed air. Every time we found a leak, we sealed the aluminium boxes using white silicone. Once we were sure the aluminium boxes were completely sealed, we cleaned the MRPCs flowing argon gas through each aluminiium box for three days.

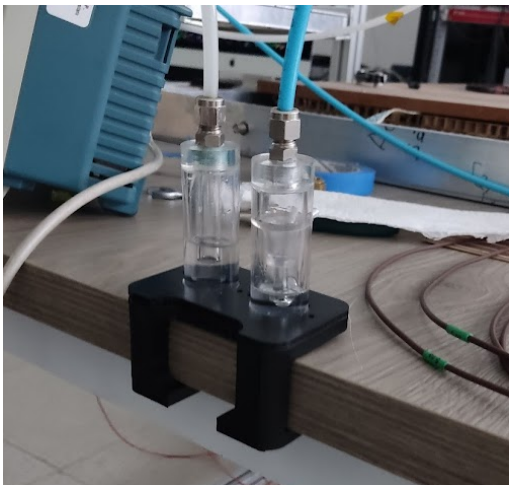

Figure 4.1: Acrylic containers to observe the gas consumption of the detectors.

To guarantee the continuity of the gas, for each pad or strip at different voltages, we used an arrangement of tubes and acrylic containers, which contained glycerin, where we could physically see that there was a bubble per second of gas consumption.

4.2 CERN MRPC's Results

We have two MRPCs from CERN built by the group of M.C.S. Williams, we will call them MRPC1 and MRPC2. We obtained the resistivity and rate capability of the both MRPCs, but due to an accident on the MRPC1, we obtained the efficiency, charge and time resolution of strips G and I of the MRPC2 with two different set ups, we call them run 1 and run 2, we described the setups in Section 3.5.

4.2.1 Resistivity

Proper resistivity ensures that the detector operates effectively, allowing it to detect charged particles. To calculate the resistivity of the detectors, we measured the current consumption, for that we used a 4 channels CAEN HV power supply and argon gas as we can appreciate in Fig. (4.2).

Figure 4.2: Experimental setup for the resistivity tests, using Argon gas, and an HV source to inject the applied voltage and obtain the current consumption from the same source.

We used channels 0 and 2 to supply MRPC1 with voltages between 4 kV and 5.7 kV, channel 2 was always at 1 kV while we changed the voltage of channel 0 by 100 V each time, resulting on the following plots. The resistivity is the product between the resistance and the area of the detector divided by the length,

$$\rho = \frac{R \times A}{L}. \tag{4.1}$$

The slope between the voltage and the electric current is the resistance of our detector [18], meaning that the average slope of the line shown in Fig. (4.3). for MRPC1, is of $1.53 \times 10^9 \Omega$, while the area is 15.4 cm^2 and the length is 22 cm, so the resistivity of

MRPC1 is $1.071 \times 10^9 \Omega \cdot cm$.

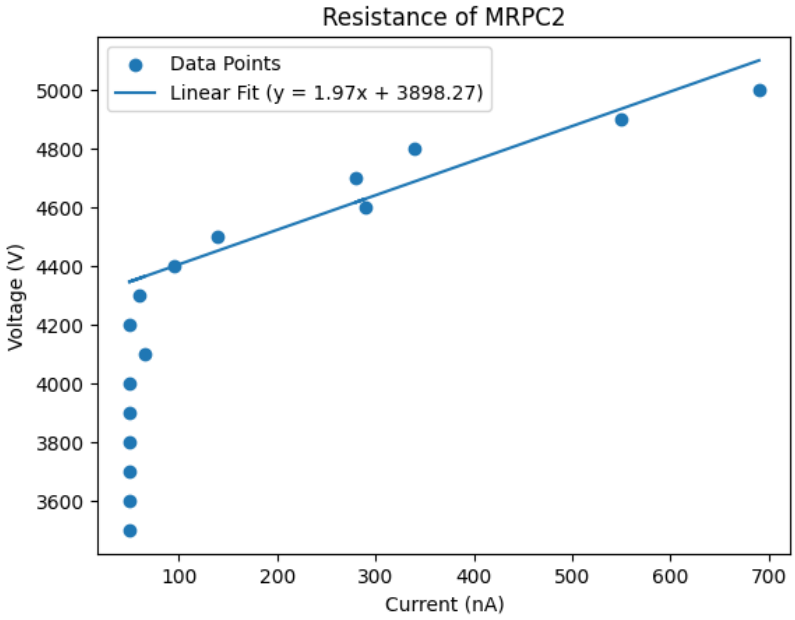

Figure 4.3: Current consumption of MRPC1, it has a $\chi^2/nd = 6.60$, and a resistance of $1.53 \times 10^9 \Omega$.

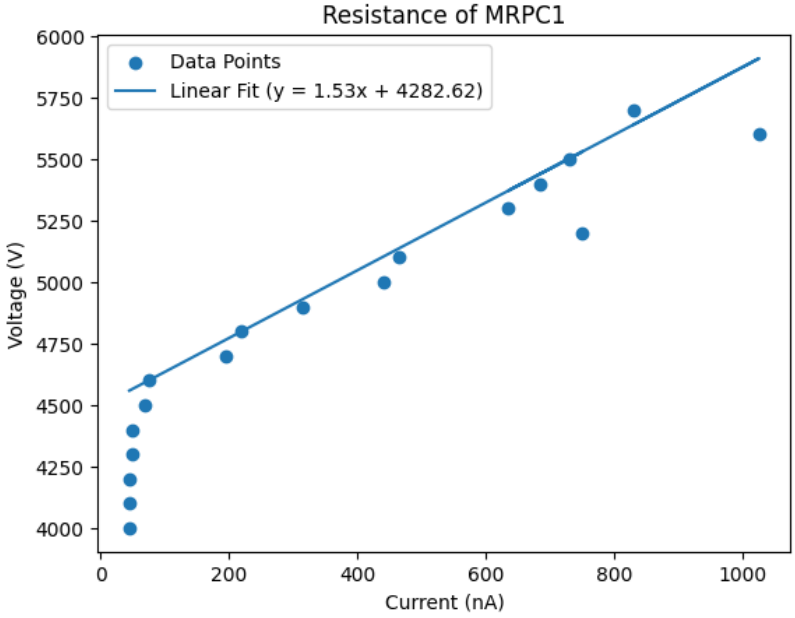

Figure 4.4: Current consumption of MRPC2, it has a $\chi^2/nd = 18.58$, and a resistance of $1.97 \times 10^9 \Omega$.

For the MRPC2, in Fig. (4.4), the average slope of the line was of $1.97 \times 10^9 \Omega$, meaning the resistivity of MRPC2 is $1.379 \times 10^9 \Omega \cdot cm$. Normally, MRPCs from CERN have a resistivity between 10^9 to $10^{12} \Omega \cdot cm$ [3]. According to [11], the resistivity of the glass used in these MRPCs is $2.1 \times 10^{10} \Omega \cdot cm$, which it means our results are in the expected range.

4.2.2 Rate capability

Rate capability can be defined as the flux of impinging particles in the detector surface. We try to normalize this flux by not exceeding the efficiency degradation of the detector. For MRPCs operated in avalanche mode, efficiency should be of 95%, meaning hundreds of hz/cm^2. The area of every strip of the MRPCs is 9.8 cm^2.

Figure 4.5: Counter made in FCFM-BUAP, which was connected to the MRPCs strips, while the detector was injected with HV and freon gas.

We used a counter made in FCFM-BUAP (Fig. (4.5)) to measure the number of counts every two minutes, to advance quickly, with a $v_{thr} = 20mV$ since below it there was a lot of noise in our signals, from 5 kV to 11 kV, in steps of 200 V, using freon. We took measurements of every two strips, meaning 12 out of the 24 total in each MRPC.

To calculate the rate we divided the number of counts between the 120 seconds we were taking data for each strip and the area of the strip [11], basically:

$$\text{Rate capability} = \frac{\text{Number of events}}{\text{Time interval} \times \text{Area}}. \tag{4.2}$$

In the case of MRPC1, Fig. (4.6), the strips that had a better rate capability were G, M, Q, A, U and Othan the rest, meaning that the best region was the third one (M-O-Q), and the rate capability was of 1.0195 Hz/cm^2.

In the case of MRPC2, Fig. (4.7), the strips that had a better rate capability were A, C, K, I, O and G, meaning that the best region was the second one (G-I-K), with a rate capability of 0.7449 Hz/cm^2.

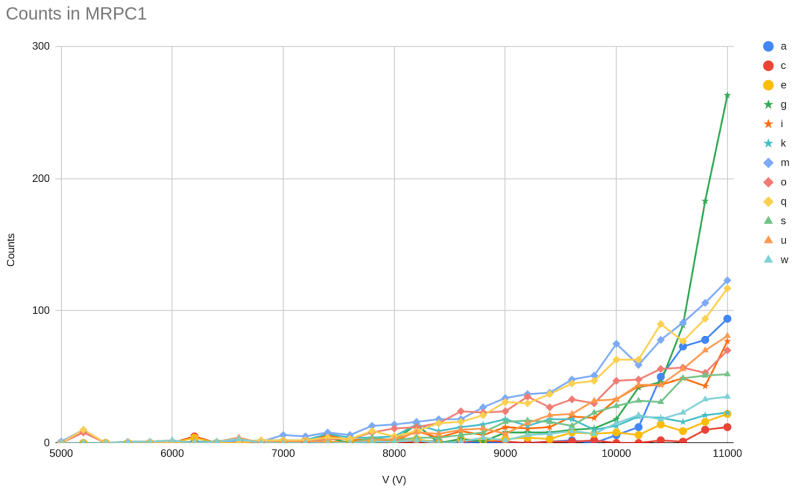

Figure 4.6: Counts vs. Applied Voltage of MRPC1.

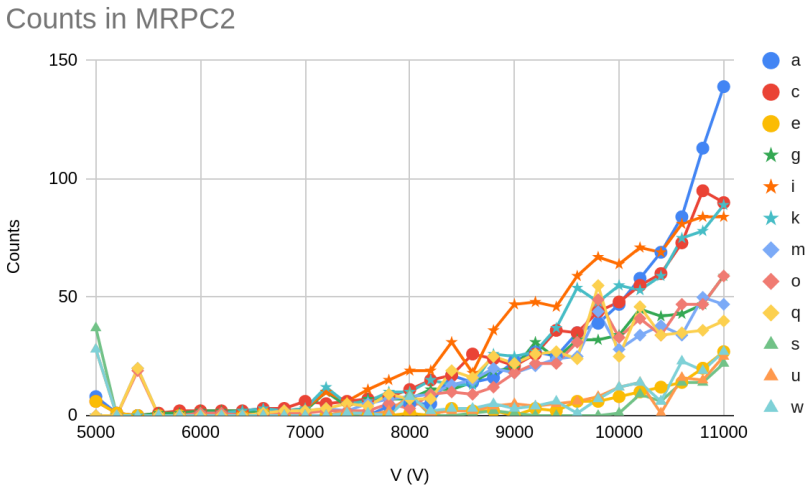

Figure 4.7: Counts vs. Applied Voltage of MRPC2.

It is important to note that these kind of MRPCs perform really well in high rate environments [11]. For our tests we used cosmic rays and we believe that this is one of the reasons why we can not get better results since about 10000 muons reach every square meter of the earths surface per minute, while in test beams like T9 we have particle fluxes of 10^6 in an area of $5 \times 12\text{m}^2$ [20]. Future tests of these MRPCs should be done with hight rate fluxes, using for example tests beams such as the ones available at CERN, like T10 in the East Area or the Prévessin area in the North Area Test Beam Facilities, or at the HZDR in Germany.

4.2.3 Efficiency

Voltage	Efficiency G1 (%)	Efficiency I1 (%)	Efficiency G2 (%)	Efficiency I2 (%)
12.8 kV	0.19			
13.8 kV			6.74	0.06
14 kV	0.11	0.01		
14.1 kV			6.57	0.83
14.2 kV			7.91	3.52
14.3 kV	4.15	2.61	10.48	4.66
14.4 kV			11.74	4.07
14.6 kV	4.12	2.61	11.98	5.11
15 kV	3.65	2.72		

Table 4.1: Efficiency at different applied voltages at strips G and I; G1 and I1 means the efficiency at strips G and I on the first run, and G2 and I2, means the efficiency at the strips on the second run.

As we where not familiar with the characteristics of these MRPC, Table 4.1 shows the data we took for MRPC2, with a wide range of applied voltage to obtain a proper efficiency curve where we can see a plateau, and we repeated the experiment twice to have more data, we called them first and second run and they area in Annexes 1 and 2.

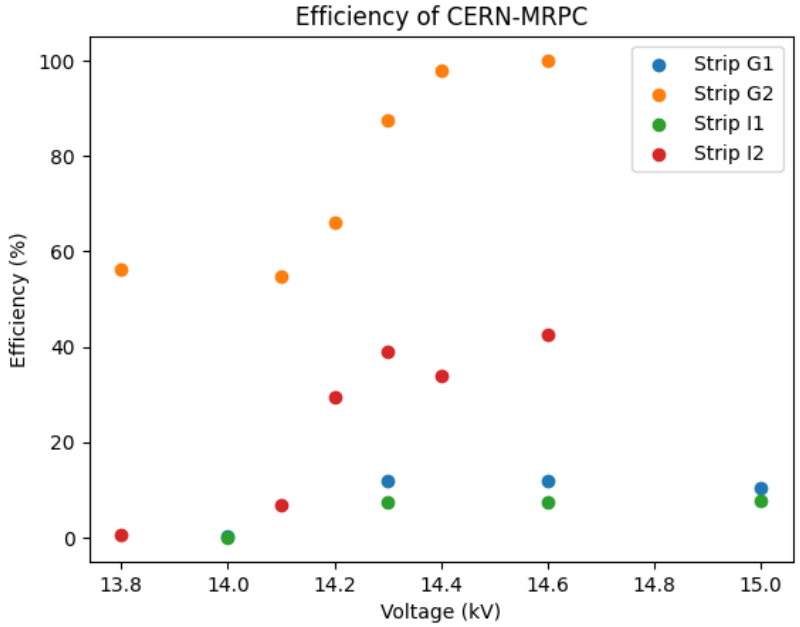

Figure 4.8: Normalized efficiency curves of the CERN MRPC.

To obtain the points in Fig. (4.8), we used the division factor (Eq. 3.1) to obtain the efficiency per area with Eq. 3.2 and then we normalized that efficiency with Eq.3.3. Although efficiency is normally expected to be around 95%, we had a maximum of 11.98% in strip G at 14.6 kV on the second run, and a minimum of 0.01% in strip I at 14 kV on the first run.

We believe that the low efficiency obtained is connected with the use of cosmic rays and the difficuty of adjusting precisely the PMTs when we used a lot of detectors in between. A higher efficiency should be expected if a radioactive source or a test beam were used [11].

4.2.4 Time Resolution

To compute the time resolution we used Eq. (2.9), according to Table 4.2 and Fig. (4.9), it is noticeable that as we increase the applied voltage, time resolution gets smaller and smaller.

Voltage	TR G1 (ns)	TR I1 (ns)	TR G2 (ns)	TR I2 (ns)
12.8 kV	10.87			
13.8 kV			1.24	26.76
14 kV	13.21	2.65		
14.1 kV			1.08	2.03
14.2 kV			0.42	0.79
14.3 kV	0.88	0.85	0.78	0.73
14.4 kV			0.58	0.64
14.6 kV	0.88	0.85	0.76	0.58
15 kV	1.37	0.58		

Table 4.2: Time resolution in nanoseconds and number of entries for different applied voltages at strips G and I. TR G1 is the time resolution of strip G run 1, TR I1 is for strip I run 1, TR G2 is for strip G run 2, and TR I2 is strip I run 2.

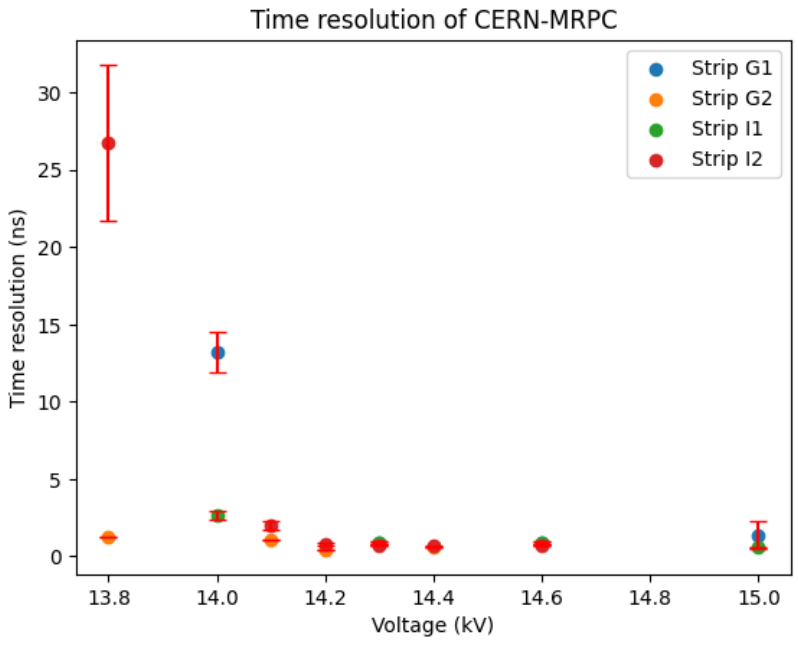

Figure 4.9: Time resolution measured in each strip.

For strip G we ave a maximum of 13.21 ns at 14 kV and a minimum of 0.42 ns at 14.2

kV. For strip I, we have a a maximum of 26.76 ns at 13.8 kV, and a minimum of 0.58 ns at 15 kV.

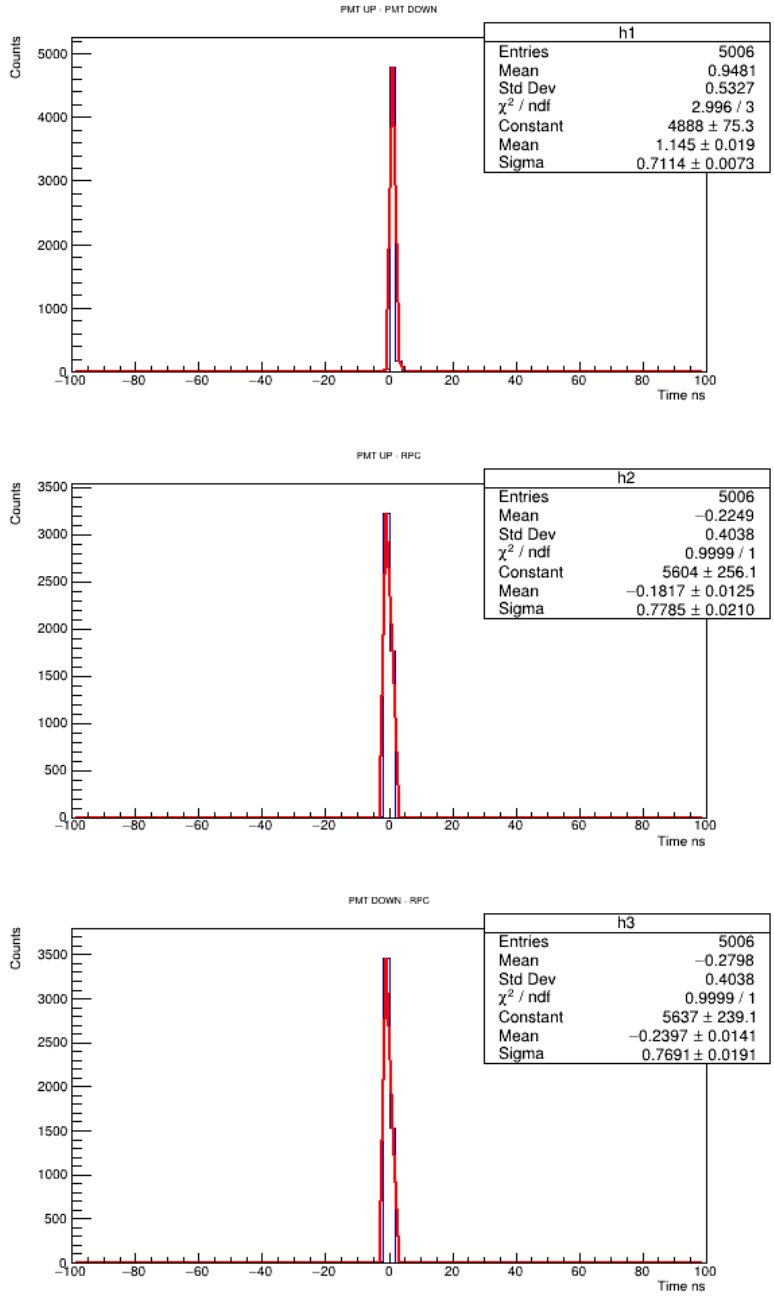

Figure 4.10: Counts vs. Time resolution at 14.4 kV on strip G.

An example of the collected data for this detector is Fig. (4.10), from where the plateau begins in strip G run 2 in Fig. (4.8. Counts are the number of particles that are crossing two detectors (PMT up-PMT down, PMT up-MRPC, or PMT down-MRPC) in a certain time.

4.2.5 Charge

Fig. (4.11) is the histogram for the charge that we obtained through the programs to reconstruct, Fig. (3.32), and plot,(3.33), the data. The entries are the number of coincidences between the three detectors (1 MRPC and 2 PMTs); the mean is the mean charge of the points that make the curve; the standard deviation is the dispersion of the Landau adjustment while sigma is the standard deviation of the data we have collected; when χ^2/ndf is 1 or close to 1, it means that the Landau adjustment is ideal; the constant ensures that total area under the curve is 1; and MPV (Most Probable Value) is the value from the data that has the highest probability of appearing.

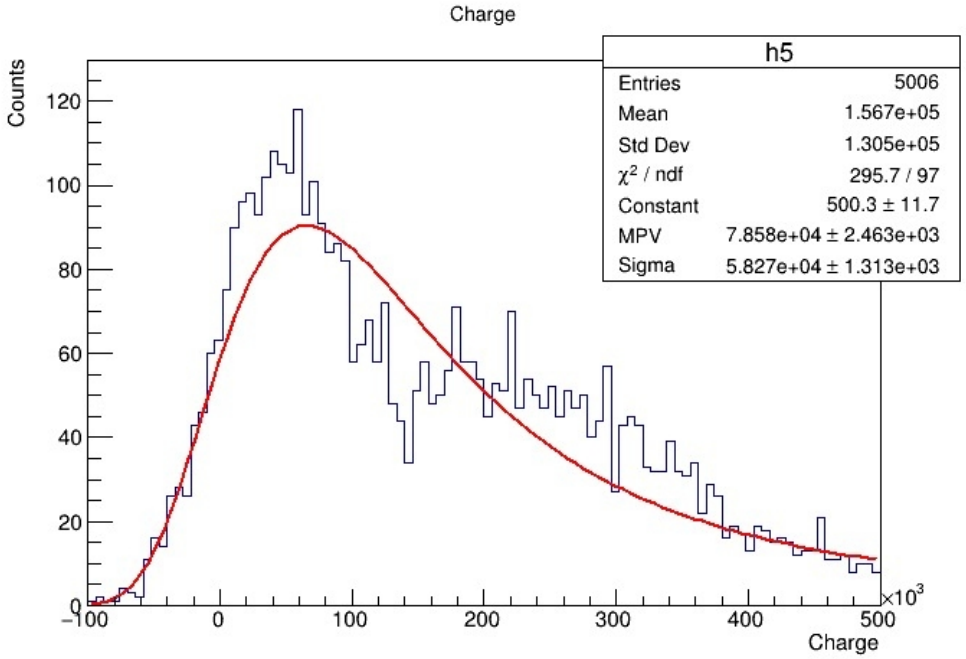

Figure 4.11: Counts vs. charge at 14.4 kV on strip G.

In this case the sigma is the half of the standard deviation, meaning we expected a higher charge than what we got, even though the adjustment to the Landau fit was 3.

4.3 ALICE-BUAP MRPC's results

For the ALICE-BUAP MRPC there are five pads, as it is shown in Table 4.3, each pad has been tested for twelve days, for three different HV points, four days per voltage point. To obtain clear signals, all the pads were tested with an oscilloscope, these pictures were taken and compared amongst themselves.

Pad Number	Voltage	Start Date	Finish Date
One	12 kV	sep 30th 2022	oct 3rd 2022
One	11.5 kV	oct 3rd 2022	oct 6th 2022
One	11 kV	oct 6th 2022	oct 10th 2022
Two	12 kV	oct 20th 2022	oct 24th 2022
Two	11 kV	oct 24th 2022	oct 28th 2022
Two	11.5 kV	nov 7th 2022	nov 10th 2022
Three	12 kV	nov 14th 2022	nov 18th 2022
Four	11.5 kV	jan 16th 2023	jan 19th 2023
Four	12 kV	jan 20th 2023	jan 23th 2023
Four	11 kV	jan 23th 2023	jan 26th 2023
Six	11 kV	jan 26th 2023	jan 30th 2023
Six	11.5 kV	jan 30th 2023	feb 1st 2023
Six	12 kV	feb 13th 2023	feb 16th 2023

Table 4.3: Data taking dates and voltage points for the ALICE-BUAP MRPC.

4.3.1 Efficiency

We got the efficiency of each pad of the MRPC, using Eq. (2.5), and compared it with each other. The table (4.4) and Fig. (4.12) show the efficiency for each pad, being 39.34% the maximum and 6.79% the minimum efficiency of the ALICE-BUAP MRPC. Efficiency is calculated through Eq. (2.5) using the code written by the group in the Ecocampus laboratory.

Pad Number	Voltage	Efficiency (%)
One	12 kV	18.9889
One	11.5 kV	20.0106
One	11 kV	8.0222
Two	12 kV	9.7614
Two	11 kV	9.6079
Two	11.5 kV	9.0909
Three	12 kV	6.7920
Four	11.5 kV	21.7938
Four	12 kV	39.3421
Four	11 kV	23.7071
Six	11 kV	8.1565
Six	11.5 kV	7.1900
Six	12 kV	7.8498

Table 4.4: Efficiency from each pad at different applied voltage points.

Fig. (4.12) shows the data from Table 4.4, where we can see the efficiency from every one of the six pads at different voltages, but normalized, and our maximum efficiency per cm^2 is $0.48\%/cm^2$, and the minimum is $0.08\ \%/cm^2$ since the pads have an area of $81cm^2$. We are in the plateau of the ALICE-BUAP MRPC's efficiency.

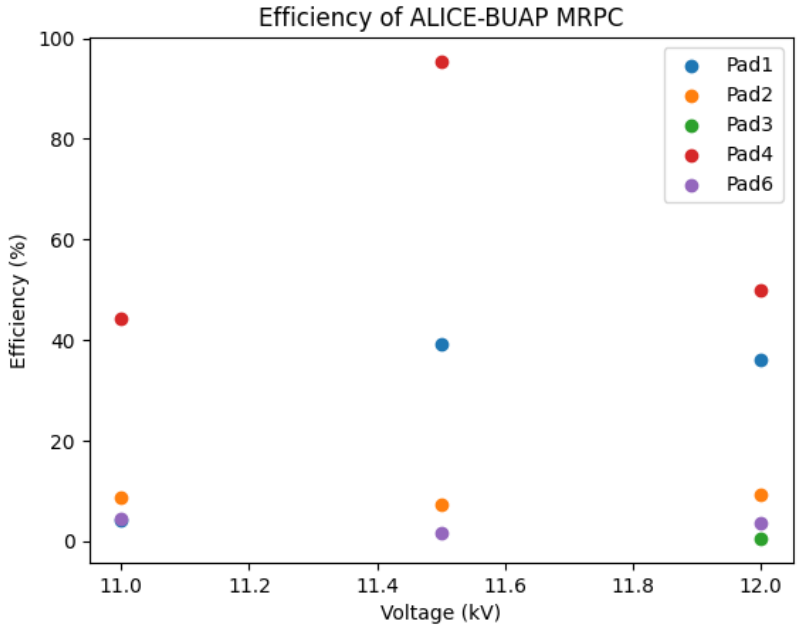

Figure 4.12: Normalized efficiency of the five pads of the ALICE-BUAP MRPC.

4.3.2 Time Resolution

Pad	Voltage	Entries	Time Resolution (ns)
One	11 kV	1429	1.97
One	11.5 kV	3405	1.56
One	12 kV	3478	1.48
Two	11 kV	1968	1.71
Two	11.5 kV	1427	2.68
Two	12 kV	2034	1.74
Three	12 kV	1459	3.42
Four	11 kV	1040	3.99
Four	11.5 kV	7128	39.60
Four	12 kV	518	21.31
Six	11 kV	1496	3.19
Six	11.5 kV	892	3.57
Six	12 kV	1533	3.92

Table 4.5: Time resolution in nanoseconds and number of entries from each pad at a certain applied voltage.

We computed time resolution with Eq. (2.9), the best time resolution is 1.48 ns in the first pad at 12 kV, while the worst is 39.60 ns in the fourth pad at 11.5 kV.

Fig. (4.13) is an example of the analysed data that we obtained, and also the one with the minimum time resolution. The first plot, from top to bottom, shows the number of coincidences between both PMTs, the value we used to compute the time resolution of the pad is the sigma, in this case 0.71 ns, for the second plot, we have the coincidences between the PMT up and the MRPC with a sigma of 1.59 ns, and the third graph shows

the coincidences between the PMT down and the RPC with a sigma of 1.60 ns. The first mean is the center of the data, the second one is the center of the fit, the χ^2/ndf is the parameter that tell us if the fit we are using is a good one, if it is 1 or closer to 1, it indicates that the observed data is consistent with the expected values, meaning that he model is providing a good representation of the data.

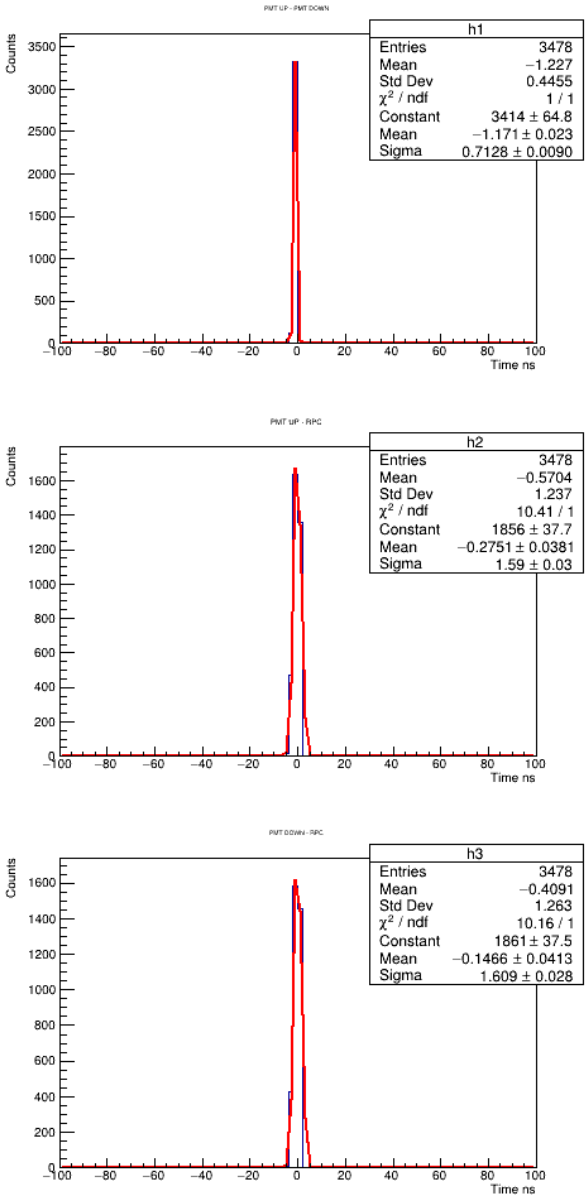

Figure 4.13: Counts vs. Time resolution at 12 kV in pad number one.

We plotted the data of Table 4.5 in Fig. (4.14), since we are in the plateau we see mostly horizontal lines, except for pad 4. The other data lines are very close within each other's value

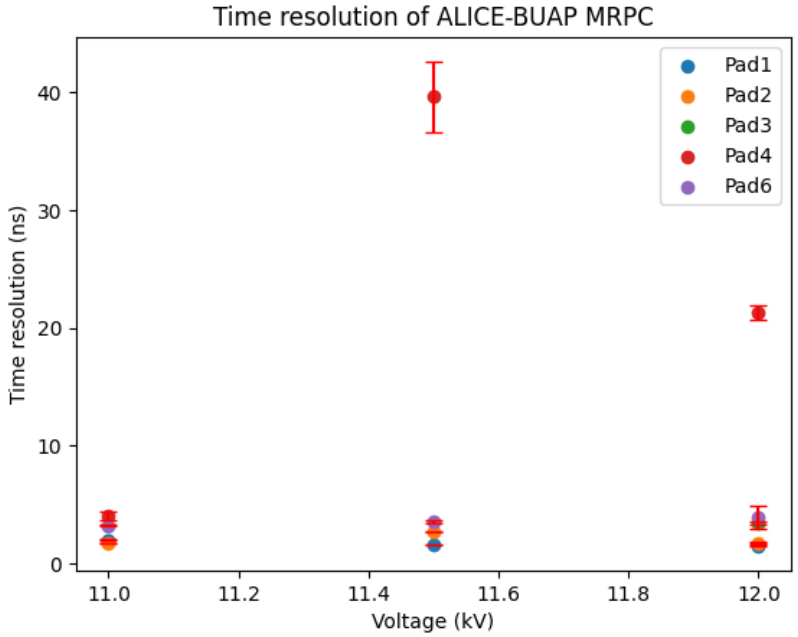

Figure 4.14: Time resolution measured in each pad.

4.3.3 Charge

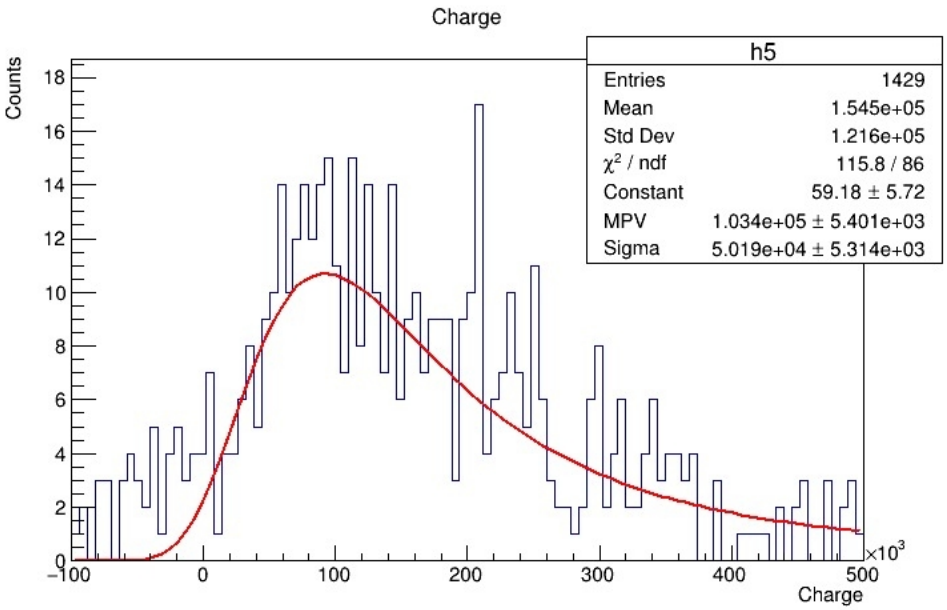

Figure 4.15: Counts vs. charge at 11 kV in pad number one.

For the charge, the plots from where we obtained the full information were just like Fig. (4.15), where the standard deviation of the Landau distribution is two times the value of sigma, which is the standard deviation of the data we acquiredprobably due to underfitting, and the adjustment is 1.34, which means it is a good adjustment.

Chapter 5

Conclusions

We learned about the creation and operation of MRPCs from various books and research papers, enabling us to begin operating the CERN MRPCs we sealed and completed constructing them. Various tests were performed so we could understand how these detectors operate since they have a different setup compared to the MRPCs from ALICE-BUAP. We had to adapt the MRPCs of CERN, MRPC1 and MRPC2, to the Ecocampus laboratory in BUAP; although the laboratory of MRPCs of the ALICE-BUAP and CMS-BUAP grous construct and operate MRPCs, we also made sure we could acquire data with the oscilloscope we will be using in the new laboratory PhD. Cecilia Uribe is creating. For each point in the plots of efficiency and time resolution we spend four to five days to collect data.

Having said that, in the case of the efficiency, CERN MRPC has seven times a better efficiency per detection area, compared to the ALICE-BUAP MRPC, and the time resolution of ALICE-BUAP MRPC is more than the double of the CERN MRPC in most of the cases. The efficiency, if we do not take into consideration the area of detection, of the ALICE-BUAP MRPC seems higher than the one of the CERN MRPC, this is due to the fact that the MRPCs we characterized were made to work in high rate environments (such as the ones in LHC) and not for cosmic rays, where the fluxes are much more smaller.

This is not all the information we got from CERN MRPCs, summarily we can say that the efficiency curve start is noticeable and the plateau starts after 14 kV, the mean time resolution has a minimum of 0.42 ± 0.0186922 ns and a maximum of 26.76 ± 5.03854 ns, the resistivity of the MRPC we studied is $0.114 \times 10^{10} \Omega \cdot cm$, while the one we could not use since there was an accident had a resistivity of $0.105 \times 10^{10} \Omega \cdot cm$.

The rate capability of the MRPC we used, CERN-MRPC2, had a maximum of 69 counts per minute at 11 kV, while the one we did not use had a rate capability of 131 counts per minute at the same voltage, as we increased the voltage, the number of counts increased too. This data also helped us know which area of the detector was the most sensitive. We divided the total area in four sections, the first one included the strips A-C-E, the second one the strips G-I-K, the third one the strips M-O-Q, and the last one the strips S-U-W.

In the case of MRPC1, he one we did not use for the efficiency, time resolution and charge tests, the second area had the best rate capability which was 60.5 counts per minute in every strip, meaning a hit every second. In the case of the MRPC we used,

MRPC2 from CERN, the best rate capability was the one from the strips G-I-K, too, with a mean rate capability of 38.6 counts per minute in every strip, meaning a hit every two seconds.

For this thesis we constructed the aluminium boxes so we could operate the MRPCs from CERN, we also made the voltage converters and cables so that they could be compatible with the instruments. Although the data collection is slow, it still can help students understand how MRPCs operate, even better since we had to change one of the aluminium lids for an acrylic lid, students can see how the MRPC is constructed while using it to acquire data.

We also used multiple setups to acquire the data from the annexes, as well as instruments and the CERN MRPCs, we acquired data with digitizer CAEN DT5742B and oscilloscope TELEDYNE LECROY HDO6104B for the efficiency, time resolution and charge. To acquire the data for the resistivity we used voltage source CAEN DT1470ET, and the data from the rate capability was acquired with a counter made in BUAP by Ph.D. Guillermo Tejeda.

Finally, we have the grounds to start operating the MRPCs as a cosmic telescope at CU-BUAP, with the oscilloscope for data acquisition, since we know how the detectors we have operate.

Chapter 6

Bibliography

[1] Santonico, Rinaldo and Roberto Cardarelli: *Development of resistive plate counters.* Nuclear Instruments and Methods in Physics Research Section A: Accelerators, Spectrometers, Detectors and Associated Equipment, 187(2–3):377–380, August 1981. http://dx.doi.org/10.1016/0029-554X(81)90363-3.

[2] The-CMS-Collaboration: *The cms experiment at the cern lhc.* Journal of Instrumentation, 3(08):S08004, aug 2008. https://dx.doi.org/10.1088/1748-0221/3/08/S08004.

[3] Giordano, Cattani: *The resistive plate chambers of the atlas experiment: performance studies.* Journal of Physics: Conference Series, 280(1):1–7, feb 2011. https://dx.doi.org/10.1088/1742-6596/280/1/012001.

[4] Blanco, A., V. Chepel, R. Ferreira-Marques, P. Fonte, M.I. Lopes, V. Peskov, and A. Policarpo: *Perspectives for positron emission tomography with rpcs.* Nuclear Instruments and Methods in Physics Research Section A: Accelerators, Spectrometers, Detectors and Associated Equipment, 508(1):88–93, 2003, ISSN 0168-9002. https://www.sciencedirect.com/science/article/pii/S016890020301283X, Proceedings of the Sixth International Workshop on Resistive Plate Chambers and Related Detectors.

[5] Sauli, Fabio: *Gaseous Radiation Detectors, Fundamentals and Applications.* Cambridge Monographs on Particle Physics, Nuclear Physics and Cosmology, 2014.

[6] Abbrescia, Marcello, Vladimir Peskov, and Paulo Fonte: *Resistive Gaseous Detectors Designs, Performance, Perspectives.* Wiley-VCH, 2018.

[7] Apollinari, G, I Béjar Alonso, O Brüning, M Lamont, and L Rossi: *High-Luminosity Large Hadron Collider (HL-LHC): Preliminary Design Report.* CERN Yellow Reports: Monographs. CERN, Geneva, 2015. http://cds.cern.ch/record/2116337.

[8] Liu, Z., F. Carnesecchi, M.C.S. Williams, A. Zichichi, and R. Zuyeuski: *Timing performance study of multigap resistive plate chamber with different gap size.* Nuclear Instruments and Methods in Physics Research Section A: Accelerators, Spectrometers, Detectors and Associated Equipment, 927:396–400, 2019, ISSN 0168-9002. https://www.sciencedirect.com/science/article/pii/S0168900219302566.

[9] Leo, William R: *Techniques for Nuclear and Particle Physics Experiments, A How-to Approach.* Springer-Verlag, 1994.

[10] Cerron Zeballos, E, I Crotty, D Hatzifotiadou, J Lamas Valverde, S Neupane, M.C.S Williams, and A Zichichi: *A new type of resistive plate chamber: The multigap rpc.* Nuclear Instruments and Methods in Physics Research Section A: Accelerators, Spectrometers, Detectors and Associated Equipment, 374(1):132–135, 1996, ISSN 0168-9002. https://www.sciencedirect.com/science/article/pii/0168900296001581.

[11] Liu, Z., R. Beyer, J. Dreyer, X. Fan, R. Greifenhagen, D.W. Kim, R. Kotte, A. Laso Garcia, L. Naumann, K. Römer, D. Stach, C. Uribe Estrada, M.C.S. Williams, and A. Zichichi: *Novel low resistivity glass: Mrpc detectors for ultra high rate applications.* Nuclear Instruments and Methods in Physics Research Section A: Accelerators, Spectrometers, Detectors and Associated Equipment, 959:163483, 2020, ISSN 0168-9002. https://www.sciencedirect.com/science/article/pii/S0168900220300875.

[12] Vásquez-Beltrán, Y., M. Rodríguez-Cahuantzi, and I. León-Monzón: *Time resolution of particle detectors based on scintillation photons.* Master's thesis, BUAP, 2023.

[13] Liu, Z., D.W. Kim, M.C.S. Williams, A. Zichichi, and R. Zuyeuski: *Multigap resistive plate chamber read out by 1×1cm2 pads with the nino asic.* Nuclear Instruments and Methods in Physics Research Section A: Accelerators, Spectrometers, Detectors and Associated Equipment, 920:115–118, 2019, ISSN 0168-9002. https://www.sciencedirect.com/science/article/pii/S0168900218318382.

[14] Liu, Z., F. Carnesecchi, O.M. Rodriguez, M.C.S. Williams, A. Zichichi, and R. Zuyeuski: *20 gas gaps multigap resistive plate chamber: Improved rate capability with excellent time resolution.* Nuclear Instruments and Methods in Physics Research Section A: Accelerators, Spectrometers, Detectors and Associated Equipment, 908:383–387, 2018, ISSN 0168-9002. https://www.sciencedirect.com/science/article/pii/S0168900218310544.

[15] Ammosov, V., V. Korablev, and V. Zaets: *Electric field and currents in resistive plate chambers.* Nuclear Instruments and Methods in Physics Research Section A: Accelerators, Spectrometers, Detectors and Associated Equipment, 401(2):217–228, 1997, ISSN 0168-9002. https://www.sciencedirect.com/science/article/pii/S0168900297008000.

[16] Cerron Zeballos, E., I. Crotty, D. Hatzifotiadou, J. Lamas Valverde, S. Neupane, V. Peskov, S. Singh, M.C.S. Williams, and A. Zichichi: *A comparison of the wide gap and narrow gap resistive plate chamber.* Nuclear Instruments and Methods in Physics Research Section A: Accelerators, Spectrometers, Detectors and Associated Equipment, 373(1):35–42, 1996, ISSN 0168-9002. https://www.sciencedirect.com/science/article/pii/0168900295014837.

[17] Sharma, Archana: *Greening gaseous detectors.* https://cerncourier.com/a/greening-gaseous-detectors/.

[18] Halliday, D., R. Resnick, and J. Walker: *Fundamentos de física, volumen dos.* Patria, 2017.

[19] Blackburn, H. and J. Heppler: *Who is writing about women in stem in higher education in the united states? a citation analysis of gendered authorship.* Frontiers of psychology, 10, 2020, ISSN 1664-1078. https://www.frontiersin.org/articles/10.3389/fpsyg.2019.02979.

[20] N/A: *Information about the t9 beam line and experimental facilities.* https://home.web.cern.ch/sites/default/files/file/spotlight_students/information_about_the_t9_beam_line_and_experimental_facilities.pdf.

Appendix A

Time resolution

Here we have the time resolution plots for each pad, in the case of the ALICE-BUAP MRPC, or strip, in the case of the CERN MRPC2, at different applied voltages, these were the plots from where we obtained the results of Tables 4.5 and 4.2.

A.1 ALICE-BUAP MRPC

The following three plots are the ones from where we obtain the time resolution of pad 1, to compute the time resolution we use the data of the sigma value of each sub plot, meaning PMT UP-PMT DOWN, PMT UP-RPC and PMT DOWN-RPC. We had more entries in the third one, where the applied voltage was of 12 kV because that is the plateu of efficiency of the ALICE-BUAP MRPC. For the applied voltage 11 kV we had a time resolution of 1.61 ns, for 11.5 kV it was slightly smaller, 1.59 ns, and finally for the 12 kV, it was of 1.51 ns, which was smaller but still around the mean value.

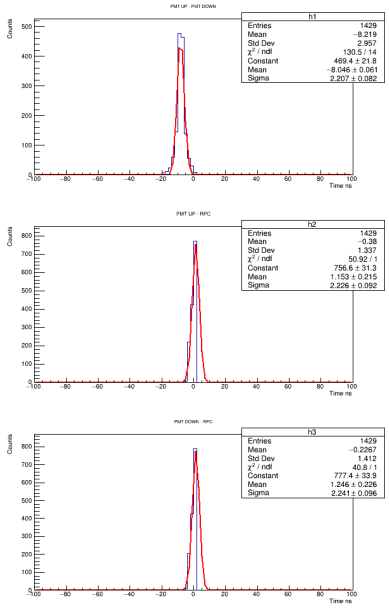

Figure A.1: Counts vs. Time resolution at 11 kV in pad number one.

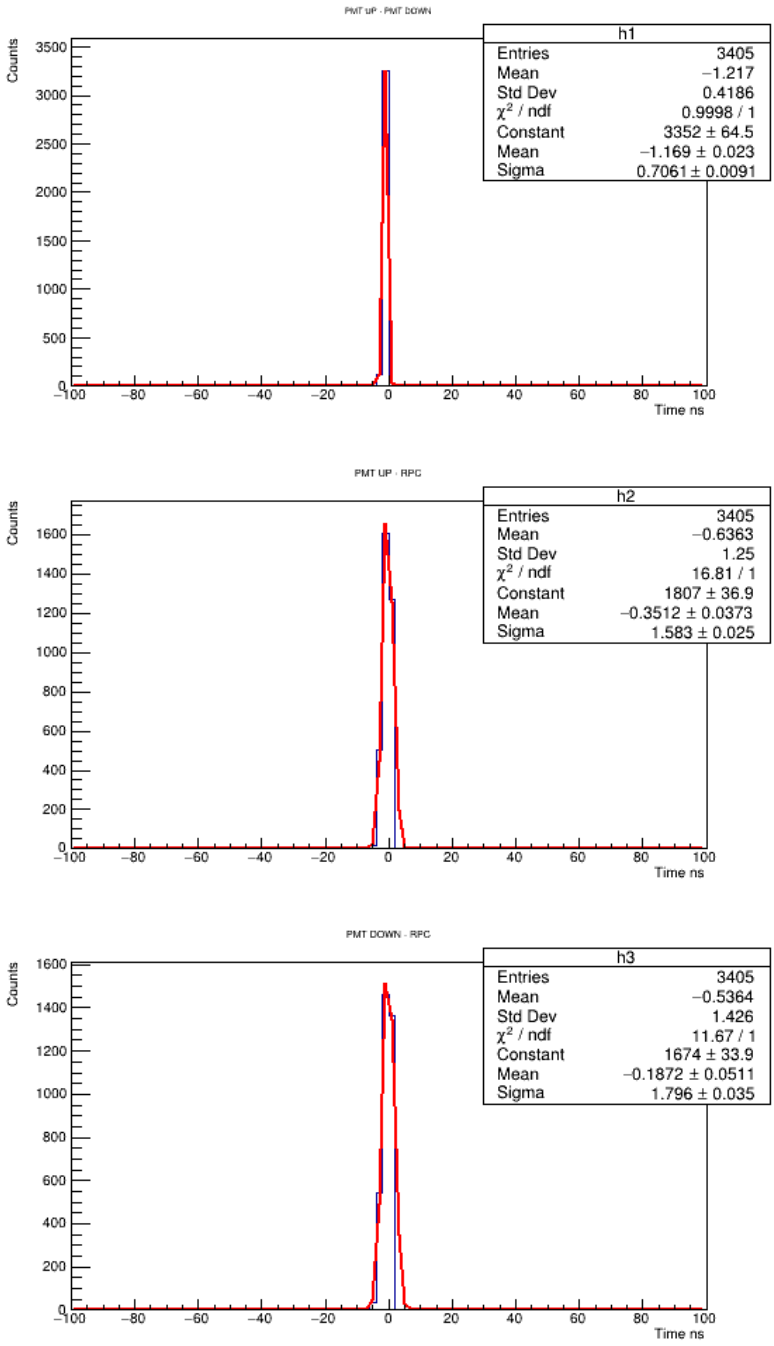

Figure A.2: Counts vs. Time resolution at 11.5 kV in pad number one.

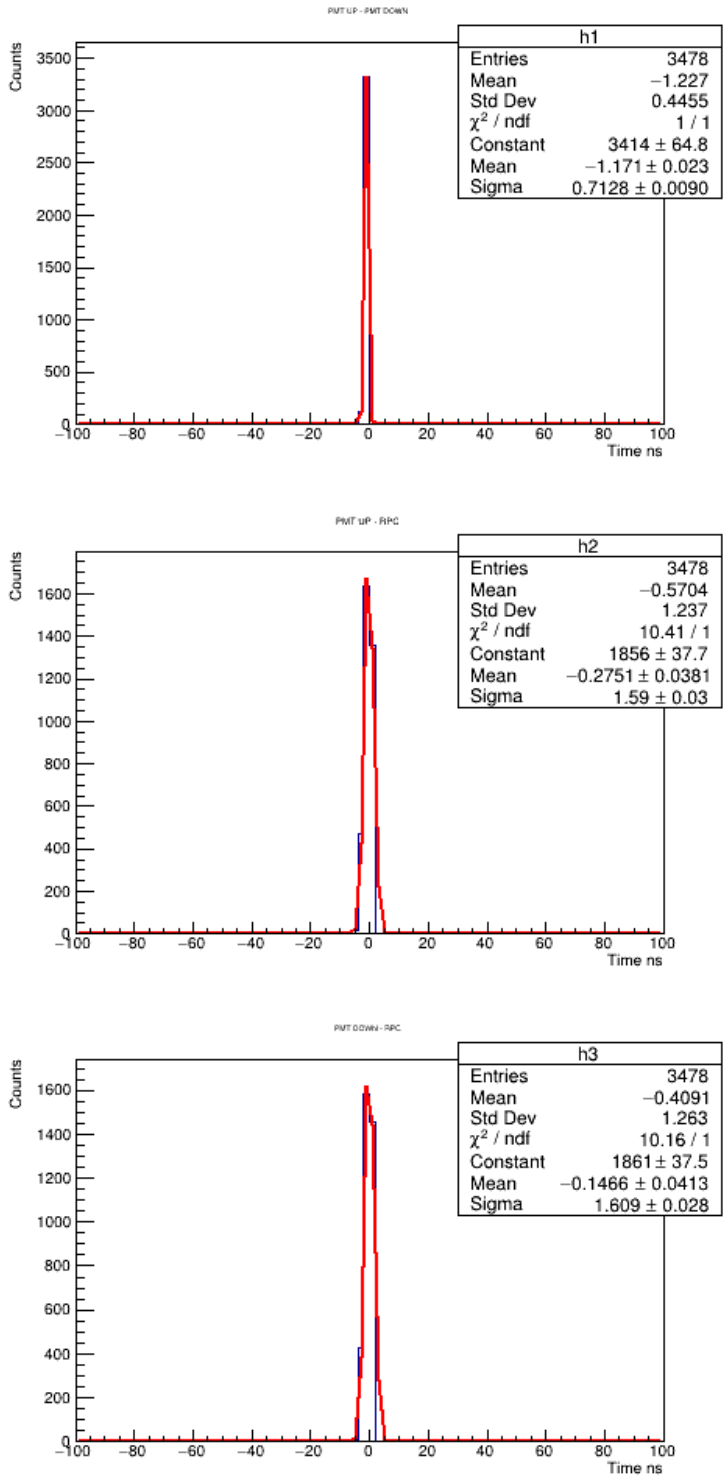

Figure A.3: Counts vs. Time resolution at 12 kV in pad number one.

For pad 2, we had more entries for the applied voltage of 11.5 kV than for the other voltages in the same pad. As for the time resolution, at the applied voltage of 11 kV we had a time resolution of 1.28 ns, for 11.5 kV it was slightly smaller, 1.17 ns, and finally for the 12 kV, it was of 2.35 ns, which is more than the double of the previous ones.

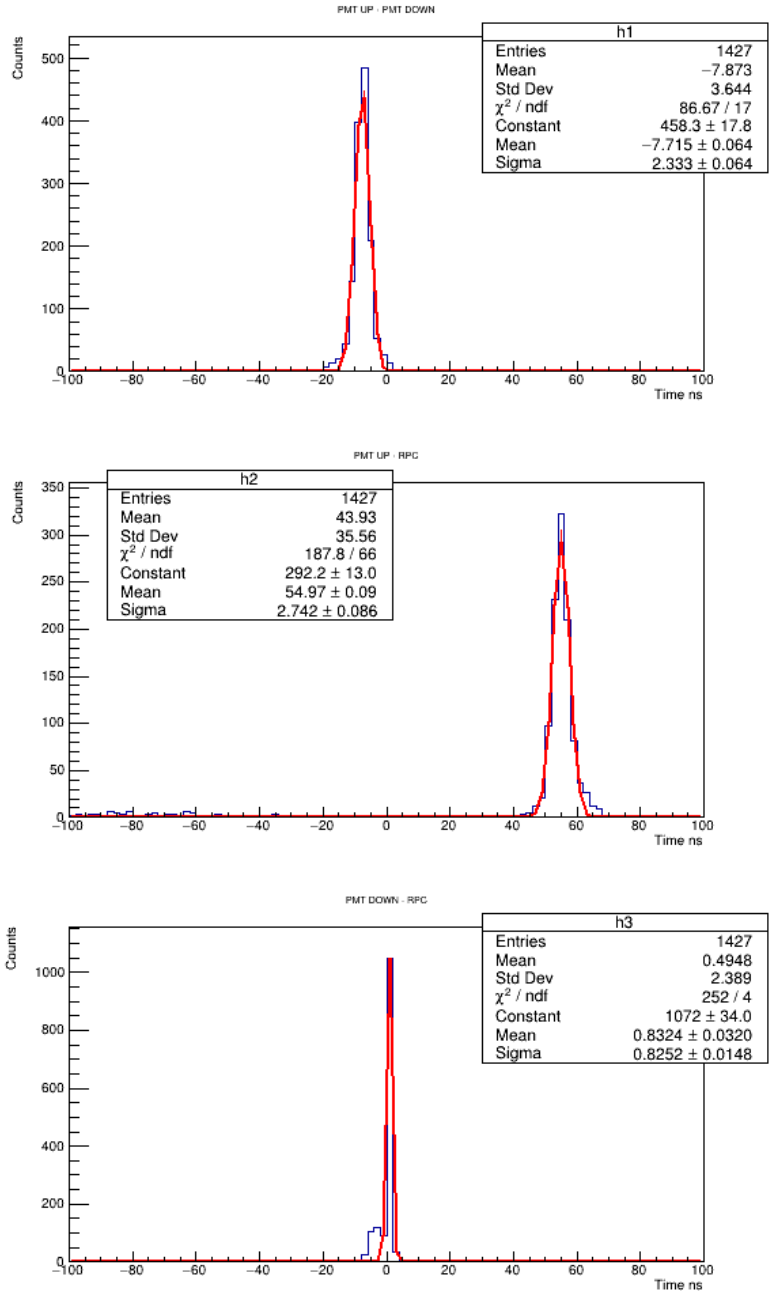

Figure A.4: Counts vs. Time resolution at 11 kV in pad number two.

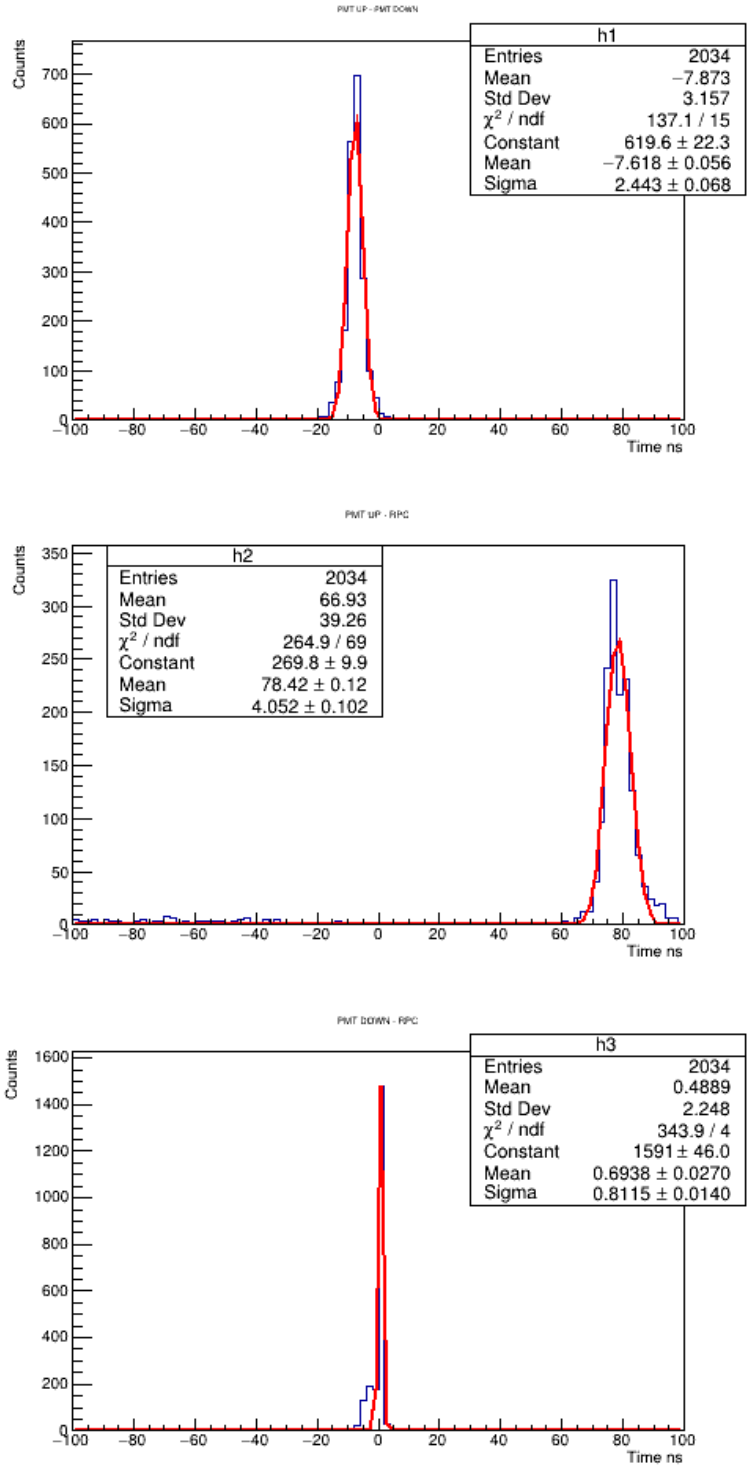

Figure A.5: Counts vs. Time resolution at 11.5 kV in pad number two.

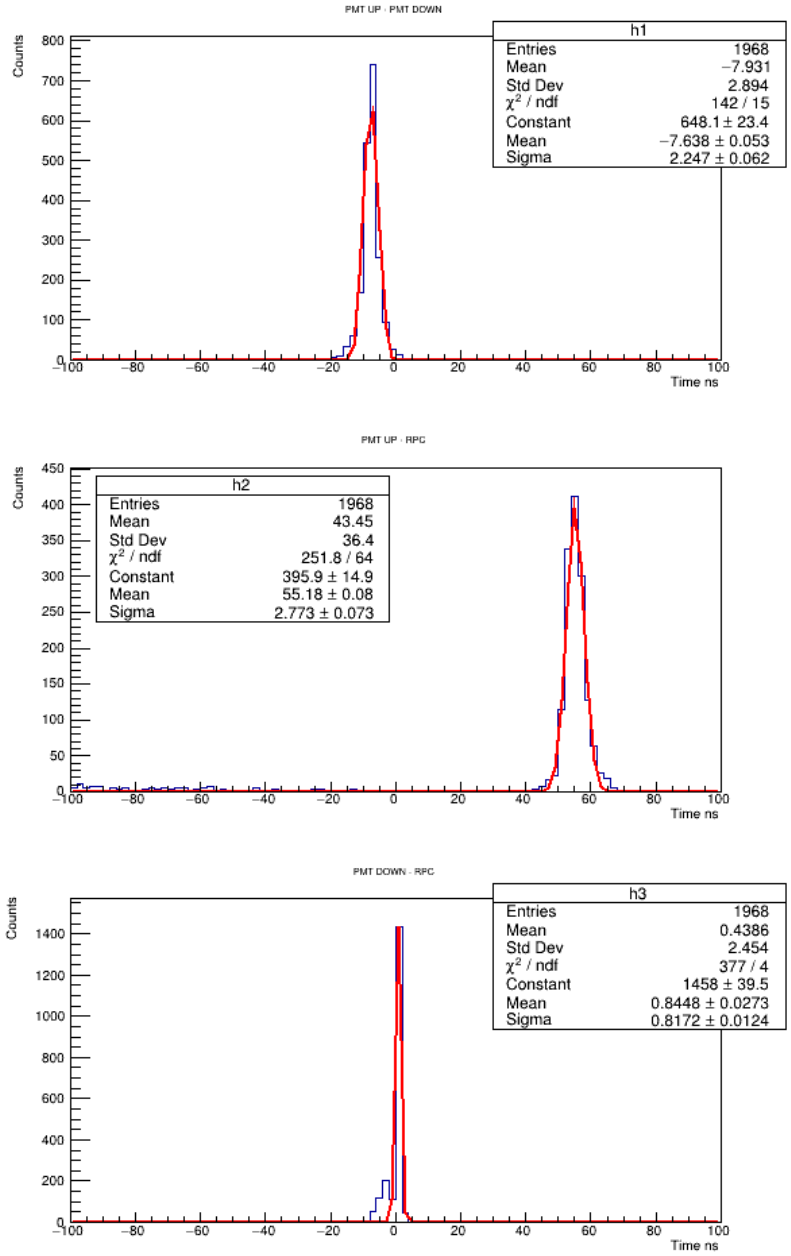

Figure A.6: Counts vs. Time resolution at 12 kV in pad number two.

For the third pad we only took data at one voltage because we had very little data at smaller applied voltages, at 12 kV we had the same number of entries as the entries at 11 kV at the previous pads. However the time resolution was of 2.90 ns, which was the biggest time resolution until now.

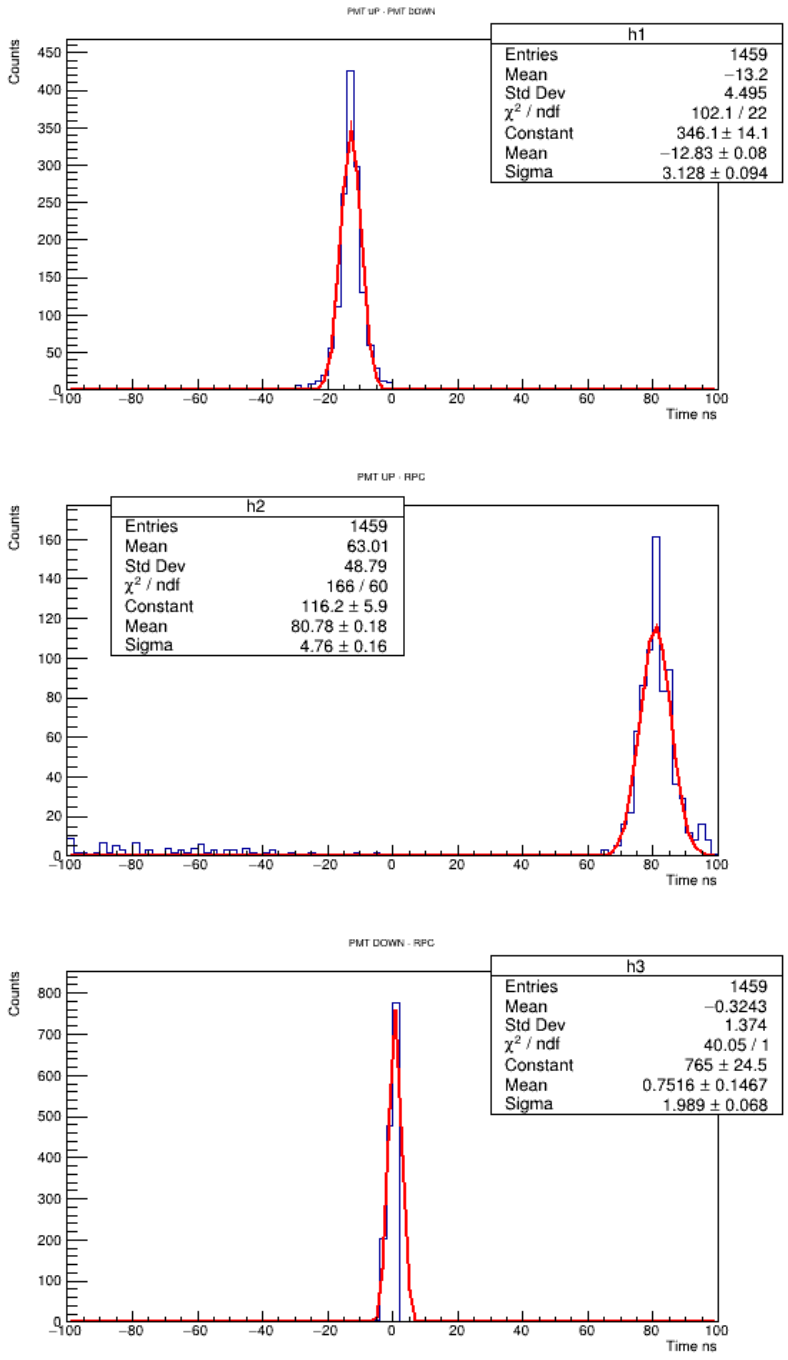

Figure A.7: Counts vs. Time resolution at 12 kV in pad number three.

The graphs for the fourth pad had bigger sigma values, and although we could think that the time resolution would be equally bigger in the three graphs, it was only true for the last two, with 39.60 ns and 21.31 ns for 11.5 and 12 kV, while the time resolution for the first one at 11 kV was 3.99 ns.

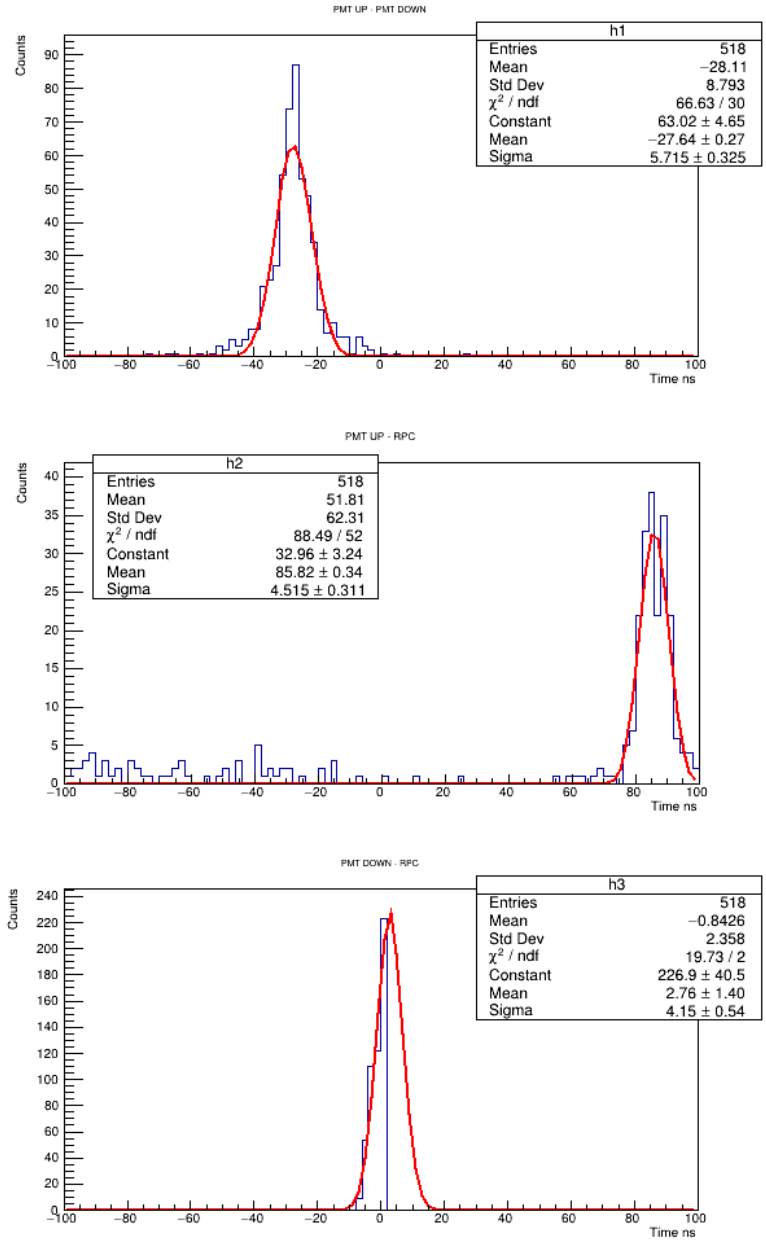

Figure A.8: Counts vs. Time resolution at 11 kV in pad number four.

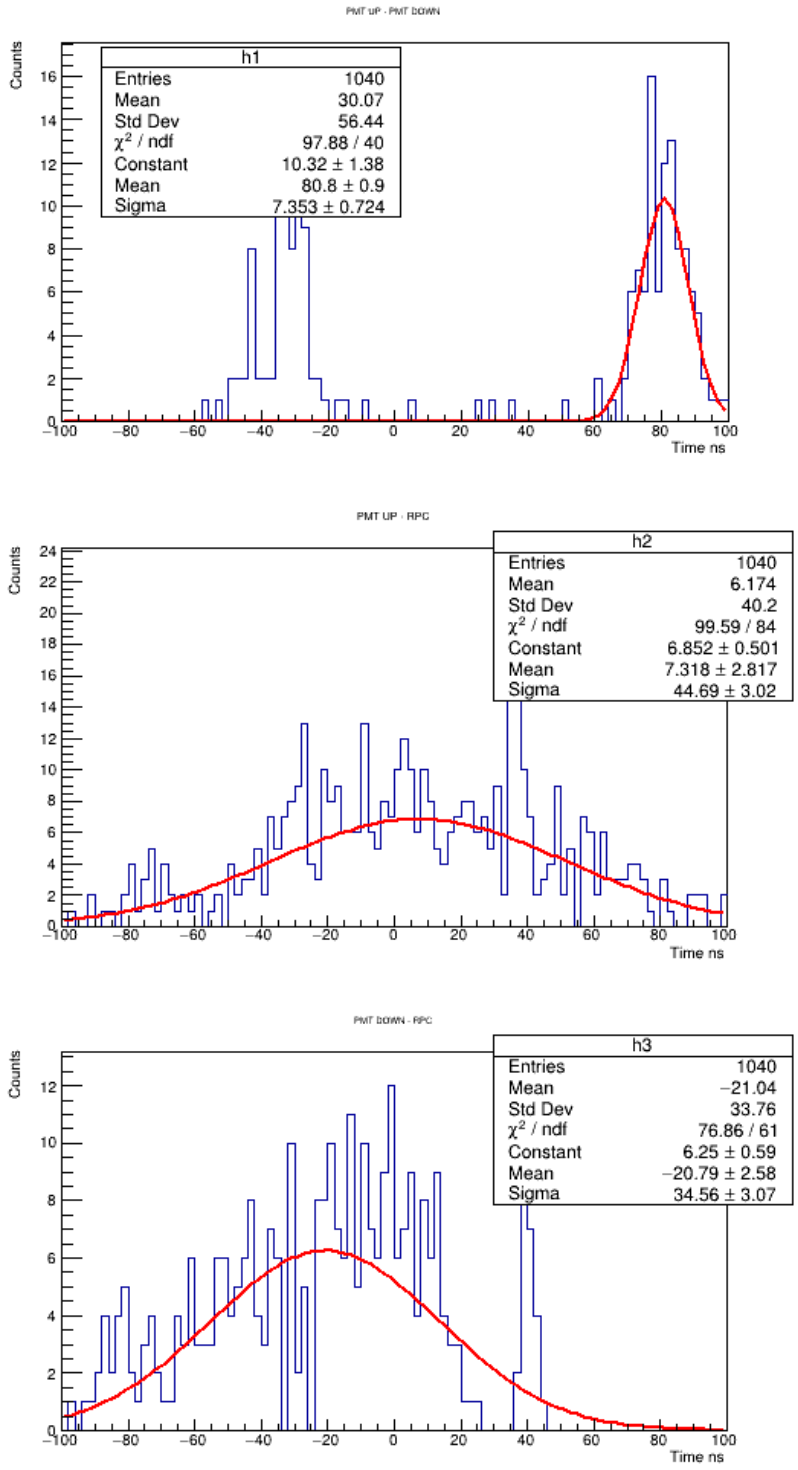

Figure A.9: Counts vs. Time resolution at 11.5 kV in pad number four.

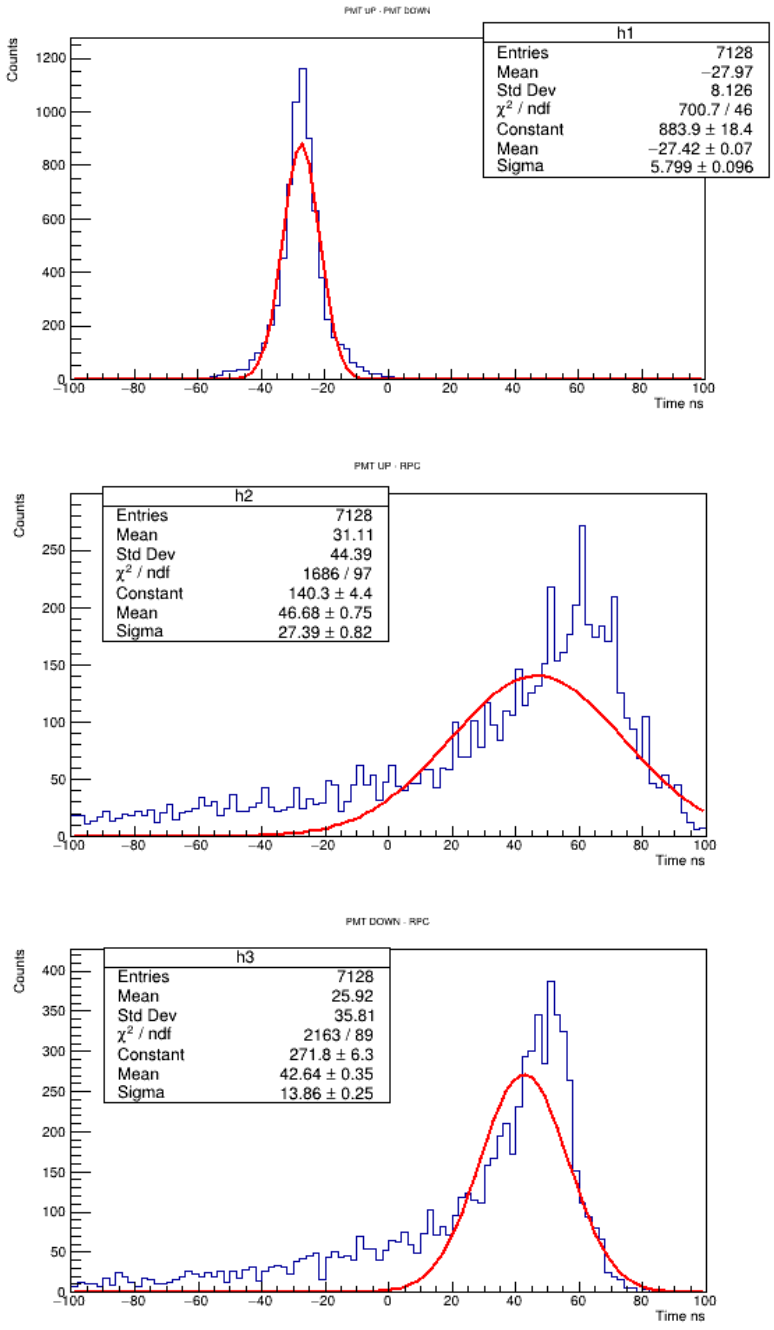

Figure A.10: Counts vs. Time resolution at 12 kV in pad number four.

The time resolution for the sixth pad was around 3.6 ns, since in all the graphs between the PMTs, the sigma value was 3 ns, and the ones between one PMT and the RPC were of 5 and 1 ns, the time resolutions were of 3.19, 3.57 and 3.92 ns for the applied voltages of 11, 11.5 and 12 kV, respectivelly.

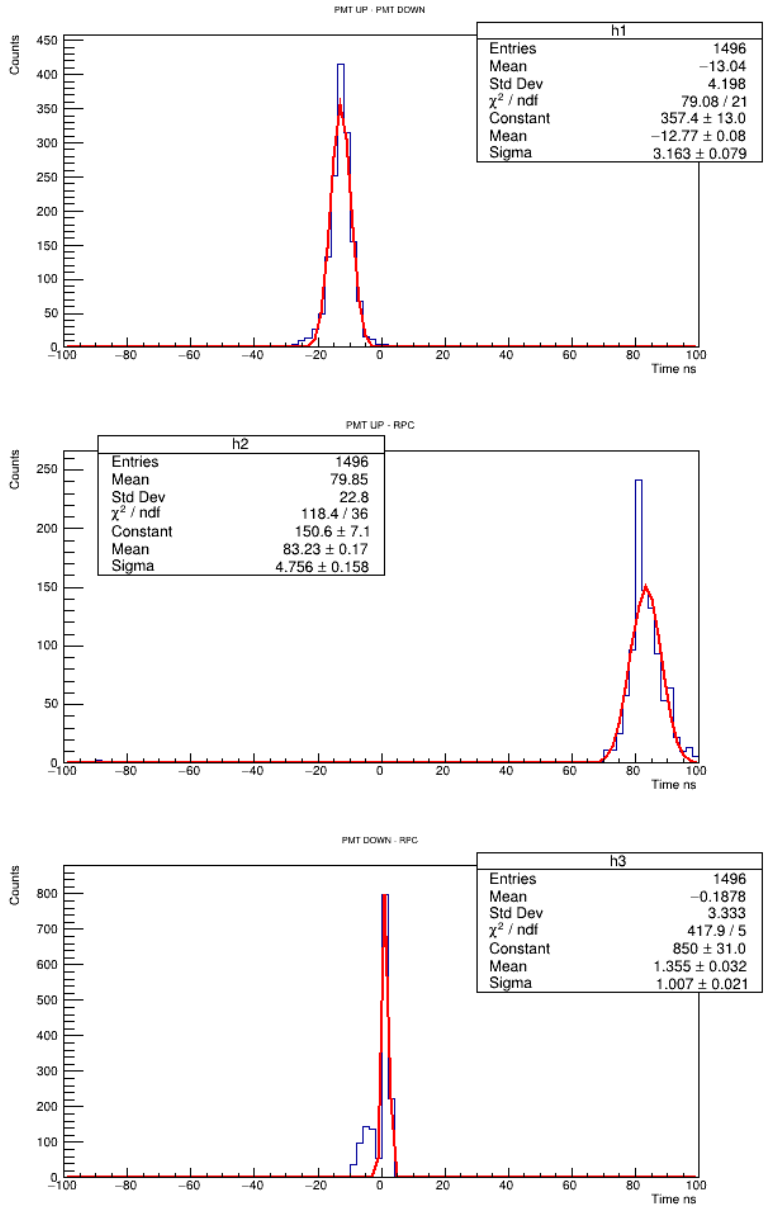

Figure A.11: Counts vs. Time resolution at 11 kV in pad number six.

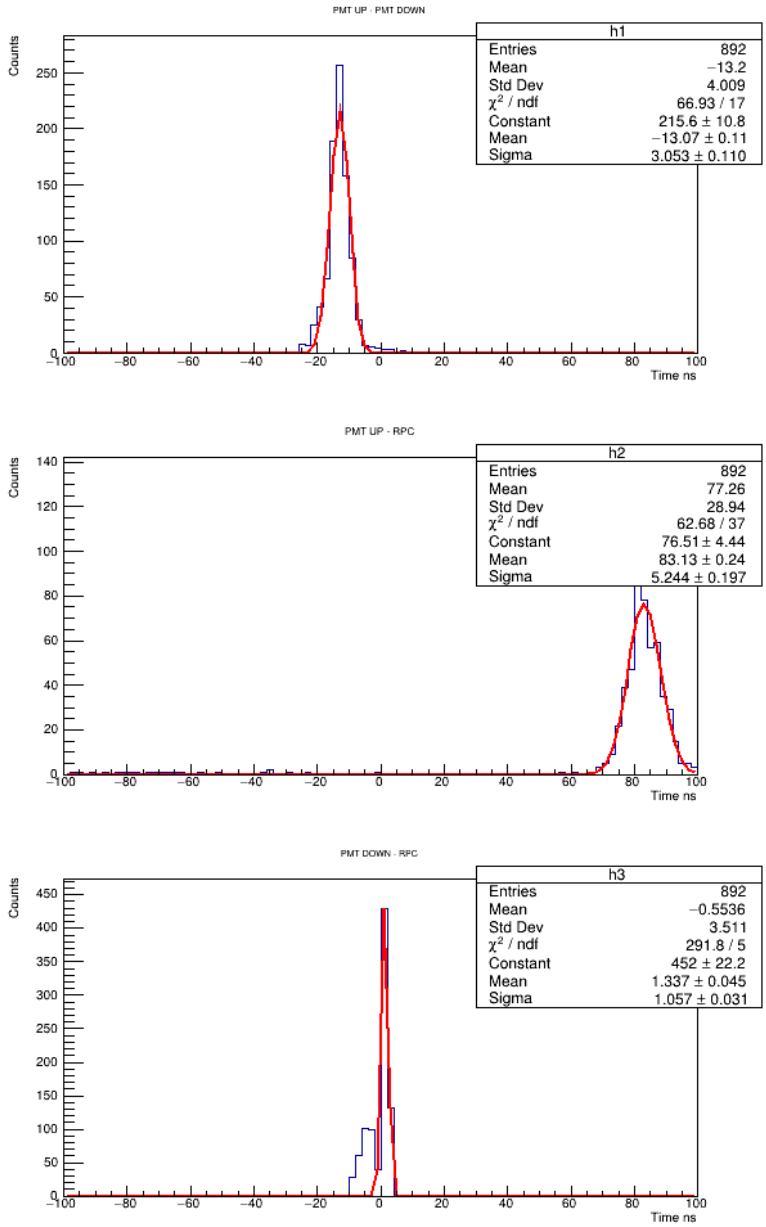

Figure A.12: Counts vs. Time resolution at 11.5 kV in pad number six.

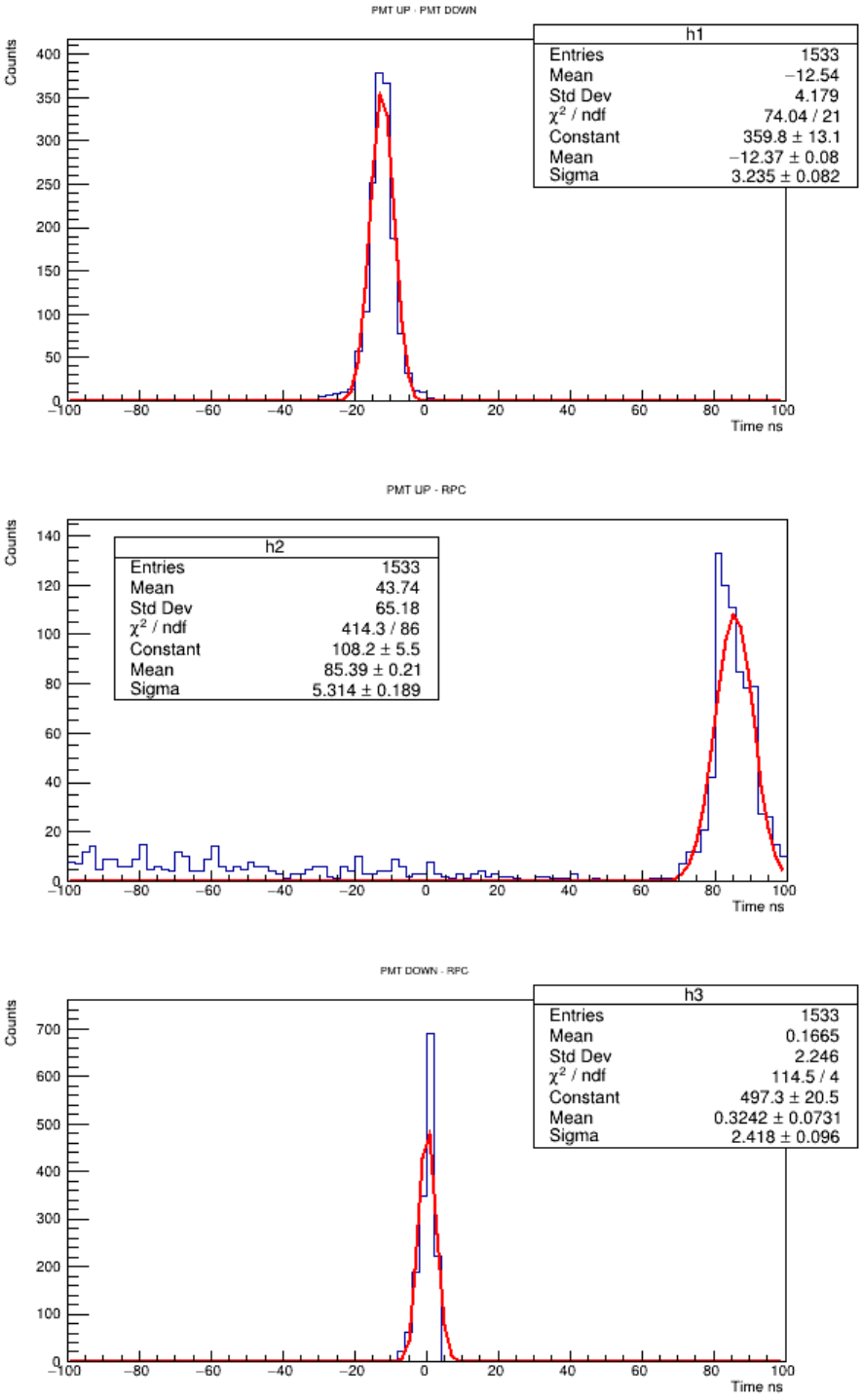

Figure A.13: Counts vs. Time resolution at 12 kV in pad number six.

A.2 CERN MRPC

A.2.1 First run

Time resolution on strip G.

For the time resolution graph at 12.8 kV, we got 104 entries, the mean of the data is at the left of the mean of the Gaussian curve, the adjustment is closer to one and the time resolution was of 10.87 ns.

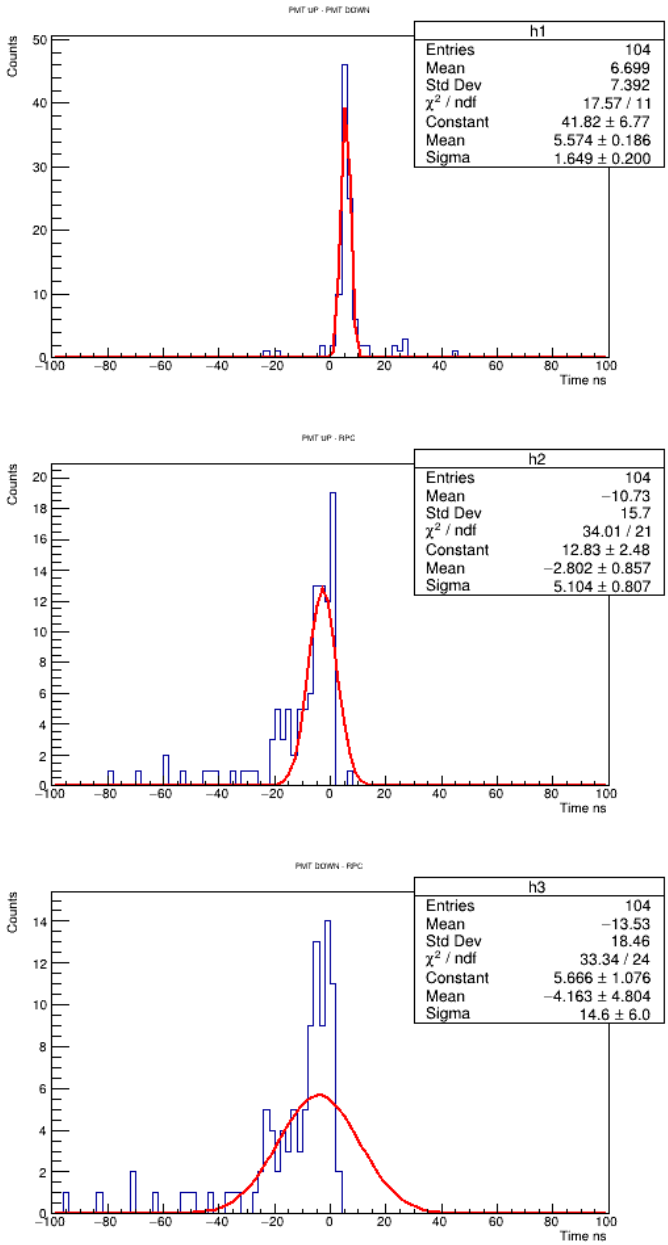

Figure A.14: Counts vs. Time resolution at 12.8 kV on strip G.

The same about the mean of the data and the mean of the gaussian curve goes for almost all of the first run of the strip G. In the case of 14 kV, since the sigmas are bigger, the time resolution is 13.21 ns, and only the graph between the PMT DOWN and RPC has a $\chi/ndf = 2$.

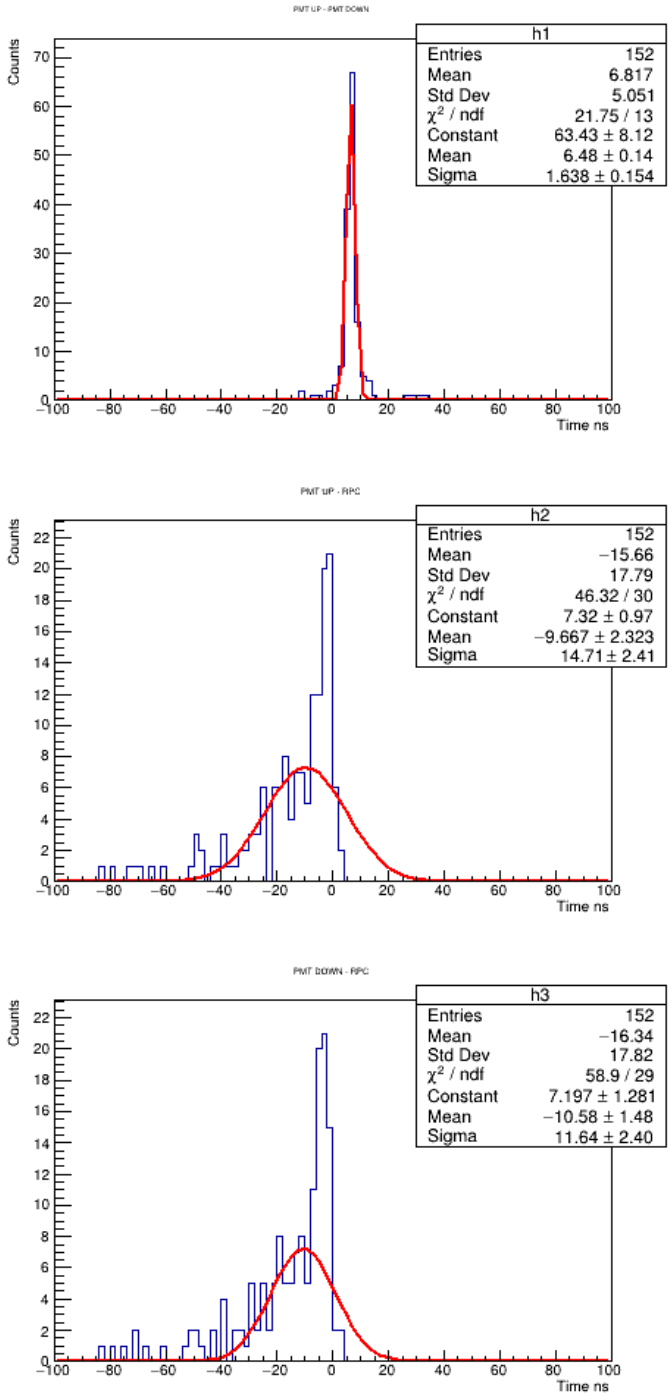

Figure A.15: Counts vs. Time resolution at 14 kV on strip G.

For 14.3 kV, the χ/ndf adjustment is almost 1 in the three cases, the mean from the Gaussian curve and the mean from the data were close, and the time resolution was of 0.88 ns.

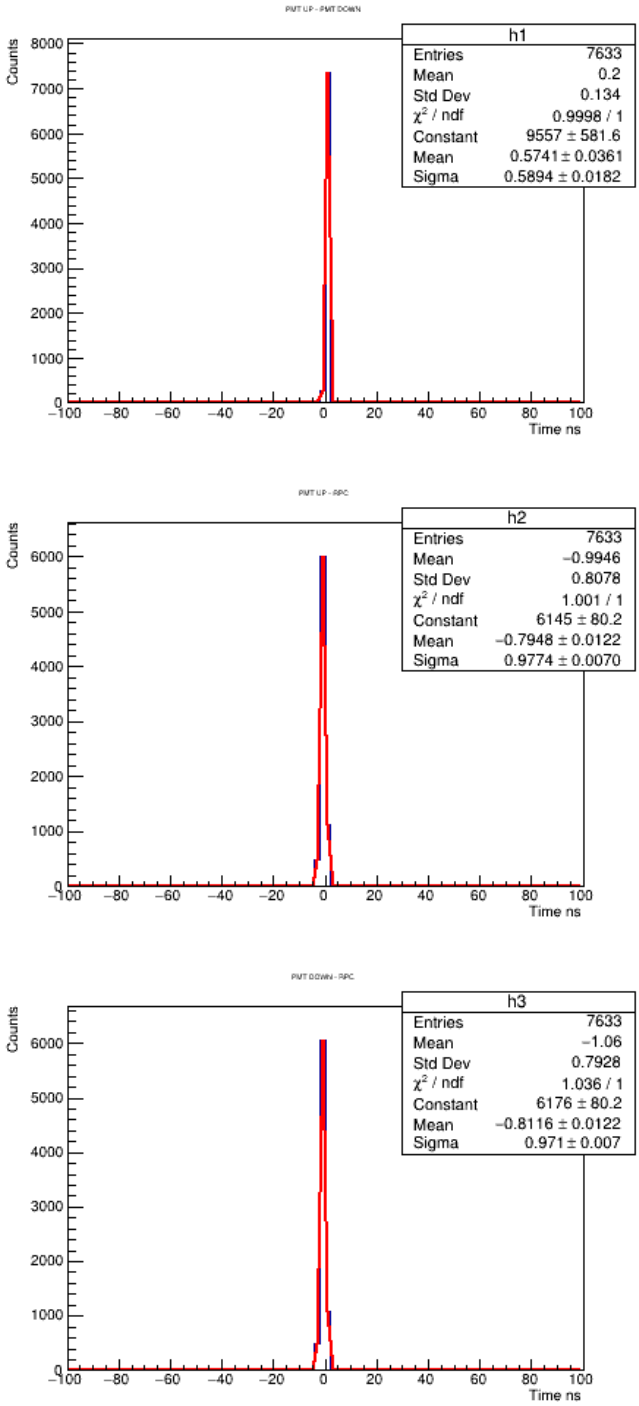

Figure A.16: Counts vs. Time resolution at 14.3 kV on strip G.

The same goes for the plots of 14.6 kV, even the time resolution is the same, the only difference is that we got more entries.

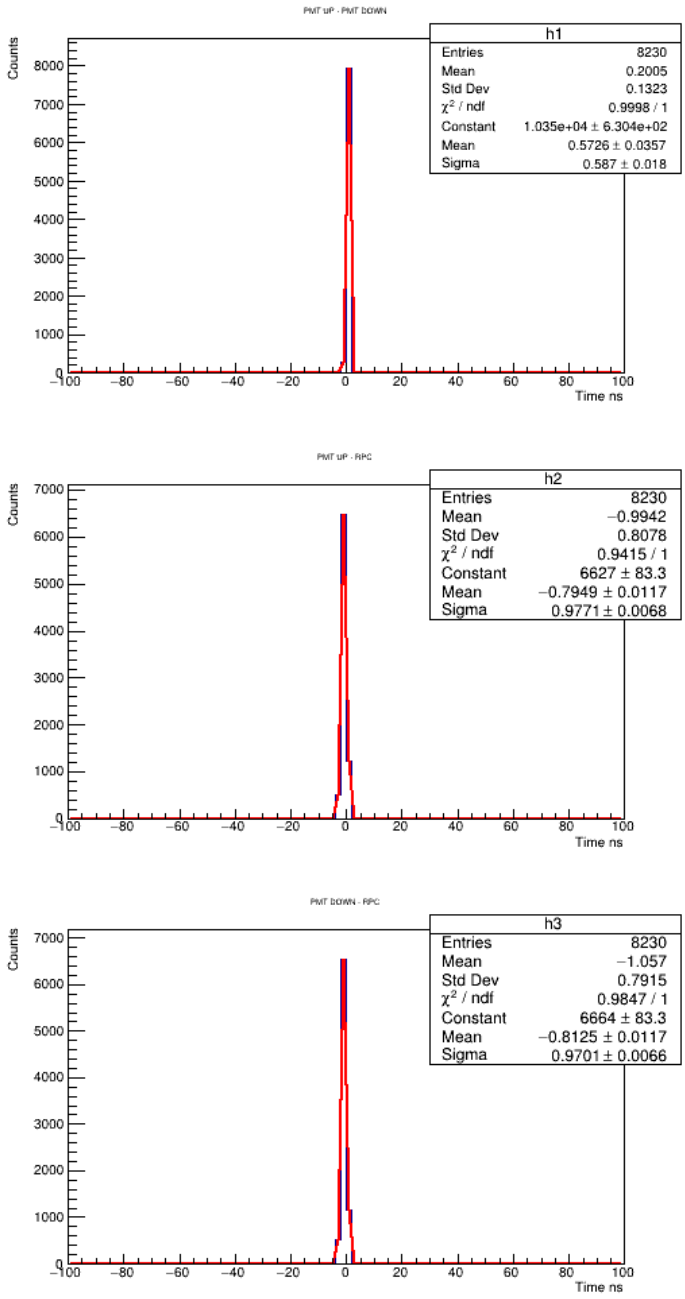

Figure A.17: Counts vs. Time resolution at 14.6 kV on strip G.

We had less entries since we took data for less days, so the adjustment is even 2 in some cases, and the plots for the PMTs and RPC are the only ones where the media of the data is at the left of the media of the Gaussian curve, and the time resolution was 1.37 ns.

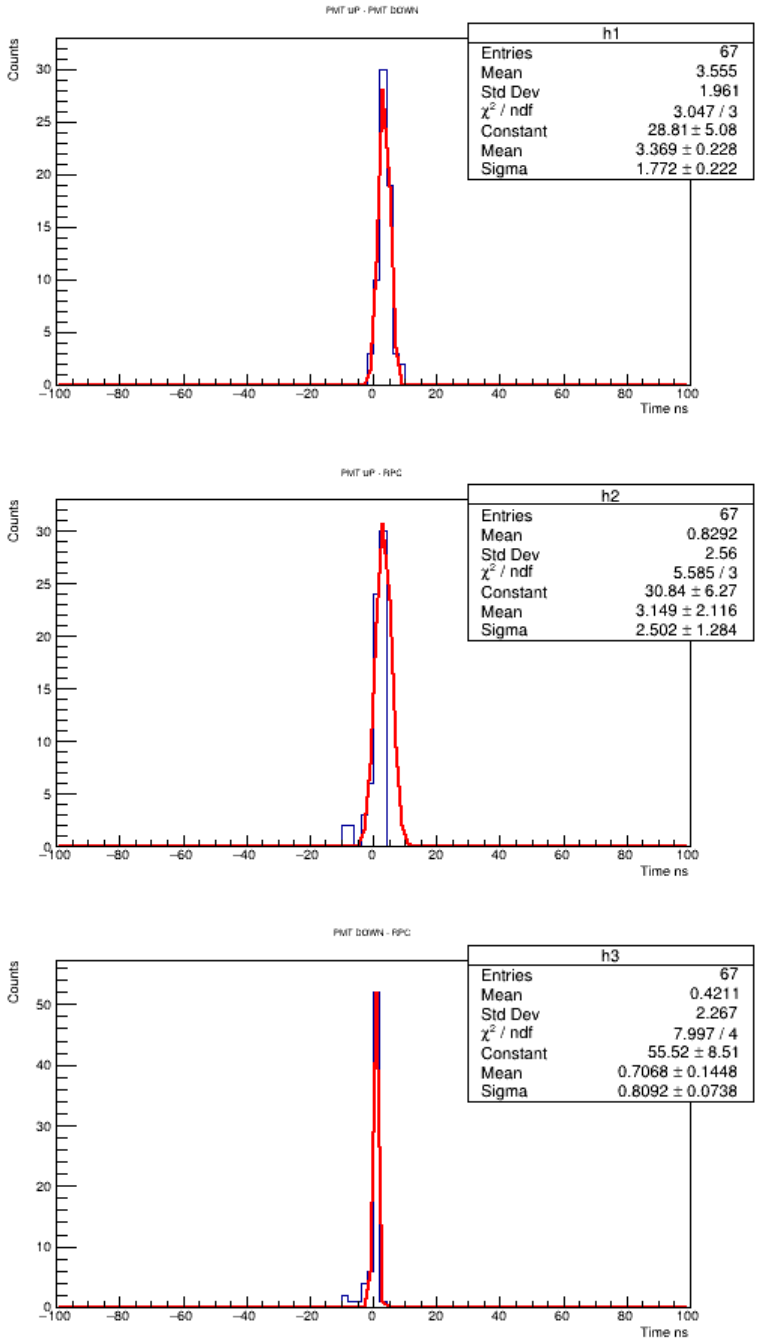

Figure A.18: Counts vs. Time resolution at 15 kV on strip G.

Time resolution on strip I.

This was the test with the least number of coincidences, whatsoever the time resolution was of 2.65 ns. The media of the Gaussian is at the left of the media of the data.

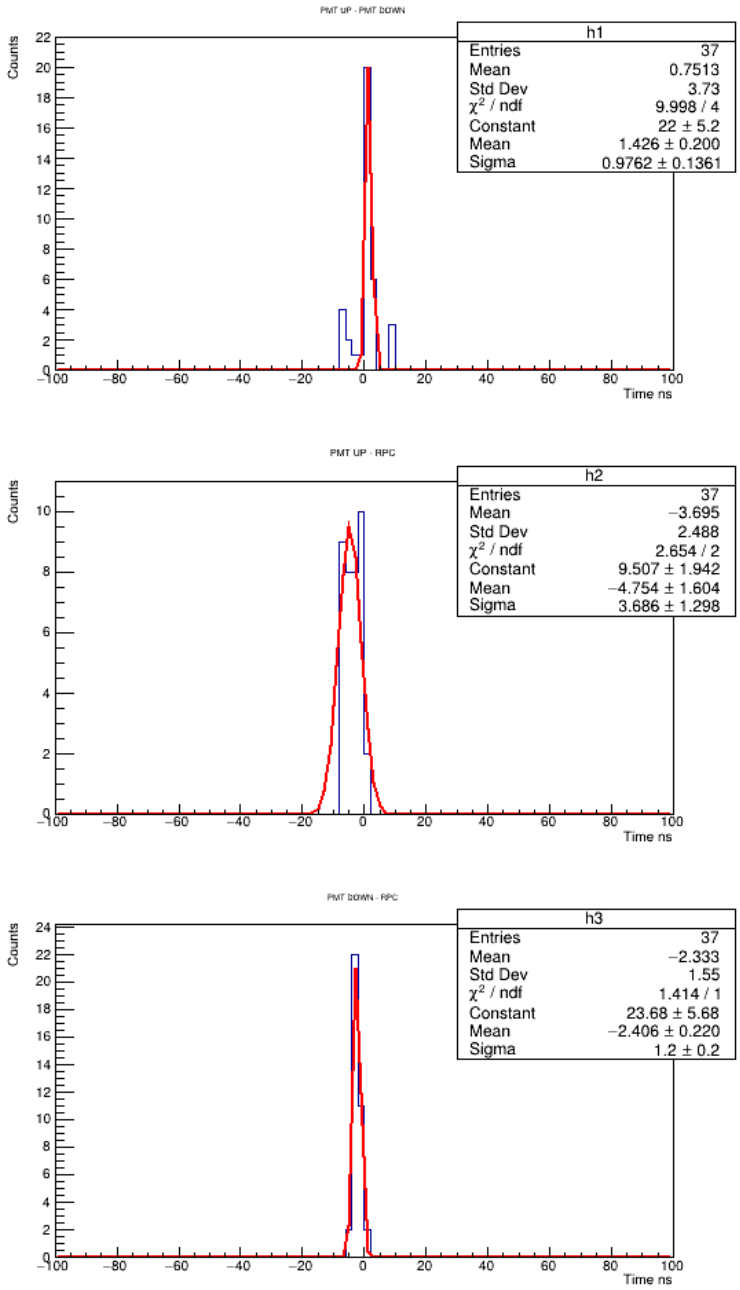

Figure A.19: Counts vs. Time resolution at 14 kV on strip I.

The adjustments of these plots is better than the first one, the Gaussian curve media is at the right of the data media, and the time resolution was of 0.85 ns.

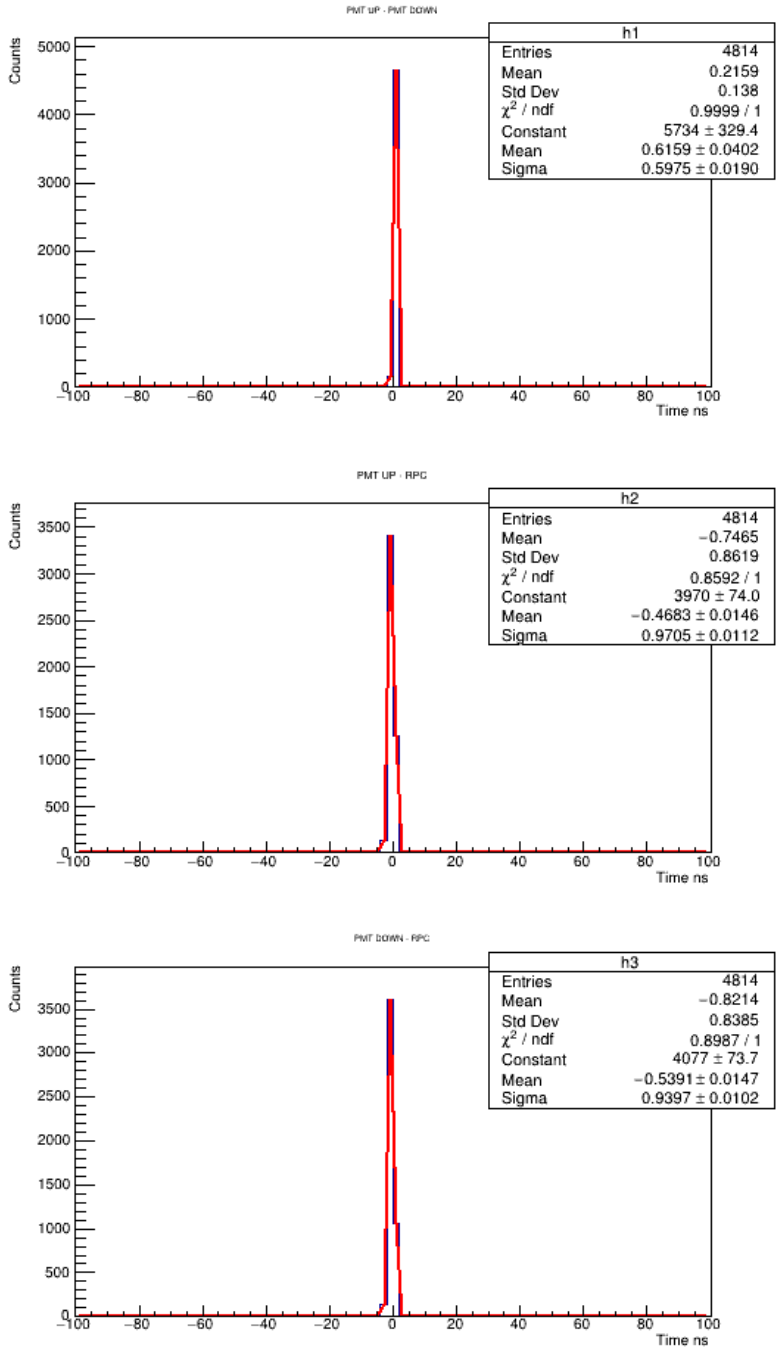

Figure A.20: Counts vs. Time resolution at 14.3 kV on strip I.

These plots are pretty similar to the previous ones, even the time resolution is the same, just with more entries because the voltage increased.

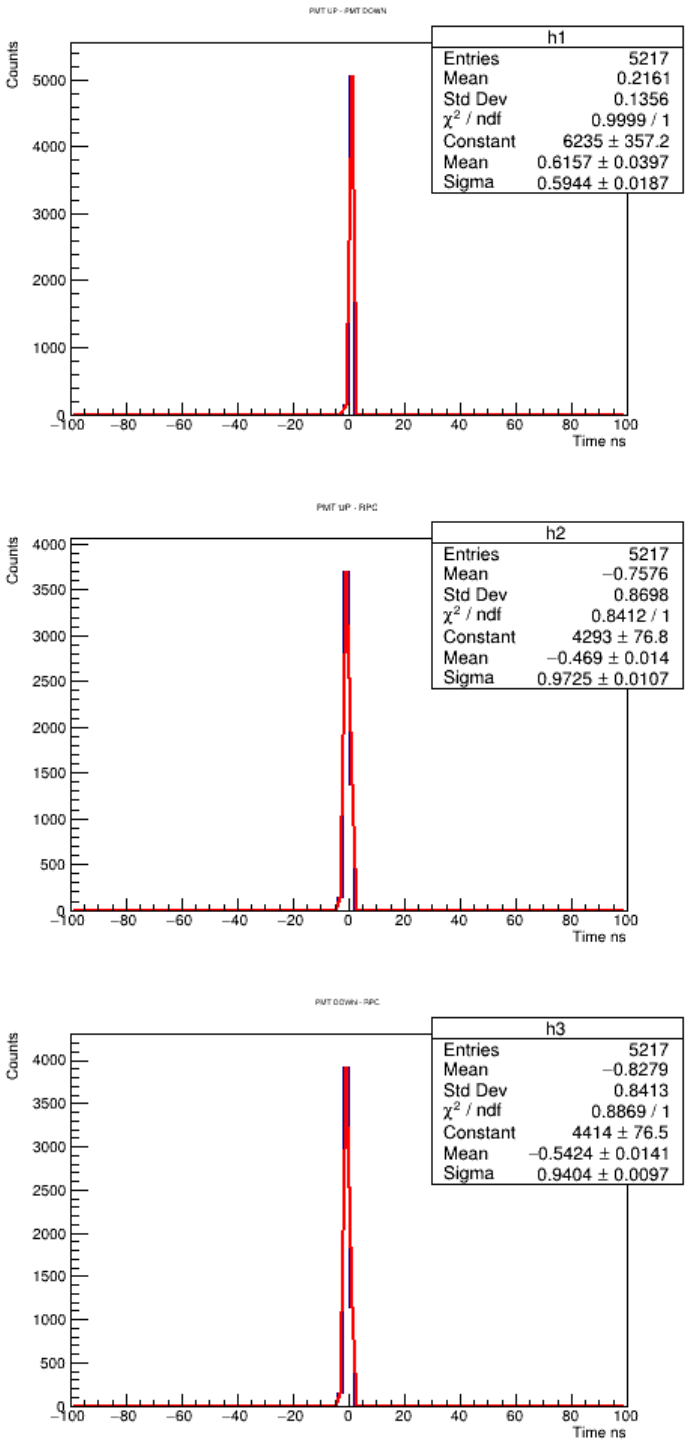

Figure A.21: Counts vs. Time resolution at 14.6 kV on strip I.

Again, the Gaussian curve media is on the right side, the adjustment is of 4, we had less entries and the time resolution was of 0.58 ns.

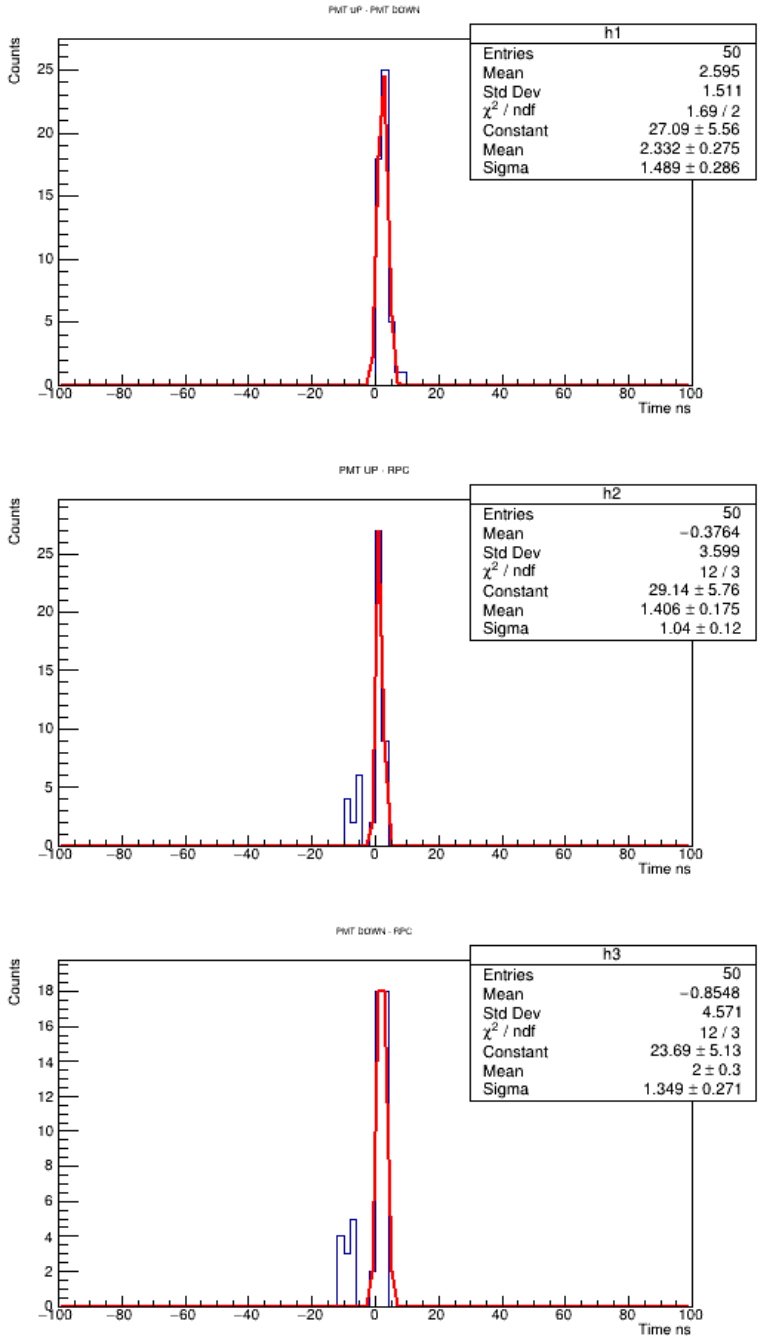

Figure A.22: Counts vs. Time resolution at 15 kV on strip I.

A.2.2 Second run

Time resolution on strip G.

The data media is at the left of the Gaussian curve media in all of the plots of the second run of the G strip between the MRPC and the PMTs, with a $\chi/ndf = (1, 1, 2)$ and a time resolution of 1.24 ns.

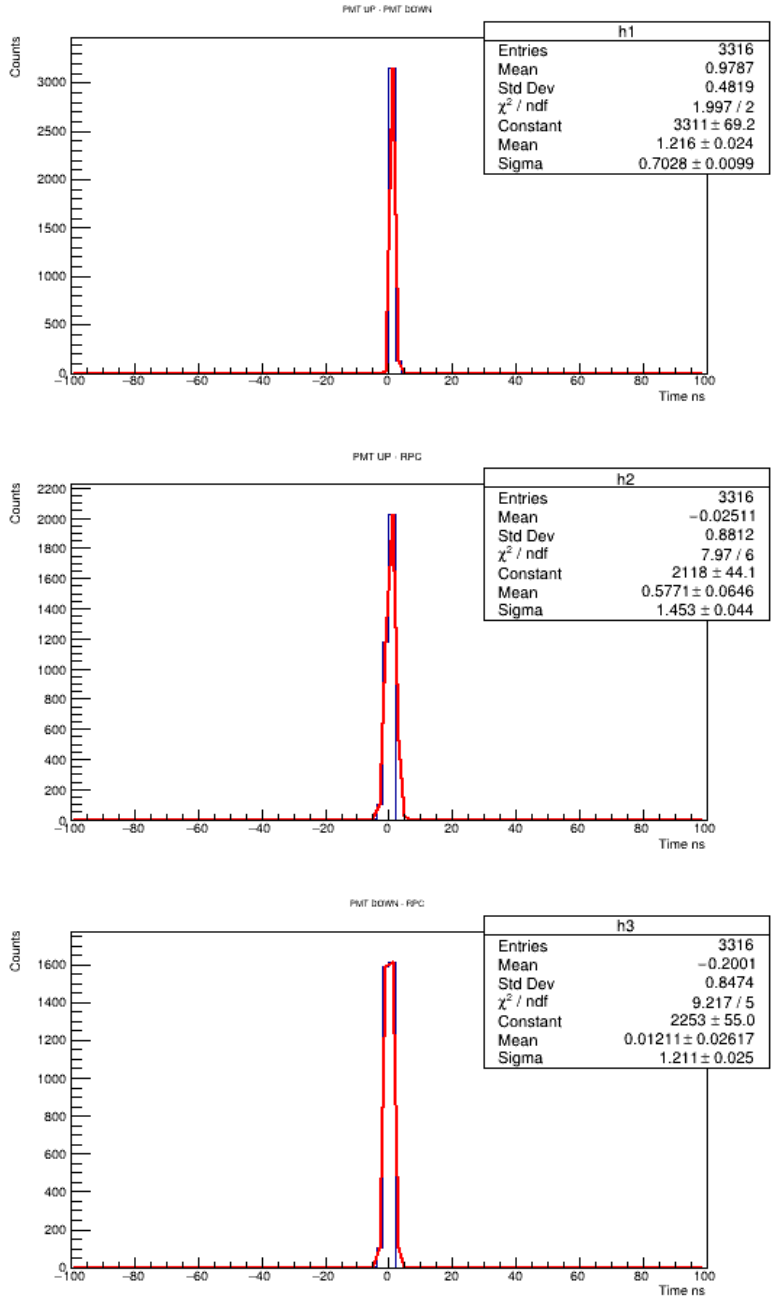

Figure A.23: Counts vs. Time resolution at 13.8 kV on strip G.

These plots have a $\chi/ndf = (1, 1.3, 1.2)$ and a time resolution of 1.08 ns, and less entries than the previous figure.

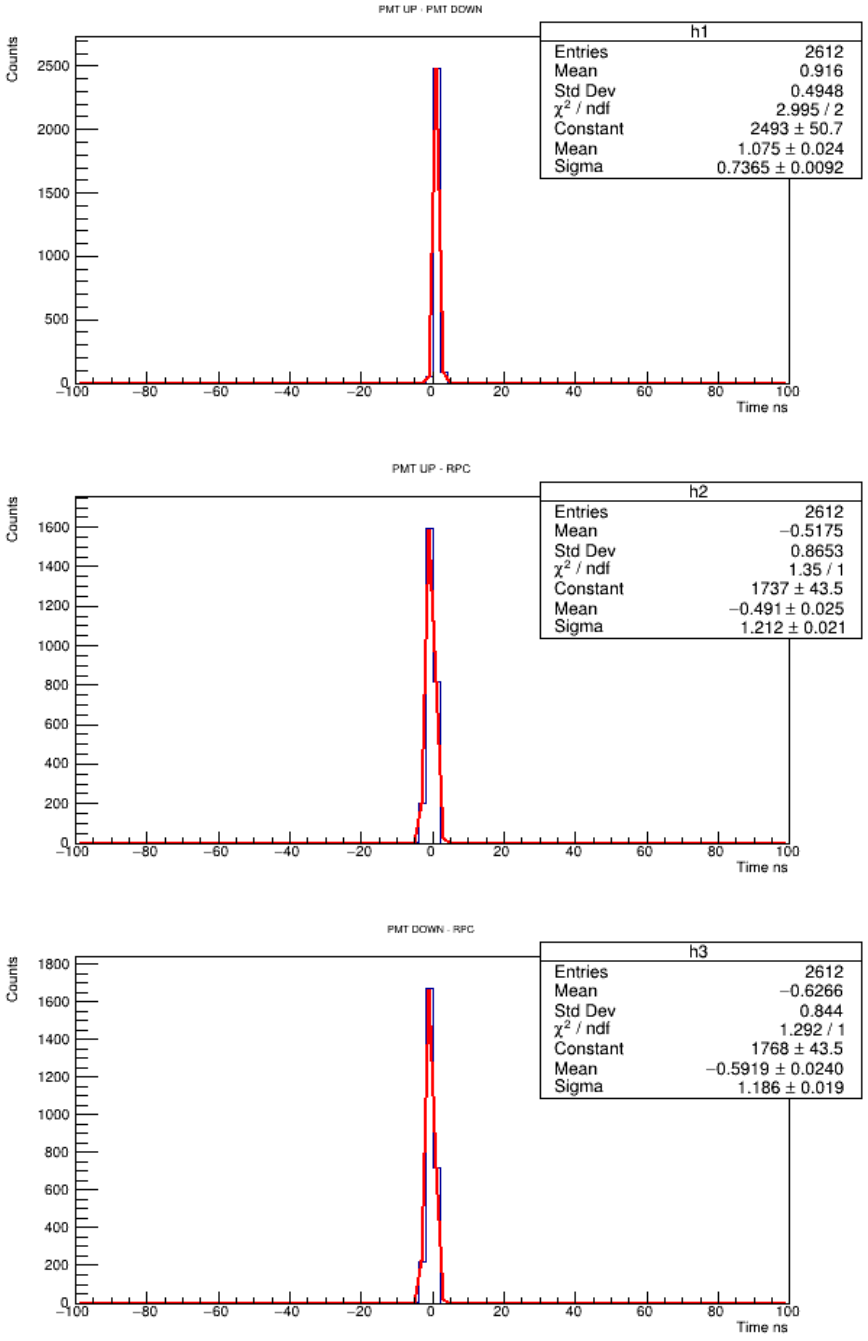

Figure A.24: Counts vs. Time resolution at 14.1 kV on strip G.

We got more entries in this case, with a $\chi/ndf = (1.2, 22.5, 23)$, which is a bigger adjustment than the previous ones, and they have a time resolution of 0.42 ns

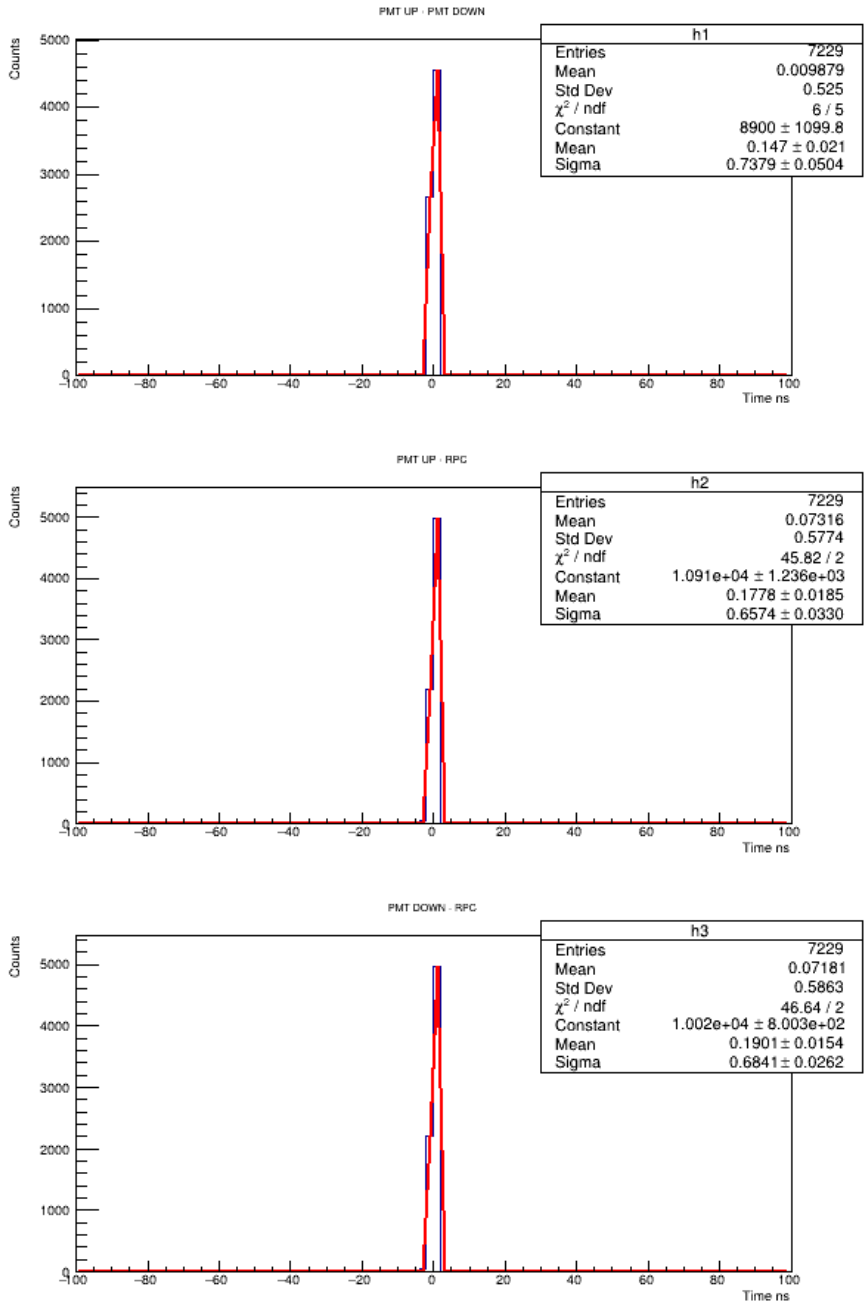

Figure A.25: Counts vs. Time resolution at 14.2 kV on strip G.

The time resolution of these plots is of 0.78 ns and the adjustment is better than the previous ones, $\chi/ndf = (1.8, 1, 1)$.

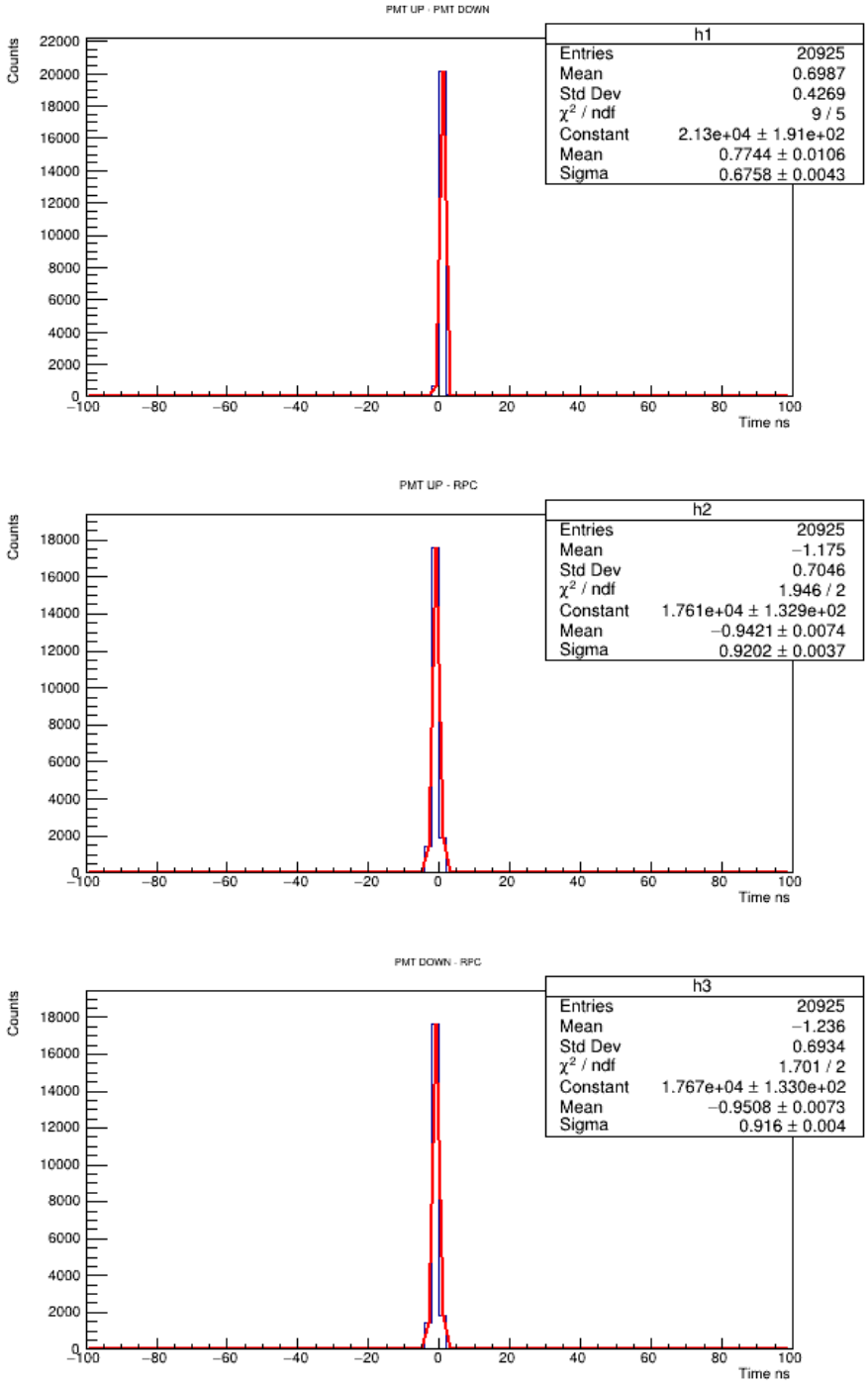

Figure A.26: Counts vs. Time resolution at 14.3 kV on strip G.

These ones has the best adjustment of all of the plots, with a $\chi/ndf = (1, 1, 1)$ and a time resolution of 0.58 ns.

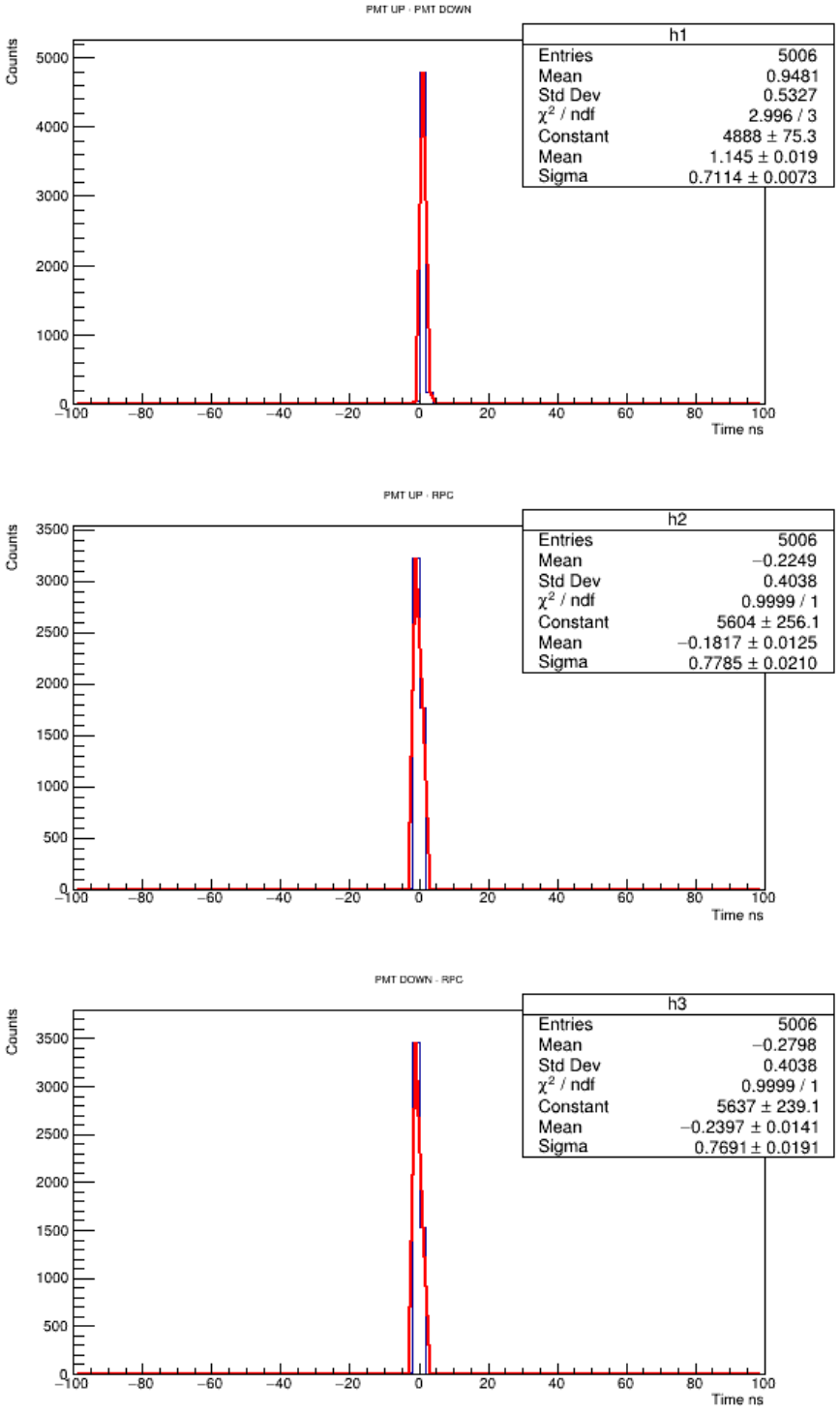

Figure A.27: Counts vs. Time resolution at 14.4 kV on strip G.

Finally, these plots has the biggest number of entries, with an adjustment of $\chi/ndf = (1.5, 1.2, 1.1)$ and a time resolution of 0.76 ns.

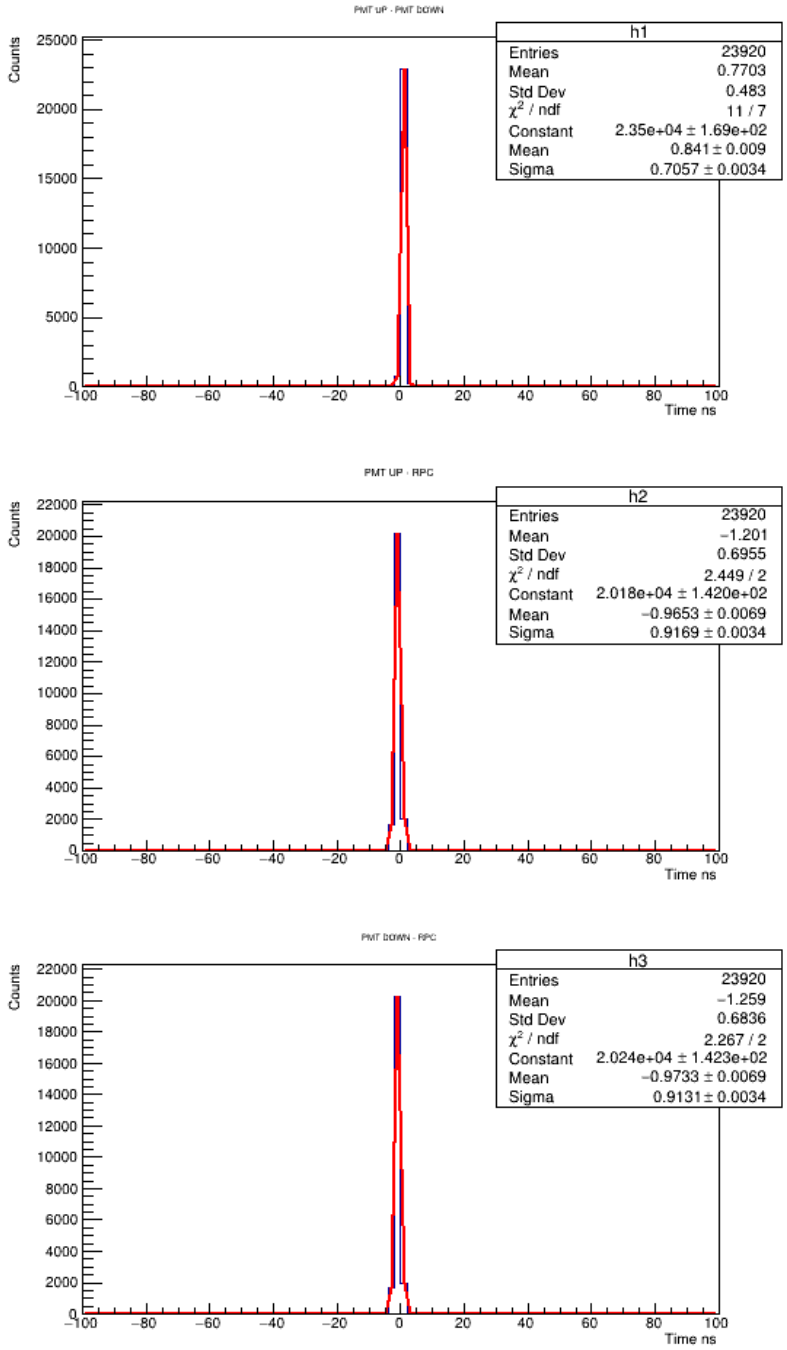

Figure A.28: Counts vs. Time resolution at 14.6 kV on strip G.

Time resolution on strip I.

We had less coincidences in he strip I, compared to strip G, we tried to keep a good adjustment of $\chi/ndf = (1, 0.7, 0.9)$, with a time resolution of 26.76 ns, which was our biggest value of time resolution n both runs. The Gaussian curve media is at the right of the data media, like in almost all of the plots between the MRPC and the PMTs.

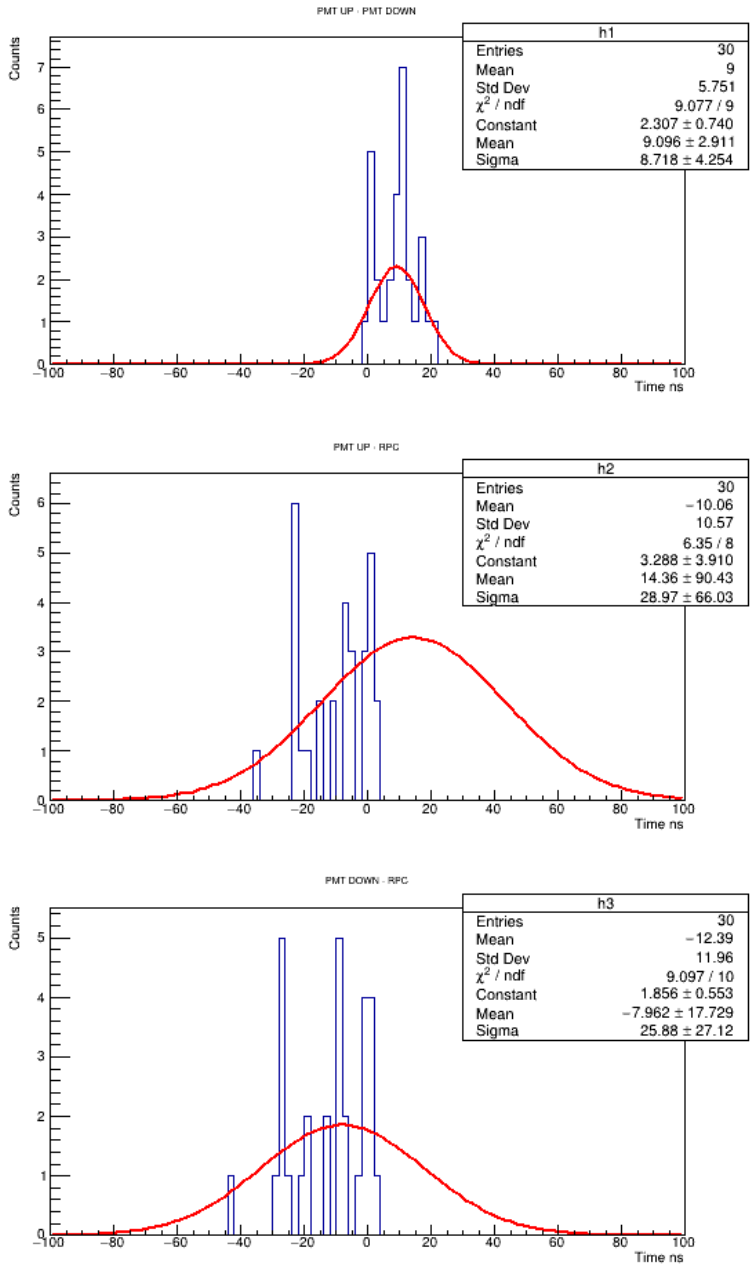

Figure A.29: Counts vs. Time resolution at 13.8 kV on strip I.

We got eleven times the coincidences compared to the last one, and equally the efficiency increased almost fourteen times. The adjustment was of $\chi/ndf = (1, 2.6, 3.2)$, with a time resolution of 2.03 ns.

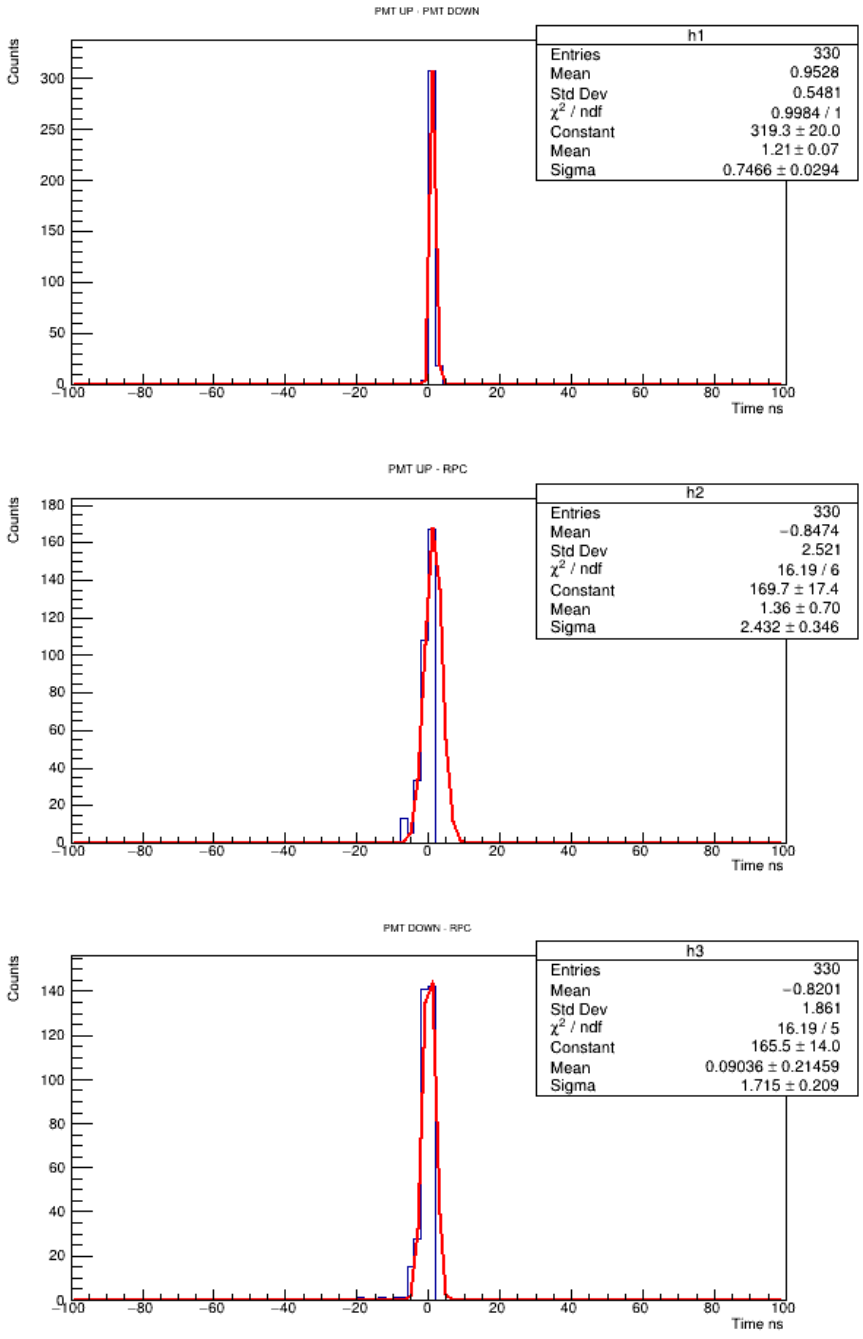

Figure A.30: Counts vs. Time resolution at 14.1 kV on strip I.

And again, the number of coincidences increased about ten times, and the efficiency increased about 4 times, with a time resolution of 0.79 ns, with an adjustment $\chi/ndf = (1, 17.4, 18.7)$. The plot between the MRPC and the PMT UP is one of the plots which has the Gaussian curve media at the left of the data mean, but its just for a difference of 0.02.

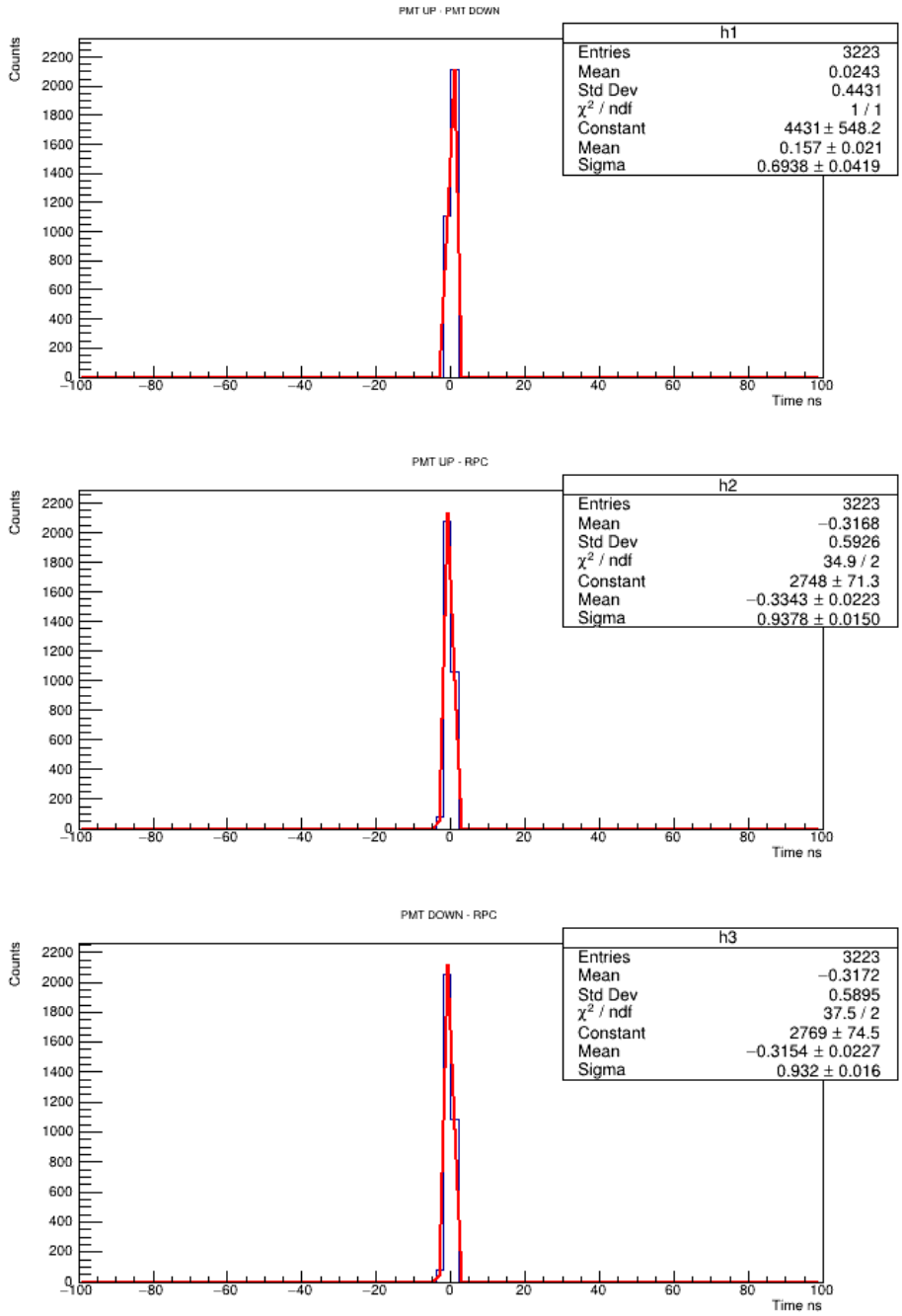

Figure A.31: Counts vs. Time resolution at 14.2 kV on strip I.

The number of coincidences increased three times, while the efficiency increased 1.3 times and the time resolution was 0.73 ns, the adjustment was better in these cases.

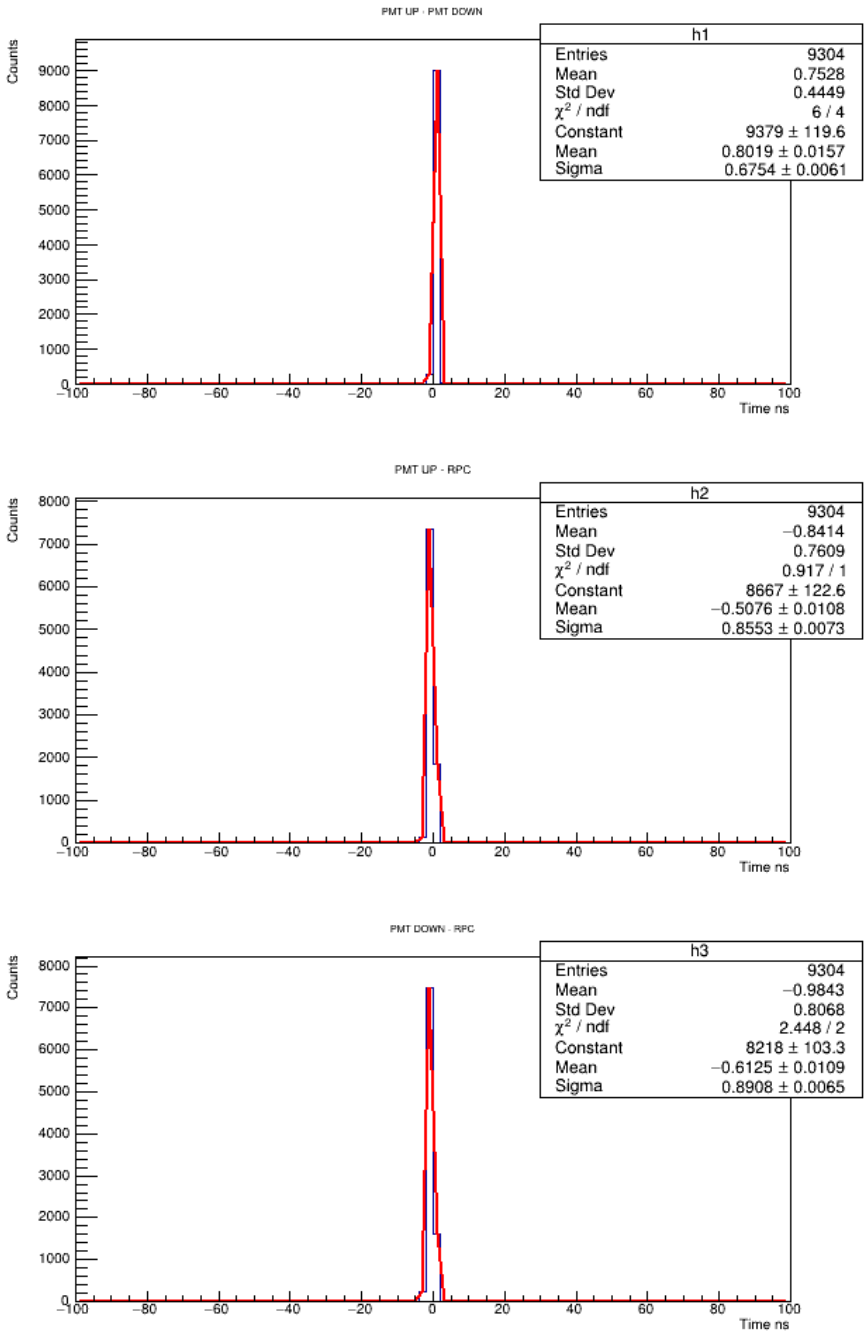

Figure A.32: Counts vs. Time resolution at 14.3 kV on strip I.

We had less coincidences here, but the efficiency was constant. The time resolution was 0.64 ns with a perfect adjustment.

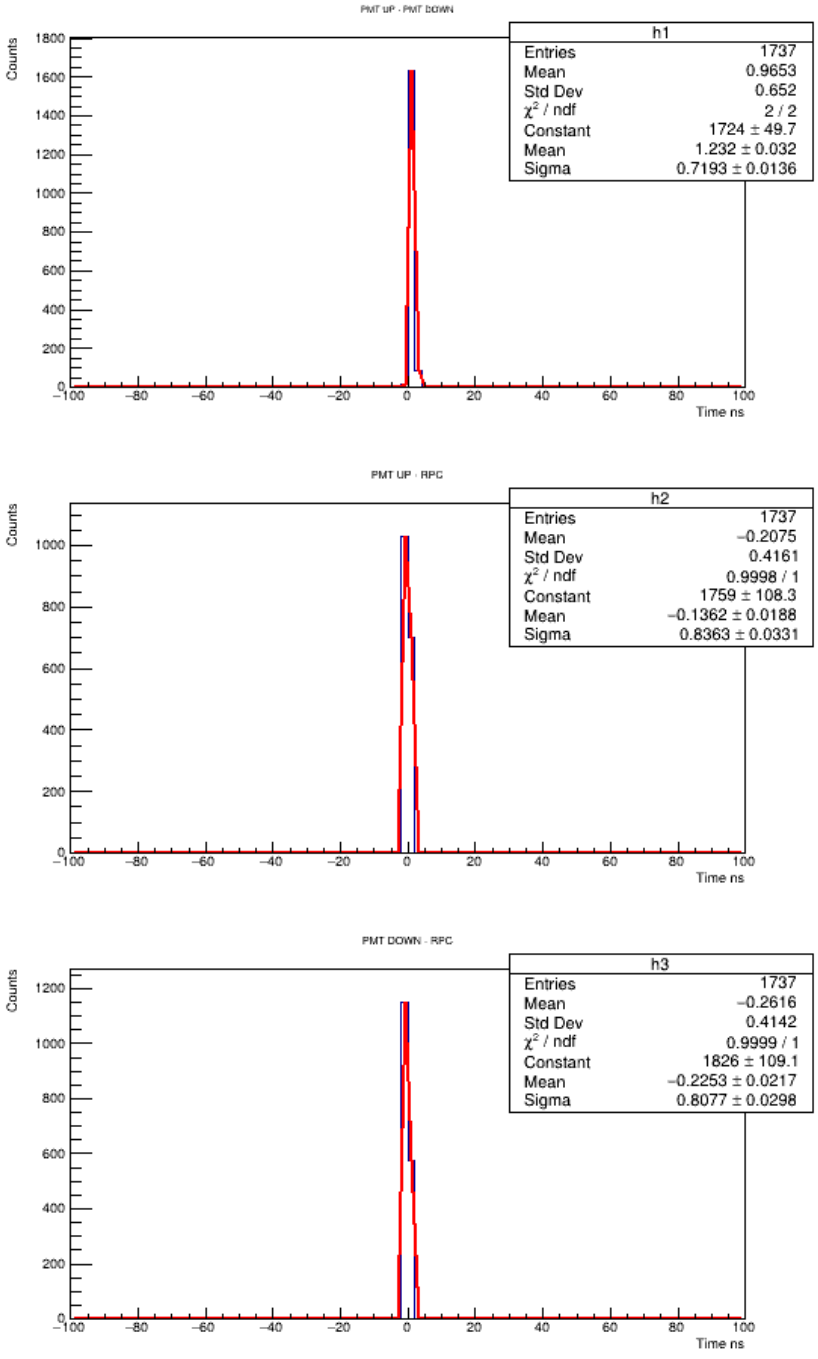

Figure A.33: Counts vs. Time resolution at 14.4 kV on strip I.

The number of coincidences increased was ten times higher than the last one, and the efficiency increased 1.2 times, and the time resolution was of 0.71 ns.

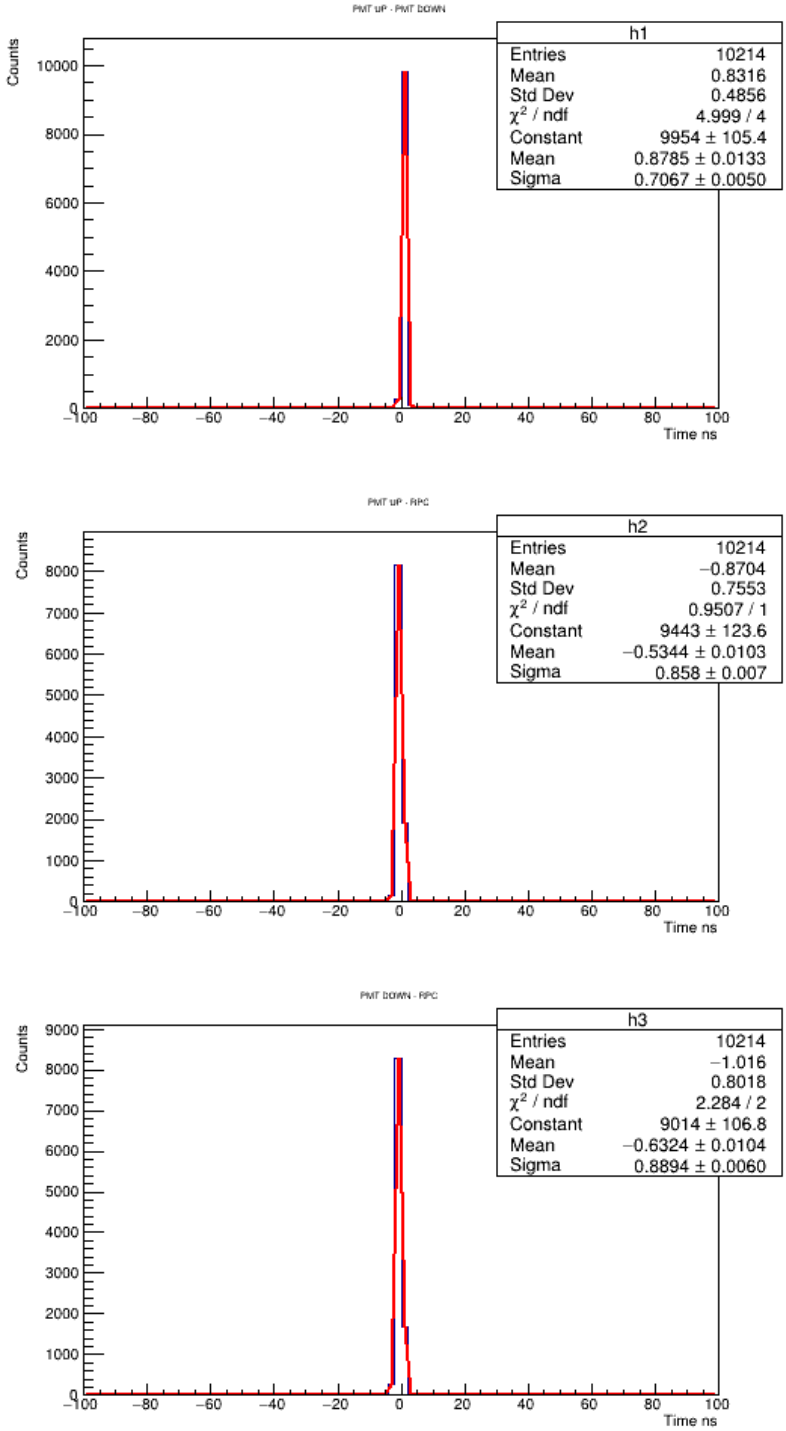

Figure A.34: Counts vs. Time resolution at 14.6 kV on strip I.

Appendix B

Charge

Here we have the charge plots for each pad, in the case of the ALICE-BUAP MRPC, or strip, in the case of the CERN MRPC2, at different applied voltages.

B.1 ALICE-BUAP MRPC

Charge of pad 1 is presented as followed.

For the pad number one, we got a $\chi^2/ndf = (1.34, 10.78, 6.602)$ for the applied voltage 11, 11.5 and 12 kV respectively, where 1 means a good adjustment. The number of entries, or coincidences, increases from 1500 to almost 3500. Just as in the plots from time resolution, the mean is the media of the data, and the MPV is the gain of the RPC, and the one we plotted and showed in the charge sub-chapters. For the 11 kV we can see the bins of the charge clearly, for 11.5 kV we can see the pedestal, or noise, of the data, and for 12 kV we got a very good fit of the charge vs. counts.

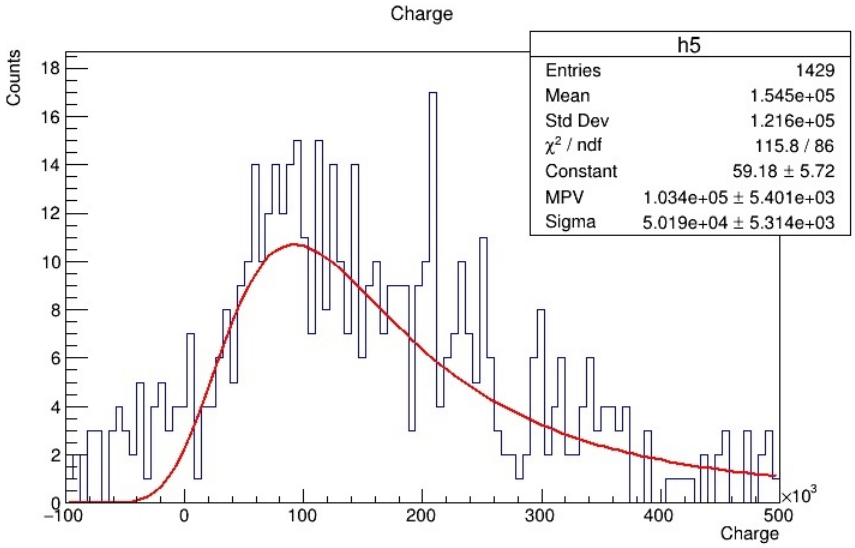

Figure B.1: Counts vs. charge at 11 kV in pad number one.

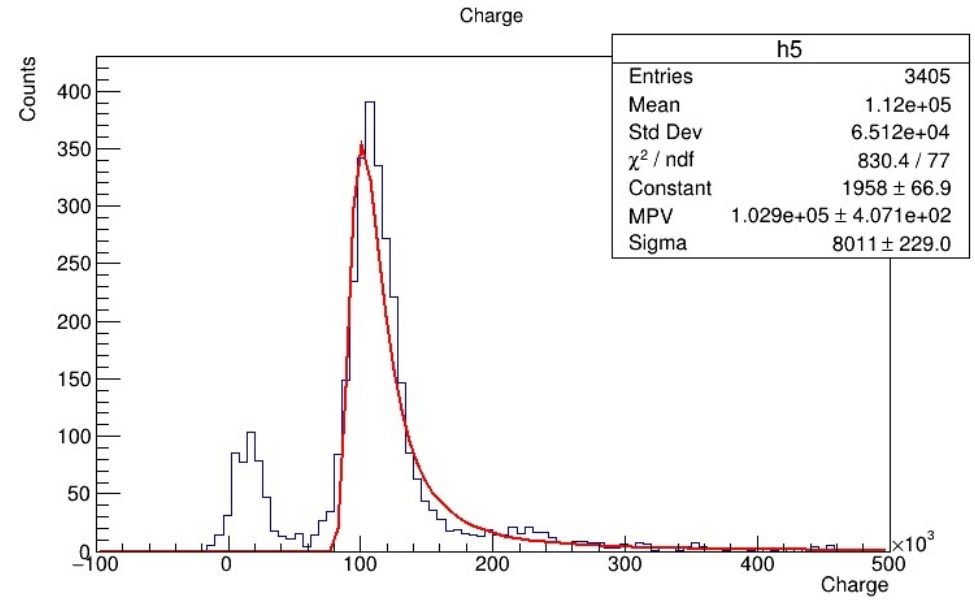

Figure B.2: Counts vs. charge at 11.5 kV in pad number one.

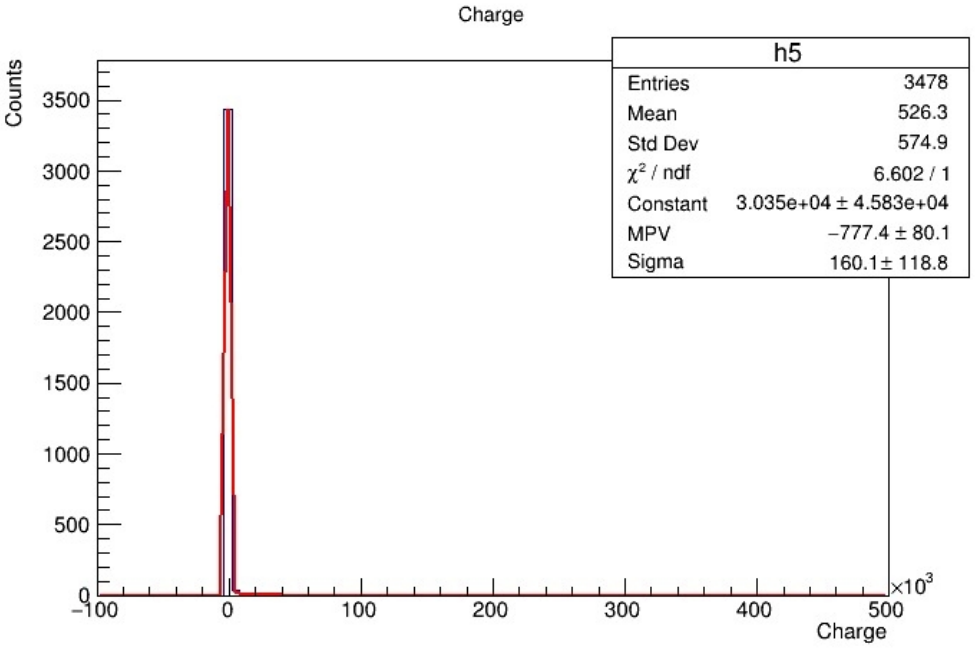

Figure B.3: Counts vs. charge at 12 kV in pad number one.

Charge of pad 2.

The number of coincidences increased between the plots of 11 and 11.5 kV, but decreased a little between the ones from 11.5 and 12 kV. For the applied voltage we got an adjustment of $\chi^2/ndf = (1.29, 1.34, 1.42)$, which means it was a very good adjustment,

in all of the plots we can see the bins of the charge, and the height of the Gaussian increases.

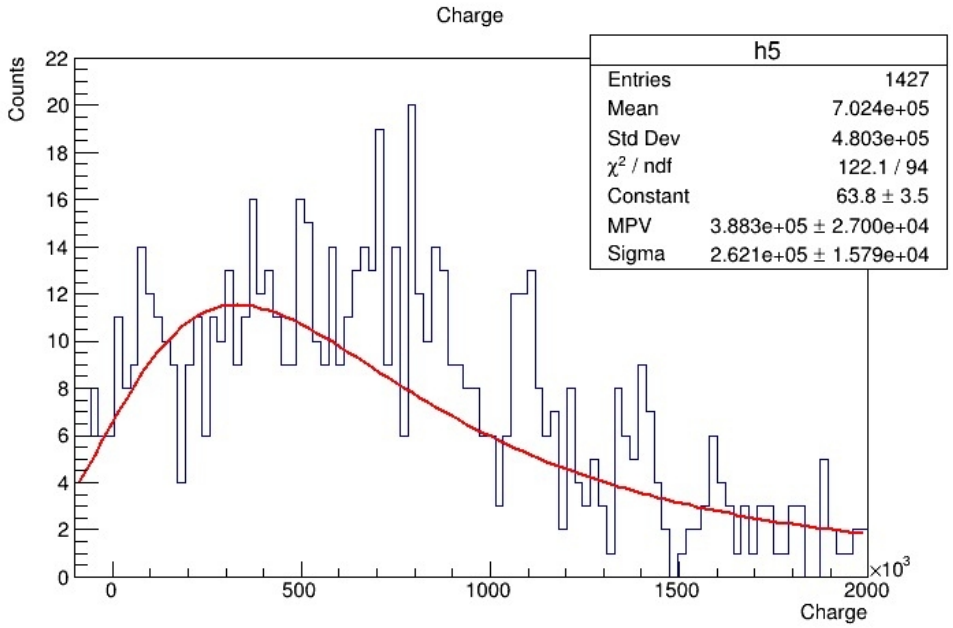

Figure B.4: Counts vs. charge at 11 kV in pad number two.

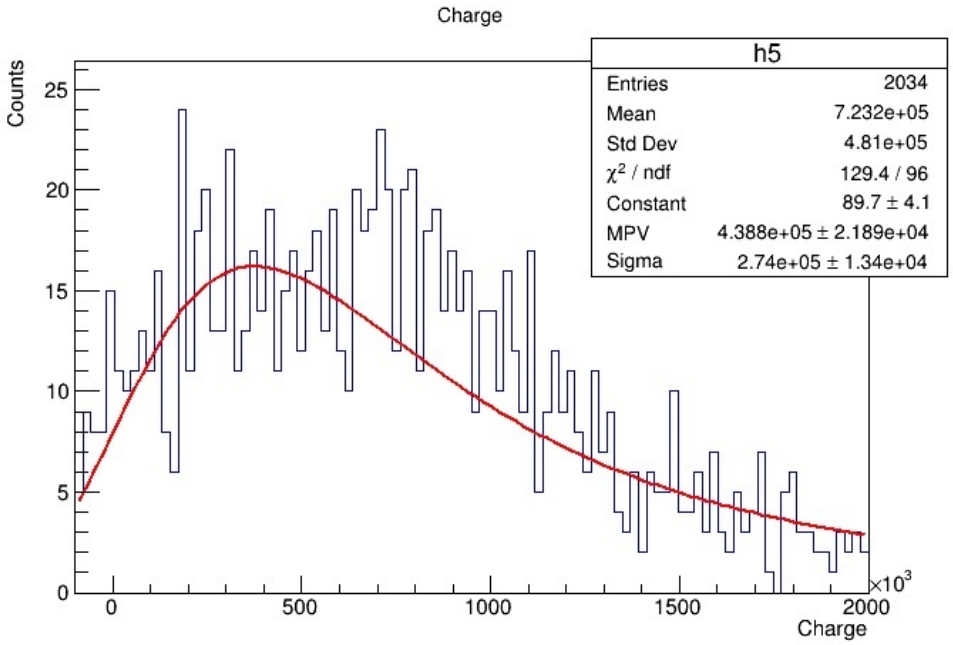

Figure B.5: Counts vs. charge at 11.5 kV in pad number two.

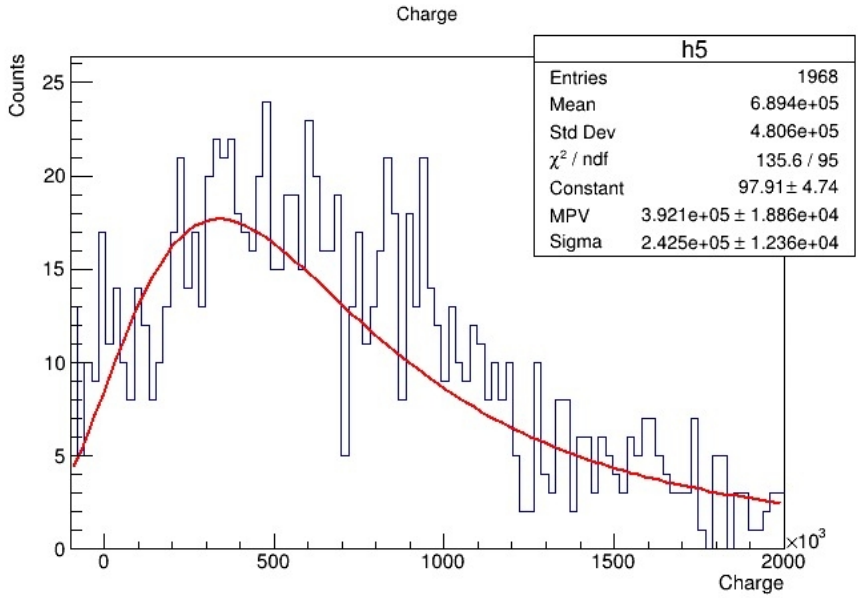

Figure B.6: Counts vs. charge at 12 kV in pad number two.

Charge of pad 3.

We got the same number of entries as the ones from 11 kV from the previous plots. It has an adjustment of 1.028, which is the best adjustment of the charge from the ALICE.BUAP MRPC until now, and the bins can be clearly seen.

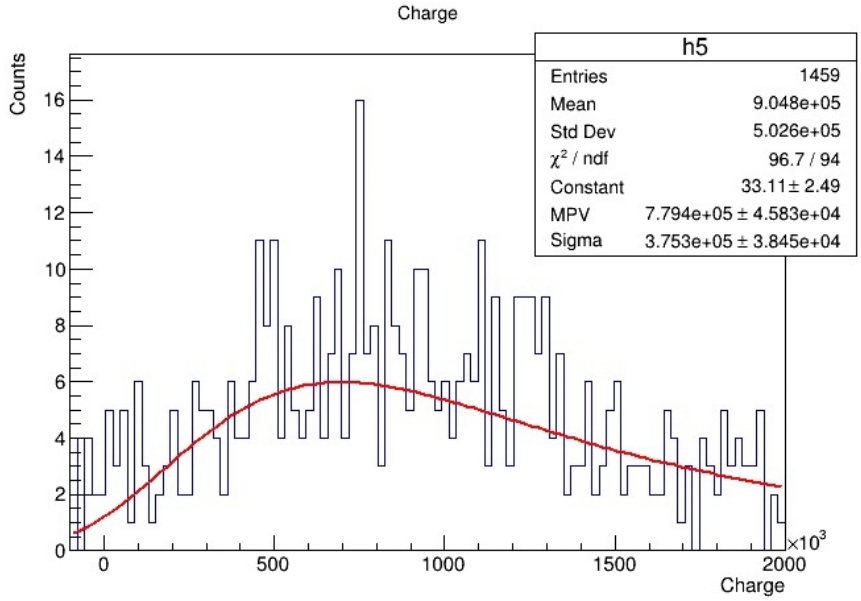

Figure B.7: Counts vs. charge at 12 kV in pad number three.

Charge of pad 4.

The number of entries increases a lot from 11 to 12 kV in this pad, the adjustments are $\chi^2/ndf = (21.76, 3.53, 14.26)$ respectively. At 11 kV, the adjustment is small, we still got a some data above the Gaussian curve, at 11.5 kV, we got two peaks of data and the Gaussian curve between them, and at 12 kV, we still got two peaks but one is clearly smaller, so the Gaussian curve stays at the bigger data peak.

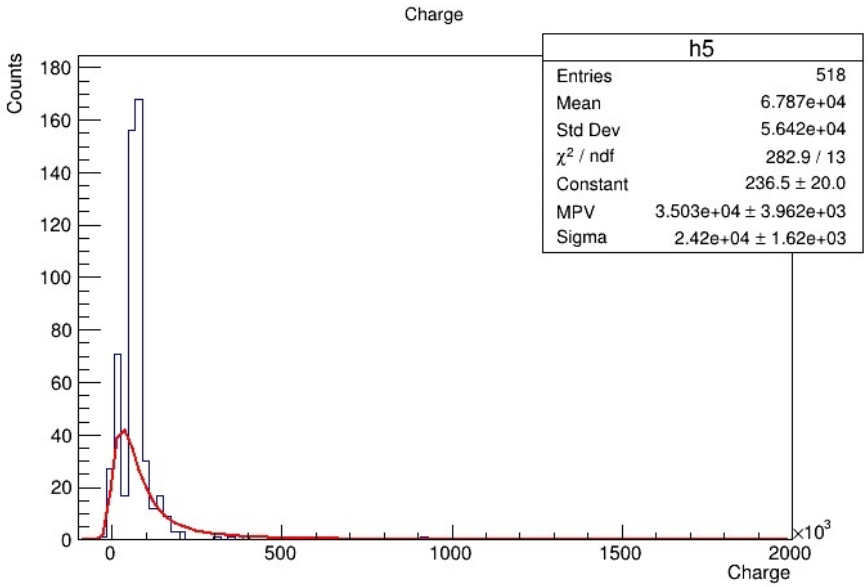

Figure B.8: Counts vs. charge at 11 kV in pad number four.

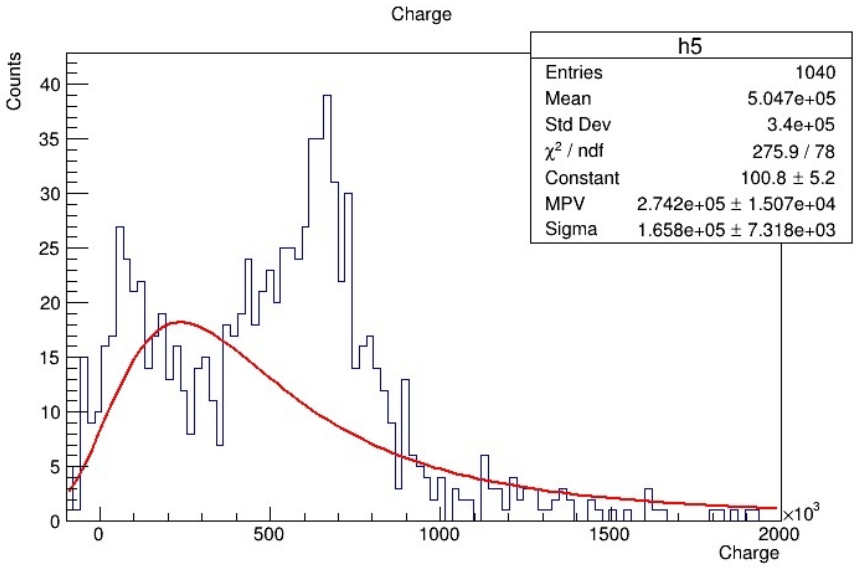

Figure B.9: Counts vs. charge at 11.5 kV in pad number four.

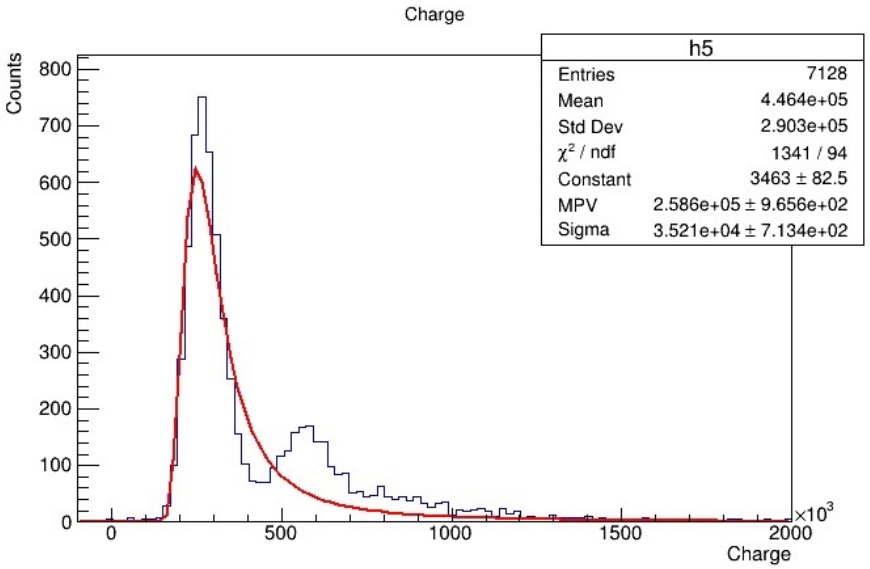

Figure B.10: Counts vs. charge at 12 kV in pad number four.

Charge of pad 6.

For all of these plots at pad six, we got two peaks of data, one bigger than the other and the adjustment goes to these ones, it just changed at the last one, where the two peaks are almost the same but the gaussian adjust goes to the first and smaller peak. Their adjustment was $\chi^2/ndf = (7.35, 5.62, 12.63)$.

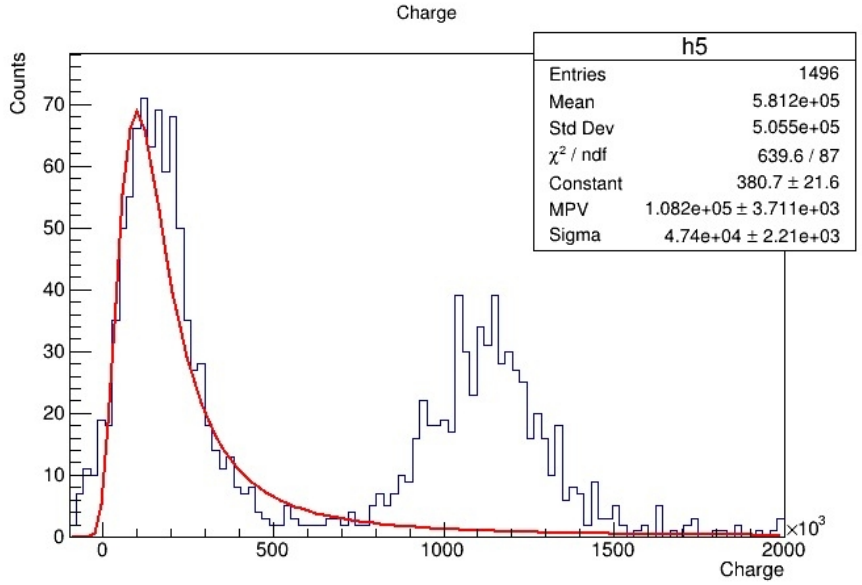

Figure B.11: Counts vs. charge at 11 kV in pad number six.

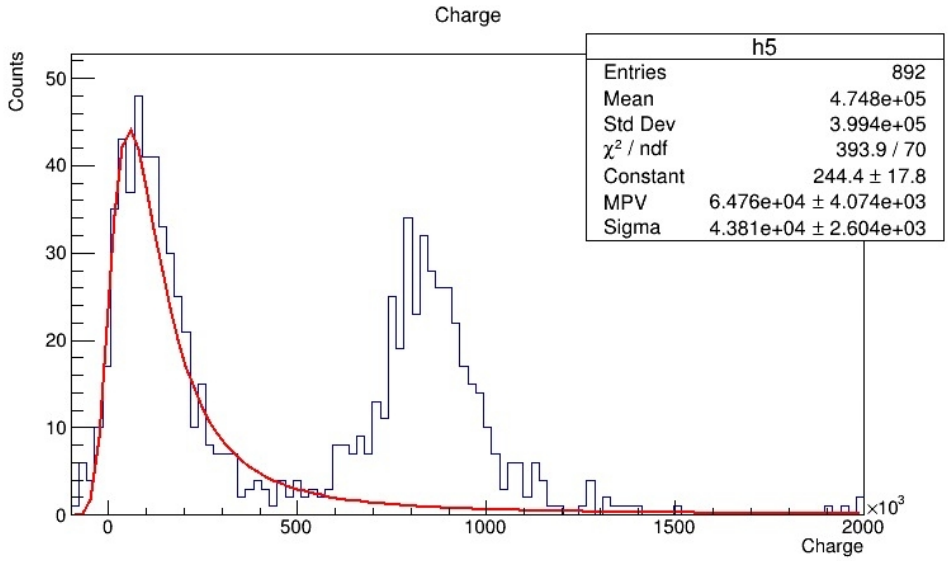

Figure B.12: Counts vs. charge at 11.5 kV in pad number six.

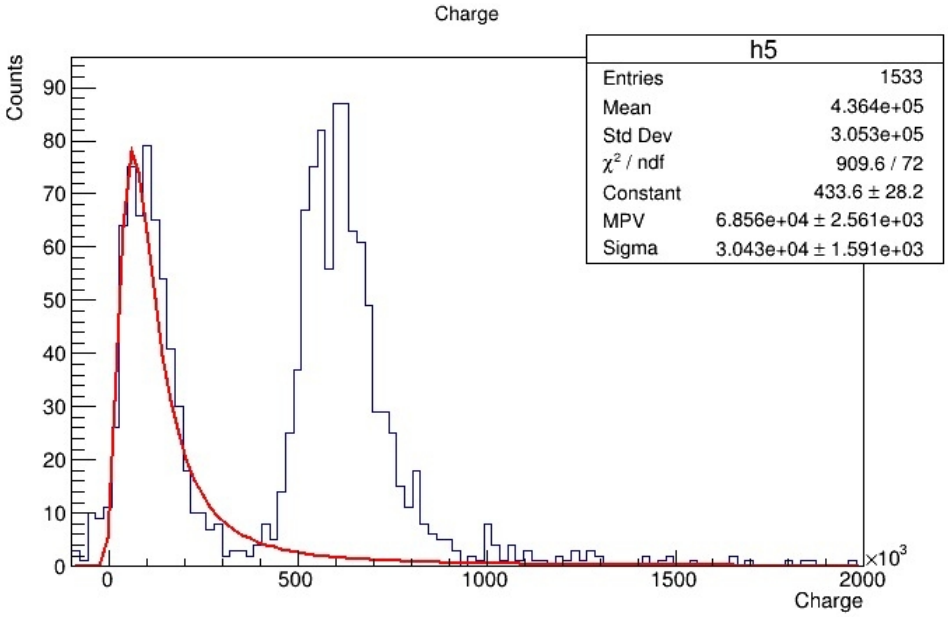

Figure B.13: Counts vs. charge at 12 kV in pad number six.

B.2 CERN MRPC

B.2.1 First run

Charge of strip G.

We had less coincidences in the CERN MRPC because the strips are smaller than the pads, we used the oscilloscope for 12.8, 14 and 15 kV. The adjustment for 12.8 kV is 1.24, which means it has a good one. For the plot of 14 kV, we had a better adjustment, which was 1.03, which was better and is higher than the first one.

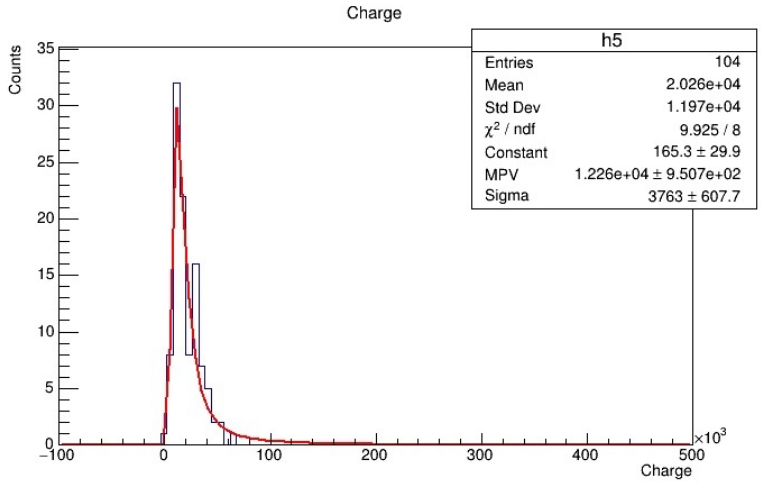

Figure B.14: Counts vs. charge at 12.8 kV on strip G.

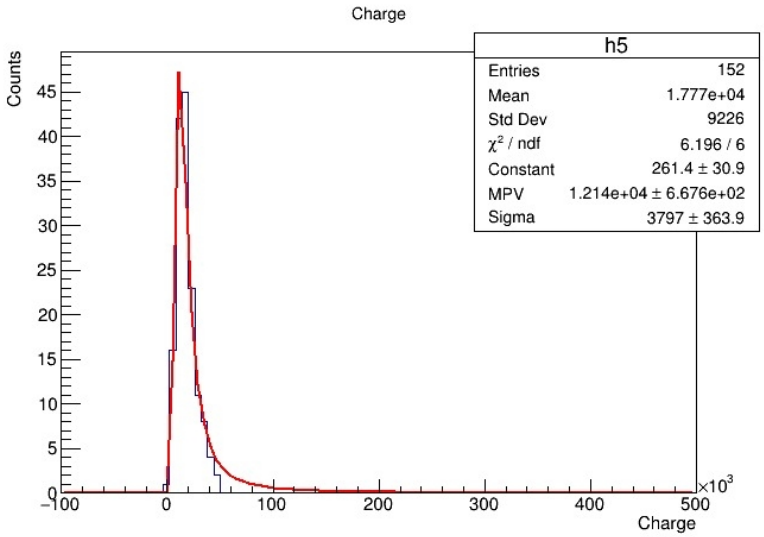

Figure B.15: Counts vs. charge at 14 kV on strip G.

At 14.3 and 14.6 we had more coincidences since we used the digitizer and detected the

signals faster, the adjustment for 14.3 kV is 2.19 and for 14.6 kV is 1.78, we can see the bins, but it as we had a lot of coincidences, they are smaller.

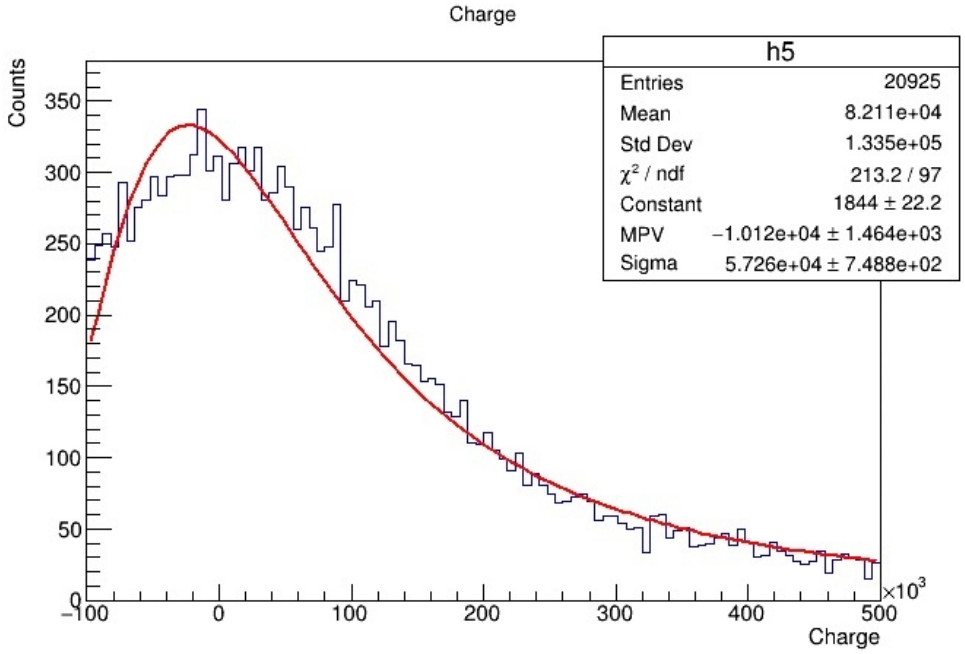

Figure B.16: Counts vs. charge at 14.3 kV on strip G.

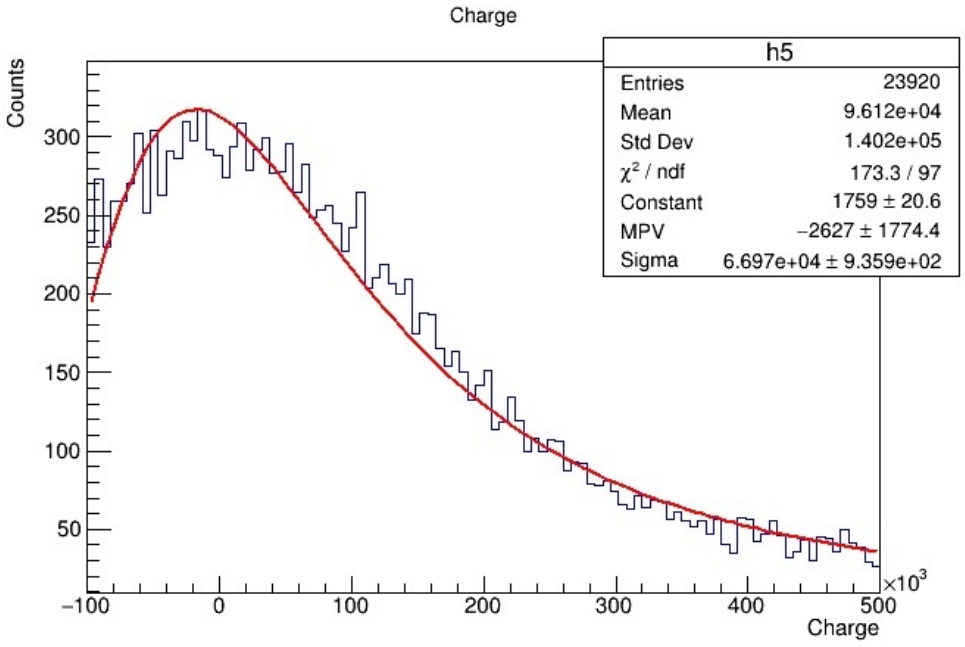

Figure B.17: Counts vs. charge at 14.6 kV on strip G.

At 15 kV, we have an adjustment of 0.95, with less entries so the bins are noticeable, but we also got data above the Gaussian curve.

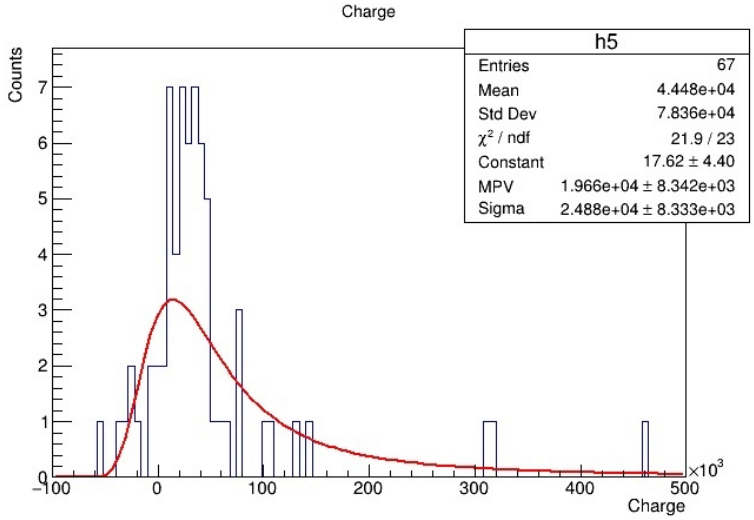

Figure B.18: Counts vs. charge at 15 kV on strip G.

Charge of strip I.

For 14 kV at strip I we had the less number of coincidences, overall, for strip I we had less coincidences, with an adjustment of 0.88, again, the bins are noticeable with some data above the Gaussian curve.

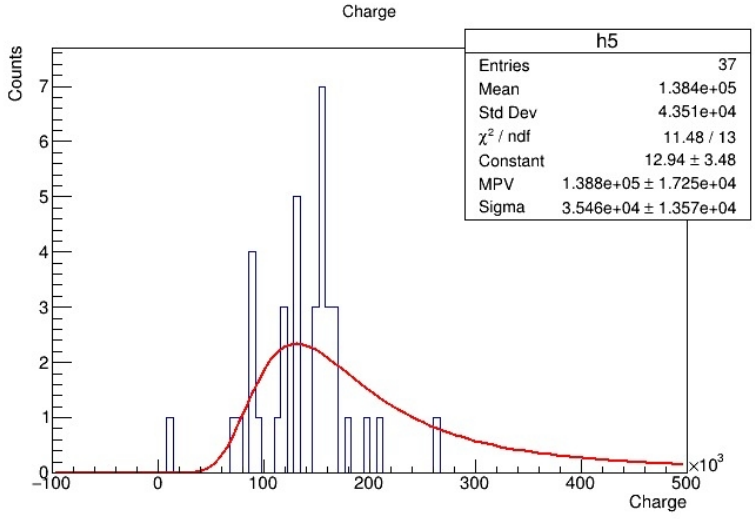

Figure B.19: Counts vs. charge at 14 kV on strip I.

Again, the number of coincidences increased a lot, and the plots for 14.3 and 14.6 kV are pretty similar to the ones from strip G, the adjustment was 1.24 and 1.26 respectively.

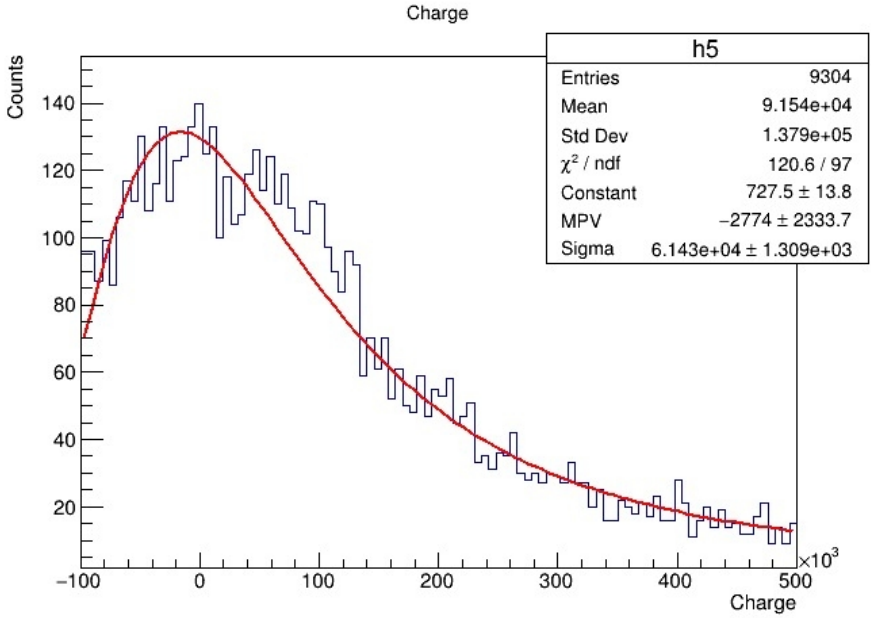

Figure B.20: Counts vs. charge at 14.3 kV on strip I.

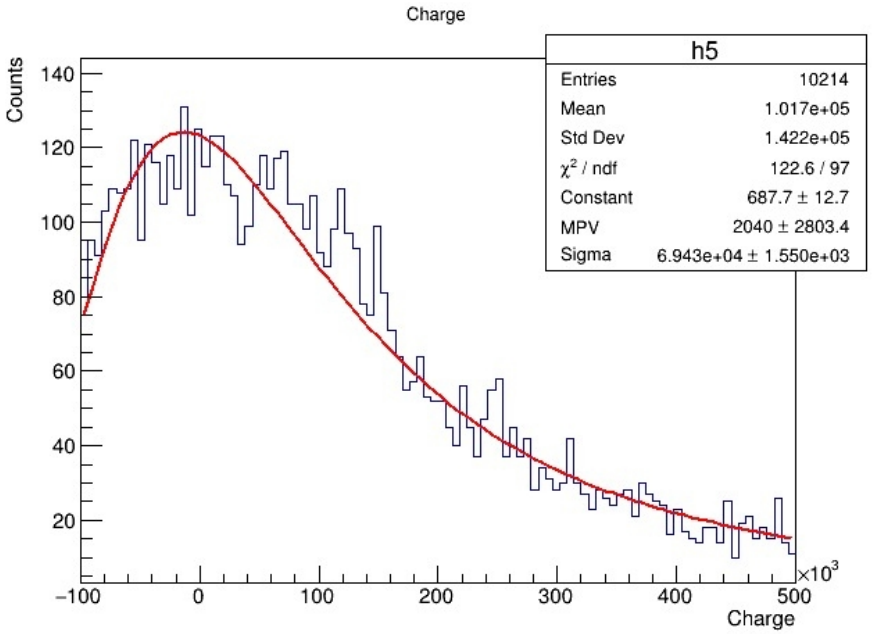

Figure B.21: Counts vs. charge at 14.6 kV on strip I.

Finally for the first run, at 15 kV, the adjustment was 0.907, and it is pretty similar to the one at 14 kV.

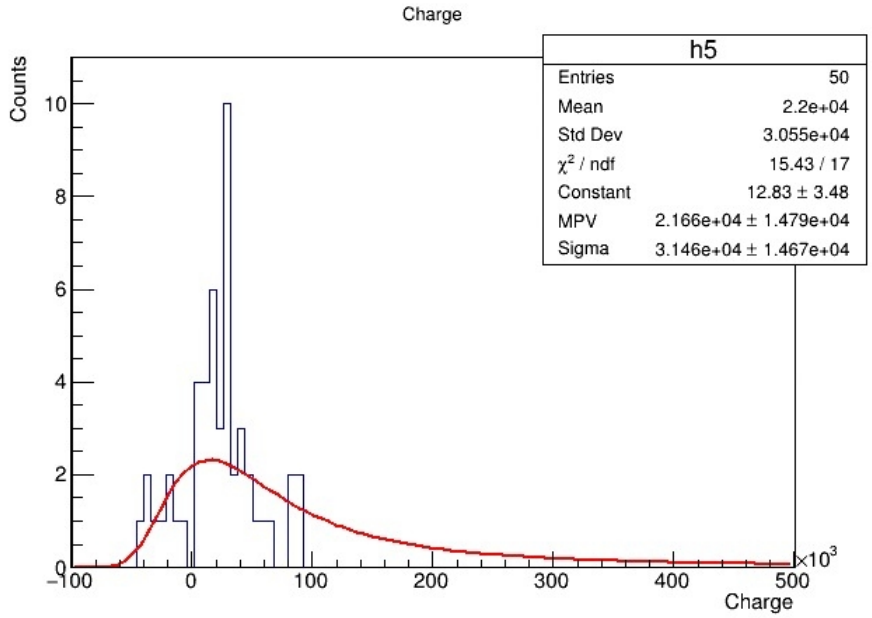

Figure B.22: Counts vs. charge at 15 kV on strip I.

B.2.2 Second run

Charge of strip G.

For the second run, all the data was obtained through the digitizer, for all the plots from strip G second run, we got the same kind of plot, where the bins are noticeable and the bell is long. The number of coincidences varies from 2612 (14.1 kV) to 23920 (14.6 kV), and the adjustment for 13.8, 14.1, 14.2, 14.3, 14.4 and 14.6 kV are $\chi^2/ndf = (4.54, 1.805, 1.63, 2.19, 3.04, 1.78)$ respectively.

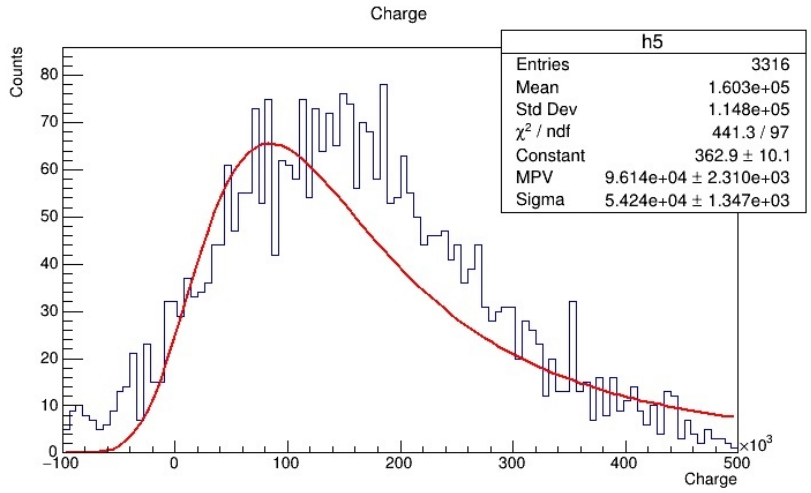

Figure B.23: Counts vs. charge at 13.8 kV on strip G.

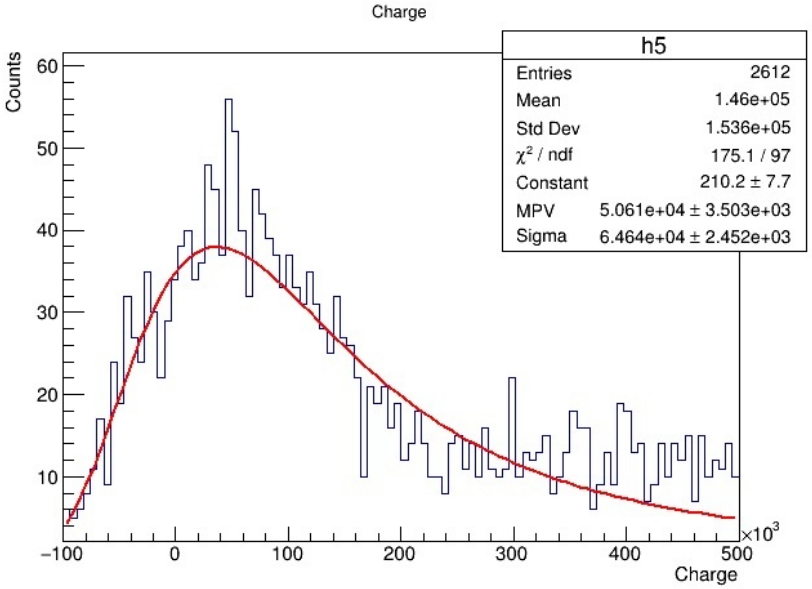

Figure B.24: Counts vs. charge at 14.1 kV on strip G.

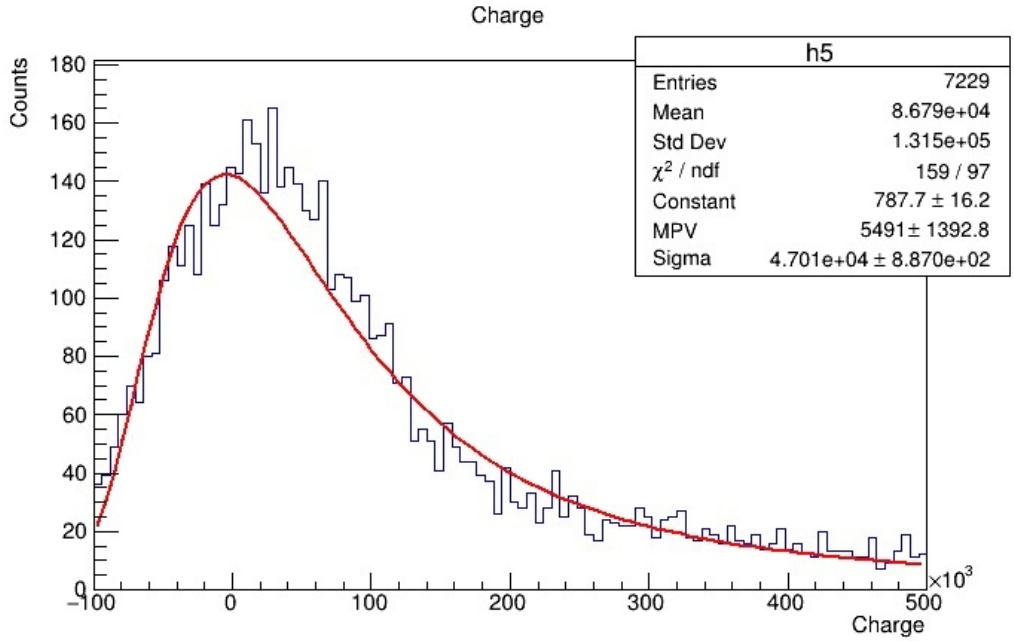

Figure B.25: Counts vs. charge at 14.2 kV on strip G.

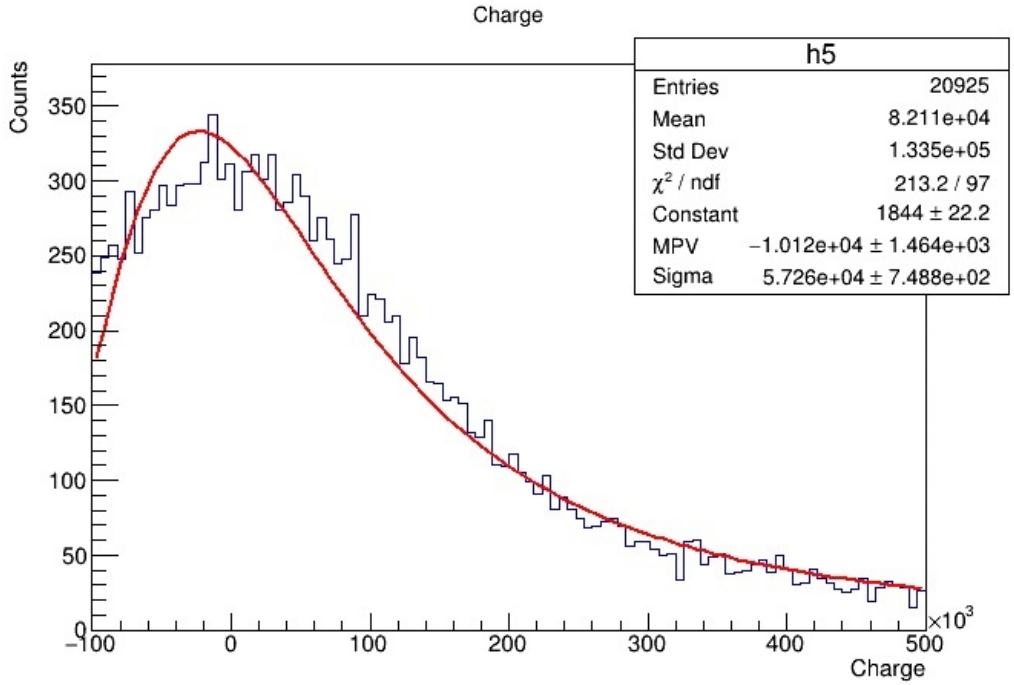

Figure B.26: Counts vs. charge at 14.3 kV on strip G.

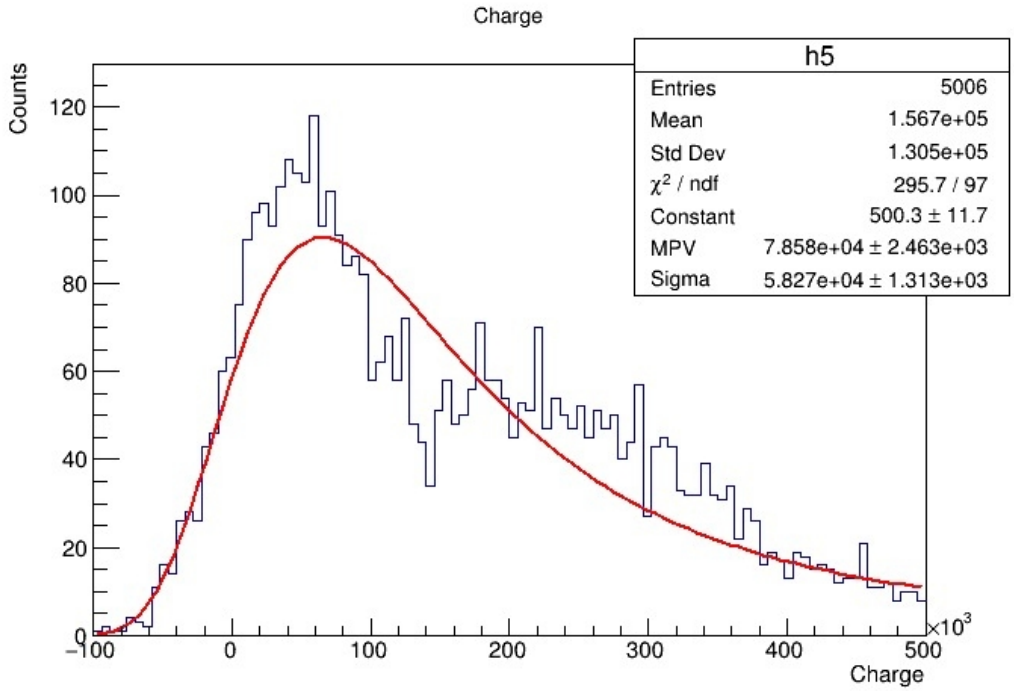

Figure B.27: Counts vs. charge at 14.4 kV on strip G.

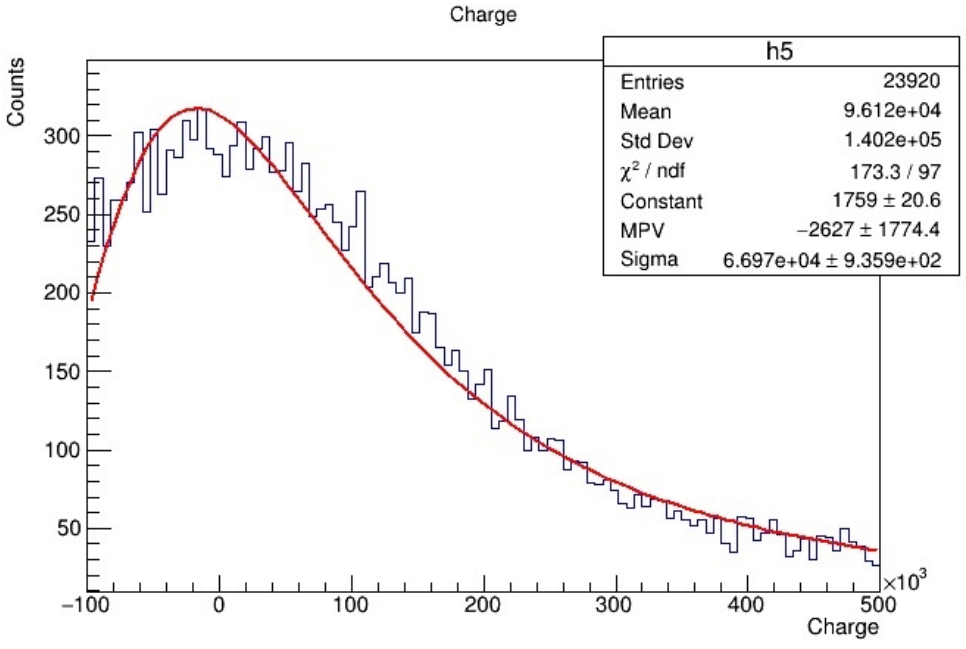

Figure B.28: Counts vs. charge at 14.6 kV on strip G.

Charge of strip I.

For the second run, we got the least coincidences at 13.8 kV on strip I, the adjustment was 0.89, very slim.

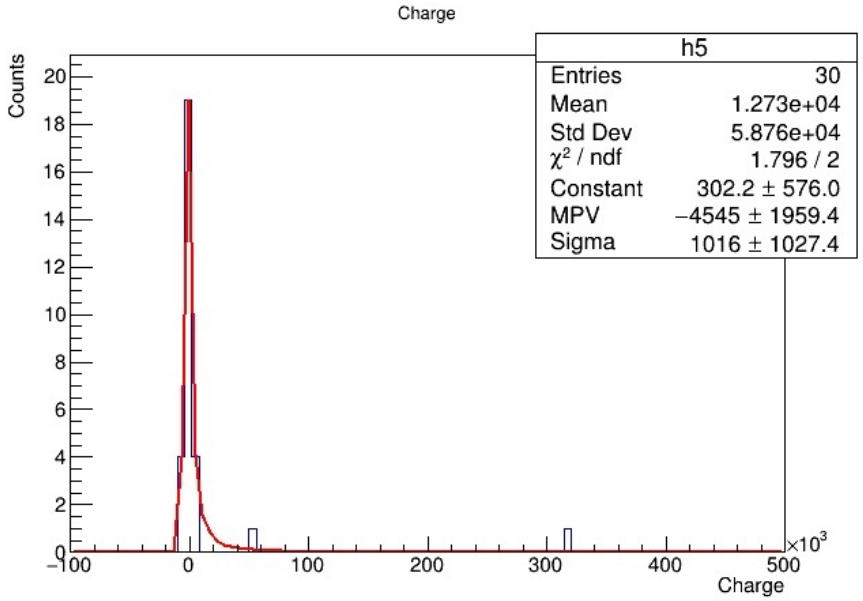

Figure B.29: Counts vs. charge at 13.8 kV on strip I.

The number of entries kept increasing until a top at 14.6 kV, so the bins kept getting slimmer, but the adjustment was pretty similar from here on. The adjustment was $\chi^2/ndf = (1.23, 1.904, 1.24, 1.64, 1.26)$ for 14.1, 14.2, 14.3, 14.4 and 14.6, respectively.

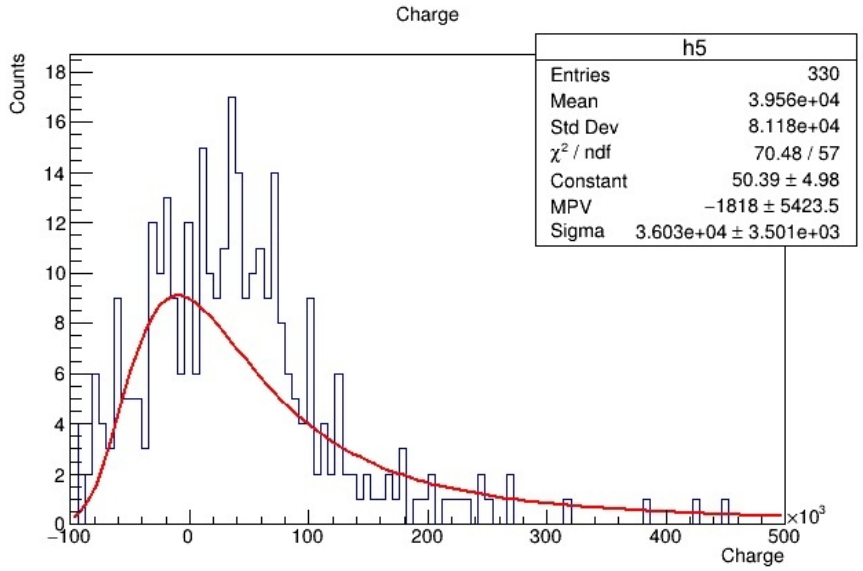

Figure B.30: Counts vs. charge at 14.1 kV on strip I.

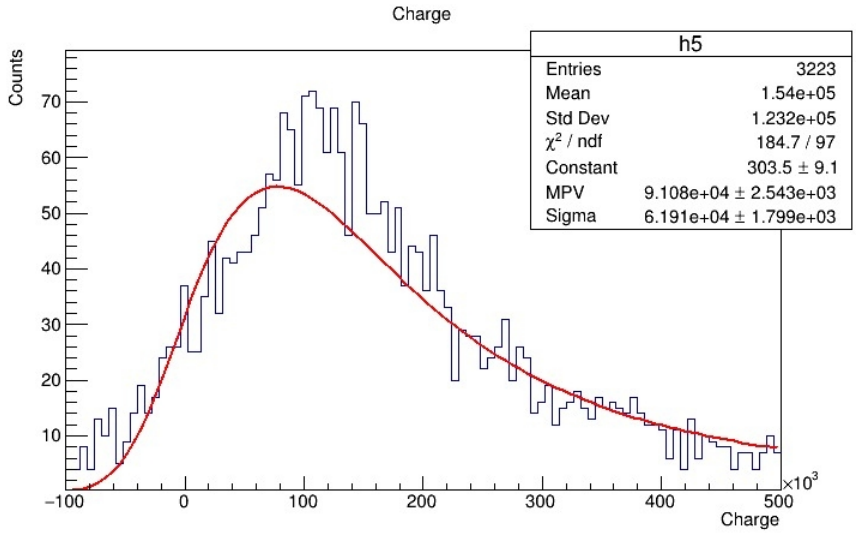

Figure B.31: Counts vs. charge at 14.2 kV on strip I.

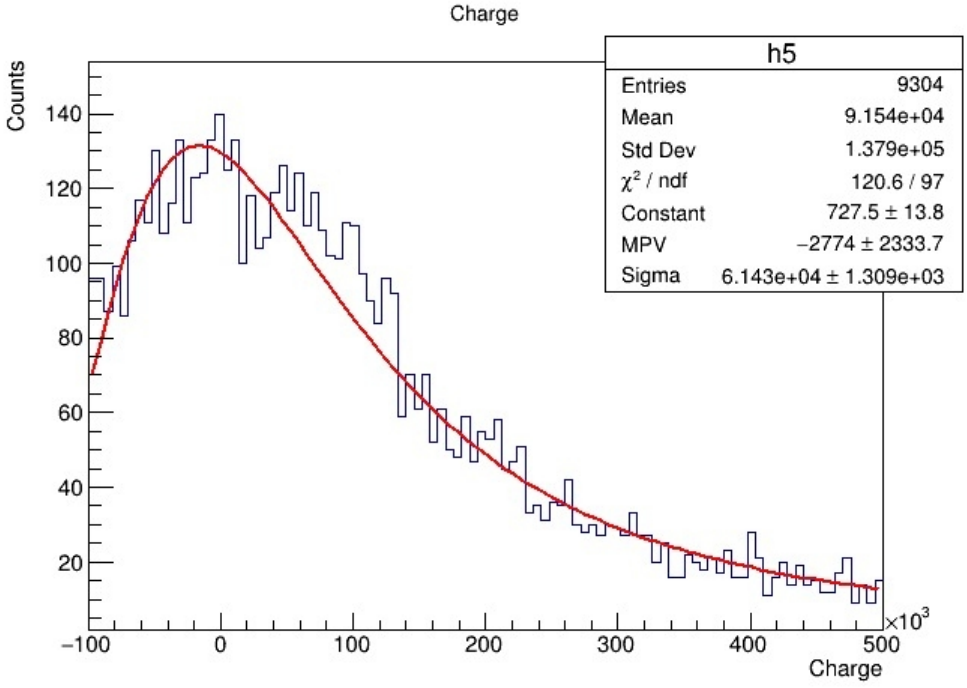

Figure B.32: Counts vs. charge at 14.3 kV on strip I.

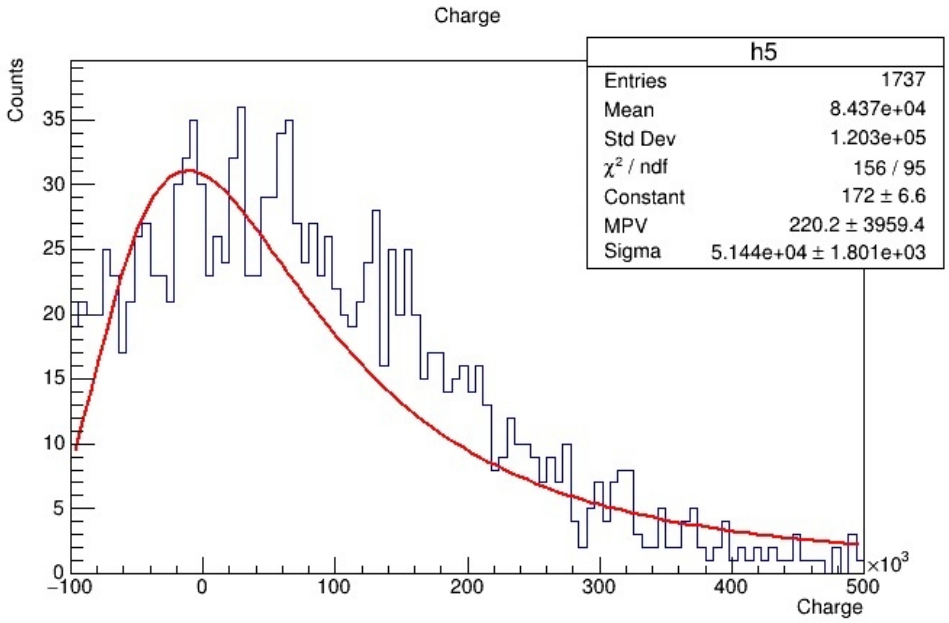

Figure B.33: Counts vs. charge at 14.4 kV on strip I.

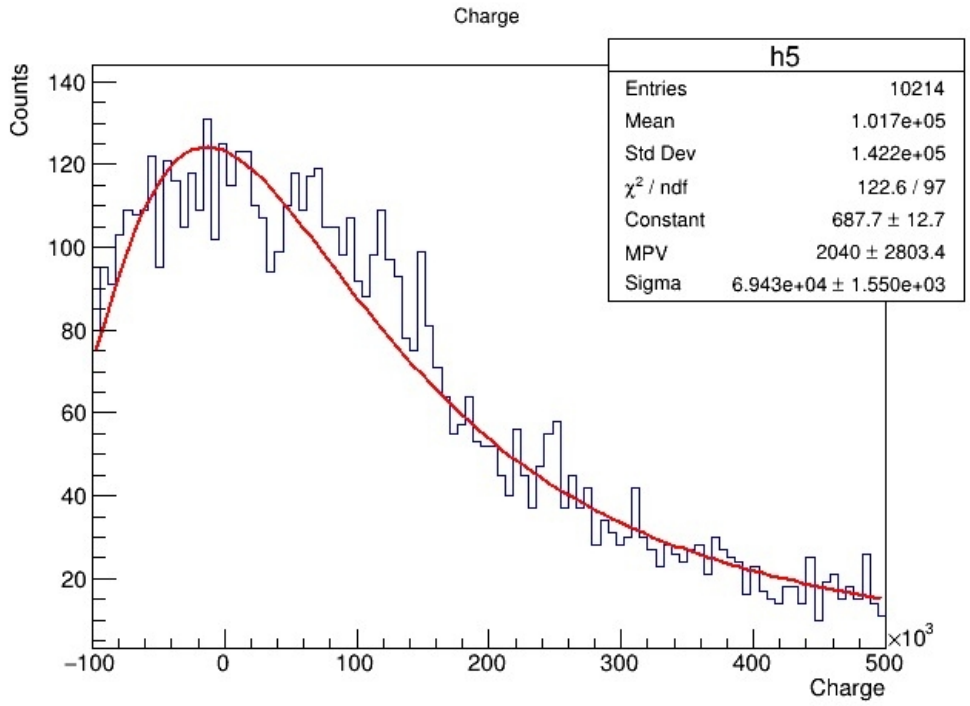

Figure B.34: Counts vs. charge at 14.6 kV on strip I.